DIRECT SPACE-TO-TIME PULSE SHAPING AND APPLICATIONS IN ARBITRARY ELECTROMAGNETIC WAVEFORM GENERATION

A Thesis

Submitted to the Faculty

of

Purdue University

by

Jason D. McKinney

In Partial Fulfillment of the

Requirements for the Degree

of

Doctor of Philosophy

May 2003

To my family and Amanda. Without your love and support this would not have been possible. Thank you.

ACKNOWLEDGMENTS

There are a great many people who have helped me in many ways throughout the course of my graduate study. I would especially like to thank Professor Andrew Weiner for his guidance, support, and encouragement throughout my graduate career. The opportunities for growth and the excitement of working in our group are deeply appreciated - I am honored to have had the chance to be part of it. Many thanks are due to Dr. Dongsun Seo for the construction of an excellent high repetition-rate fiber laser - without his efforts much of this work would not have been possible. I would like to thank Dan Leaird for his friendship, many fruitful discussions on a variety of topics, and for invaluable help in the lab.

I would also like to thank the various faculty with whom I have worked in a teaching capacity over the years. Access to your classrooms, teaching abilities, and feedback have been vital to my growth as a future educator. Many thanks to all the students I have had the pleasure of interacting with are in order as well - they have taught me equally as much as the faculty.

Finally, I would like to thank all the staff of our department with whom I have interacted during my time here. You have made being part of our School an extremely enjoyable experience and have provided me with more help than is imaginable over the years.

TABLE OF CONTENTS

LIST OF FIGURES

ABSTRACT

McKinney, Jason D. Ph.D., Purdue University, May, 2003. Direct Space-to-Time Pulse Shaping and Applications in Arbitrary Electromagnetic Waveform Generation. Major Professor: Andrew M. Weiner.

Direct space-to-time (DST) pulse shaping, with its straightforward mapping of an input spatial pattern to an output temporal pattern, has been shown to be an effective method to create ultrafast optical data packets. To our knowledge, we introduce the first DST pulse shaper operating in the 1.5 μm lightwave communications band, which is compatible with high-speed ($\geq$ 100 Gb/s) optical communication systems. Novel features of our pulse shaper include polarization-independent operation, utilization of diffractive optical elements for spatial pattern generation, and a telescopic, fiber-coupled configuration. These features collectively enable the creation of equal intensity optical pulse sequences over a time aperture in excess of 100 ps and at rates of $\sim$ 100 GHz. These pulse sequences enable us to overcome electrical limitations and generate arbitrary electromagnetic waveforms in the GHz to multiple tens of GHz range through a novel optical technique.

Although creation of arbitrary optical waveforms is achievable through established methods - such as Fourier transform pulse shaping - arbitrary waveform generation capabilities in the microwave and millimeter-wave range are quite limited. We demonstrate, for the first time to our knowledge, cycle-by-cycle generation of broadband burst and continuous electromagnetic waveforms at center frequencies from $\sim$2-50 GHz. Our simple, reconfigurable method uses tailored optical pulse sequences from our 1.5 μm DST pulse shaper to drive a high-speed optical-to-electrical converter. By appropriately tailoring the input optical spatial pattern of the pulse shaper, arbitrarily phase- and frequency-modulated electromagnetic waveforms are achieved.

1. INTRODUCTION

Techniques for obtaining arbitrarily shaped optical waveforms have been of great interest for many years. One such technique, which is now widely accepted, is Fourier transform (FT) pulse shaping [1]. Using a combination of phase- and amplitude-modulation in the pulse shaper, nearly arbitrarily shaped optical waveforms can be obtained, with the shape of the output temporal waveform given by the Fourier transform of the applied spatial masking function in the FT pulse shaper. While this technique allows synthesis of virtually any temporal waveform, the method is limited by the update rate of the modulator and by the time to compute the requisite masking function. For optical communications applications, such as optical time-division multiplexed systems, where "packets" of information are desired, slow modulator updates and lengthy computation time limit the overall system bit rate. For these type systems, a more direct method of packet generation is desirable.

Direct space-to-time (DST) pulse shaping, originally demonstrated in the mid-1970s with pulses in the 30 ps range [2], provides a straight-forward method for creating such optical data packets, by exploiting the coupling between space and time in dispersive optical systems. While techniques to measure this coupling have been demonstrated [3, 4] and FT pulse shaping systems utilizing this coupling have been constructed [5, 6], only recently has this effect been exploited for high-rate optical pulse sequence generation [7]. This pulse shaping geometry which consists of a diffraction grating, lens and thin slit, gives a temporal output which is a directly scaled version of a spatially patterned fs input beam. This mapping of a parallel spatial pattern to a serial temporal pattern is compatible with high-speed modulator arrays allowing packet generation by parallel manipulation of each bit in the packet. Operation of this pulse shaper in the femtosecond regime has been thoroughly an-

alyzed by Leaird [8] and has been shown to be a simple method for the creation of ultrafast optical data packets [7]. We now extend this work by moving DST pulse shaping to the 1.5 μm communications band in a manner compatible with high-speed optical fiber communications systems.

Through a novel telescopic, optical fiber-coupled DST pulse shaping geometry [9] we demonstrate, for the first time to our knowledge, high-rate optical pulse sequence generation over a time aperture in excess of 100 ps. Additional novelties of our pulse shaper include the use of diffractive optical elements to improve the spatial patterning operation and polarization-independent operation. The combination of the above features enables high-rate optical pulse sequence generation over a time aperture $\sim$3 times greater than previously demonstrated. This apparatus, when coupled with a 10 GHz actively modelocked input source [10], allows generation of continuous optical pulse sequences at rates approaching 100 GHz - more than two times higher than the commercial state-of-the-art.

Though the intended optical application of our 1.5 μm DST shaper is optical packet generation, aimed toward high-speed optical networks, the ability to generate arbitrary pulse sequences over a 100 ps temporal window also enables another novel experiment - generation of arbitrarily shaped electromagnetic waveforms. By using tailored optical pulse sequences from our DST pulse shaper to drive a high-speed photodiode (optical-to-electrical) converter, we generate arbitrarily phase- and frequency-modulated broadband burst millimeter waveforms at center frequencies approaching 50 GHz[11]. We also demonstrate how predistortion of the driving optical pulse sequence in our experiment allows amplitude equalization of the output electrical waveform. Our technique, when coupled with a high repetition rate optical source, is demonstrated to be extendible to generation of continuous millimeter-wave signals [12]. Utilizing the physics of our pulse shaping apparatus, namely the ability to impart a frequency modulation, or chirp, onto the pulse shaper output waveform [13] and dispersive stretching, we have also demonstrated generation of microwave signals in the $\sim$2 GHz range [14, 15]. Our reprogrammable cycle-by-cycle electrical

waveform generation technique could be an enabling technology for various applications in including RF communication systems, electronic countermeasures and pulsed radar.

This work is organized in the following manner. In Chapter 2, a brief discussion of the theory of operation of the telescopic DST shaper(Sec. 2.2) will be followed by discussions of the temporal window of our pulse shaper in Section 2.3, frequency modulation behavior of the pulse shaper in Section 2.4, and effects of this frequency modulation on the pulse shaper output in Section 2.5. The experimental realization of the pulse shaper will be discussed in Section 2.6, along with generation of high-rate burst optical pulse sequences, and Section 2.7 will present continuous 100 GHz optical pulse sequence generation. Our novel electromagnetic waveform generation technique will be explained in Chapter 3 and Chapter 4 will describe the extension of this technique to electrical waveforms in the low GHz range. In Chapter 5, we will summarize and present future research directions. The diffraction analysis of the telescopic DST shaper is included, in its entirety, in Appendix A.

2. DIRECT SPACE-TO-TIME PULSE SHAPING

2.1 Motivation and Previous Work

Techniques for generation of high-rate arbitrary optical pulse sequences are of importance to many applications, ranging from coherent control to optical communication. Specifically for optical communications applications, e.g. optical packet generation, direct space-to-time pulse shaping [8] has been demonstrated to be a straightforward manner by which to generate these pulse sequences.

Direct space-to-time (DST) pulse shaping was first demonstrated by Colombeau et al. in the mid-1970s, with pulses in the ~30 ps range [2]. This initial work was further explained during the late eighties and early nineties using more standard measurement techniques (optical auto- and cross-correlation) to verify the resulting shaped pulses [16], and to theoretically explain the pulse shaping mechanism [16, 17].

DST pulse shaping was brought into the femtosecond regime by Leaird and Weiner [8] in the latter half of the 1990s. Thorough analysis of the pulse shaping apparatus has been performed and generation of high-rate optical pulse sequences at Ti:sapphire wavelengths has been demonstrated [7, 8]. Chirp control in the apparatus has also been presented [13]. The work of Leaird and Weiner [7, 8, 13], while providing the fundamental description of the pulse shaping apparatus on a femtosecond time scale, also illustrated several areas which could be further engineered to enhance the overall system performance for optical packet generation in optical communications applications. In particular, improvements in the pulse shaping time aperture and equalization of optical pulse sequences from the pulse shaper are of primary interest.

The focus of this chapter is a novel direct space-to-time optical pulse shaper, constructed for the first time in the 1.5 μm lightwave communications wavelength band. The pulse shaper exhibits a novel telescopic, fiber-coupled configuration which

enables generation of nearly equal amplitude, high-rate optical pulse sequences over a time aperture in excess of 100 ps - more than two times greater than previously demonstrated. In addition to the pulse shaping apparatus itself, a theoretical analysis of previously unknown chirp and temporal window behavior will be given. The remainder of the chapter is organized in the following manner. In Section 2.2, the theory of operation of the DST pulse shaper is discussed and novel temporal window and frequency modulation (chirp) behavior are presented in Sections 2.3 and 2.4, respectively. Effects of frequency modulation in the DST shaper are analyzed in Section 2.5. The implementation of the pulse shaping apparatus, and the novel features thereof, are addressed in Section 2.6 along with generation of high-rate burst optical pulse sequences. Section 2.7 presents experimental results in generation of high-rate ($\sim$100 GHz) continuous optical pulse sequences from the DST shaper.

2.2 Theory of Operation for the Fiber Coupled DST Pulse Shaper

Though not as widely known as Fourier transform (FT) pulse shaping [1, 18], DST pulse shaping provides a simple manner by which to generate optical pulse sequences. The basic functionality of the DST shaper is illustrated in Figure 2.1. In contrast to the Fourier relation between the spatial mask and temporal output in FT shaping, the output temporal waveform from a DST shaper is a directly scaled version of the spatial pattern applied to a short pulse at the input of the shaper. Functionally, the DST shaper acts as a parallel-to-serial converter for this short pulse input. Changes in the output pulse sequence are induced simply by changing the applied spatial pattern at the pulse shaper input. This straightforward relationship between the applied spatial pattern and the pulse shaper temporal output makes the system ideally suited for optical pulse sequence generation.

The mapping from space to time, or optical parallel-to-serial operation, can be illustrated in a number of ways. Calculation of the pulse tilt [19] or a simple geometric argument for the delay across a plane wave diffracted off a grating [20] both give the time-to-space mapping exactly. A diffraction analysis of the DST shaper, similar to [5, 8, 21] also illustrates how the DST shaper converts a spatially patterned fs input

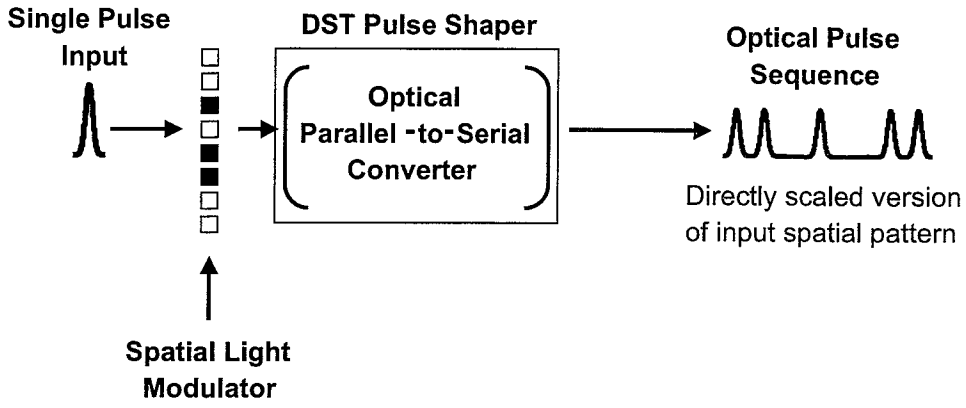

Fig. 2.1. Schematic operation of the DST pulse shaper. A spatially patterned short pulse input is converted to a temporal output which is a directly scaled version of the applied spatial pattern. The DST shaper essentially performs optical parallel-to-serial conversion.

beam into a temporally patterned output waveform. The results of this analysis will be discussed in this section. The specific point of this discussion is to point out the effects of the telescope on the achievable pulse shaping temporal window and new control of the frequency modulation (chirp) behavior of the pulse shaper, as compared to previous analysis [8, 13].

The diffraction analysis was performed for the system shown in Figure 2.2. The derivation in its entirety is included in the appendix; only key results and the basic operation of the DST shaper will be included here. For a spatially patterned beam $s(x)$ just after the diffraction grating ($\mathbf{P_2}$), the field at the pulse shaper output, prior to the slit ($\mathbf{P_5}$) is given by

$$\mathbf{E_5}(x) = C_{DST} e^{-j\frac{k}{2d_2}\left(\frac{f_1 - d_1 A_1}{f_1}\right)x^2} S'\left(\frac{k}{f_1} A_1 x\right) \tag{2.1}$$

where

$$S'\left(\frac{k}{f_1} A_1 x\right) = \mathcal{F}\left\{ s(x)\, e^{-j\frac{k}{2d_1}\left(\frac{f_1 - d_2 A_1}{f_1}\right)x^2} \right\} = \mathcal{F}\{s'(x)\} \tag{2.2}$$

$$A_1 = \frac{f_1^2}{f_1 d_1 + f_1 d_2 - d_1 d_2} \tag{2.3}$$

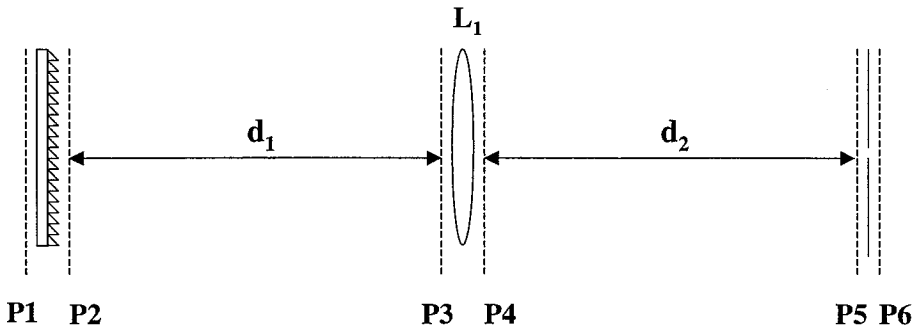

Fig. 2.2. Definition of planes relevant to the diffraction analysis of the DST pulse shaper.

and $\mathcal{F}\{\}$ denotes the spatial Fourier transform

$$S'(\xi) = \int_{-\infty}^{\infty} dx'\ s(x')\, e^{j\xi x'}. \tag{2.4}$$

Here, A_1 is a unitless scaling factor arising from the position of the pulse shaping lens. This quantity takes on a maximum value of 1 for $\mathbf{d_1}$ and / or $\mathbf{d_2} = \mathbf{f_1}$. In the expression for $\mathbf{E_5}$ given by Eq. 2.1, C_{DST} is a constant arising from the diffraction analysis of the field at the input to the pulse shaper. For a full expression for this constant, please consult Appendix A. In order to relate the field at the pulse shaper output to the spatial input pattern of the DST before the grating ($\mathbf{P_1}$), the effect of the diffraction grating must be taken into account. If a spatially patterned Gaussian fs input beam [22, 23, 8], of radius w and with phase-front radius of curvature R, is assumed just prior to the grating,

$$\mathbf{E_1}(x,\omega) = m(x)\ e^{-\frac{x^2}{w^2}}\ e^{-j\frac{k}{2R}x^2}\ E(\omega) \tag{2.5}$$

where

$$m(x) = \text{applied spatial pattern} \tag{2.6}$$

$$e^{-\frac{x^2}{w^2}} = \text{intensity distribution of the Gaussian beam} \tag{2.7}$$

$$e^{-j\frac{k}{2R}x^2} = \text{phase distribution of the Gaussian beam} \tag{2.8}$$

the field after the grating ($\mathbf{P_2}$), taking into account the change in beam size after the grating (α) and the dispersion of the grating (γ) is

$$\mathbf{E_2}(x) = s(x)\, e^{-j\gamma\omega x} E(\omega), \tag{2.9}$$

where

$$s(x) = m(\alpha x)\; e^{-\frac{\alpha^2 x^2}{w^2}}\; e^{-j\frac{k\alpha^2}{2R}x^2}. \tag{2.10}$$

In the above expression,

$$\alpha = \frac{\cos\theta_i}{\cos\theta_d} \tag{2.11}$$

$$\gamma = \frac{\lambda}{cd\cos\theta_d}\ (\text{ps/mm}) \tag{2.12}$$

where λ is the source wavelength, c is the speed of light, d is the period of the diffraction grating and θ_i, θ_d are the incident and diffracted angles of the beam off the grating. Inserting the expression for $s(x)$ (Eq. 2.10) into 2.2 and taking the spatial Fourier transform, the field prior to the output fiber in the DST is

$$\mathbf{E_5}(x,\omega) = \frac{C_{DST}}{\alpha} E(\omega)\, e^{-j\frac{k}{2d_2}\left(\frac{f_1 - d_1 A_1}{f_1}\right)x^2} S'\left\{-\frac{\gamma}{\alpha}\left(\omega - \frac{k}{f_1\gamma}A_1 x\right)\right\}. \tag{2.13}$$

In order to express the temporal output of the DST, the effect of the slit (which samples the Fourier transform of the input spatial pattern) must be taken into account and an inverse temporal Fourier transform performed. In contrast to previous work, where the slit was treated as an ideal spatial δ function [7, 8, 13], the output in the 1.5 μm DST shaper is sampled with a single-mode fiber. To find the field coupled into the fiber, an overlap integral must be performed between the field just before the fiber and the effective spatial mode of the fiber. The method used to find this overlap integral is similar to [24]. Assuming the fiber mode is centered at $x = 0$ and of the general form $f\left(\frac{x}{w_0}\right)$, where w_0 allows scaling of the width of the mode, and has the property

$$\int_{-\infty}^{\infty} dx \left| f\left(\frac{x}{w_0}\right)\right|^2 = 1 \tag{2.14}$$

this overlap integral can be written as

$$E_{DST}(x,t) = \frac{C_{DST}}{\alpha} f\left(\frac{x}{w_0}\right) \frac{1}{\sqrt{2\pi}} \int_{-\infty}^{\infty} d\omega\ E(\omega)\, e^{j\omega t} \cdot \int_{-\infty}^{\infty} dx'\ f\left(\frac{x'}{w_0}\right) e^{-j\frac{k}{2d_2}\left(\frac{f_1 - d_1 A_1}{f_1}\right)x'^2} S'\left[-\frac{\gamma}{\alpha}\left(\omega - \frac{k}{f_1 \gamma} A_1 x'\right)\right] \tag{2.15}$$

Interchanging the order of integration and taking the inverse temporal Fourier transform, we have

$$E_{DST}(x,t) = \frac{C_{DST}}{\gamma} f\left(\frac{x}{w_0}\right) \int_{-\infty}^{\infty} dx'\ f\left(\frac{x'}{w_0}\right) e^{-j\frac{k}{2d_2}\left(\frac{f_1 - d_1 A_1}{f_1}\right)x'^2} e(t) * \left\{ s'\left(-\frac{\alpha}{\gamma} t\right) e^{j\frac{k}{\gamma f_1} A_1 x' t} \right\} \tag{2.16}$$

where $*$ denotes convolution. Interchanging the order of the convolution and the dx' integral, and treating the dx' integral as a spatial Fourier transform, the temporal output of the DST shaper can be written as

$$E_{DST}(x,t) = \sqrt{2\pi} w_0 \frac{C_{DST}}{\gamma} f\left(\frac{x}{w_0}\right) e(t) * \left\{ s'\left(-\frac{\alpha}{\gamma} t\right) \left[F\left(\frac{k w_0}{\gamma f_1} A_1 t\right) * e^{j\frac{k}{2\gamma^2 f_1^2} A_1^2 \left(\frac{f_1 d_2}{f_1 - d_1 A_1}\right) t^2} \right] \right\} \tag{2.17}$$

where $e(t)$ represents the temporal shape of the input fs pulse, $s'\left(-\frac{\alpha}{\gamma} t\right)$ is the spatial pattern, including a quadratic spatial phase, evaluated as a function of time, and $F\left(\frac{k w_0}{\gamma f_1} A_1 t\right)$ is the Fourier transform of the fiber mode as a function of time. If we take the fiber mode to be a Gaussian of the form

$$f(x) = \frac{1}{\sqrt{2\pi} w_0} e^{-\frac{x^2}{w_0^2}} \overset{\mathcal{F}}{\Leftrightarrow} F(\xi) = e^{-\frac{\xi^2 w_0^2}{4}} \tag{2.18}$$

and evaluate $s'\left(-\frac{\alpha}{\gamma} t\right)$, the DST shaper output is now given by

$$E_{DST}(x,t) = \frac{C_{DST}}{\gamma} e^{-\frac{x^2}{w_0^2}} e(t) * \left\{ m\left(-\frac{\alpha}{\gamma} t\right) e^{-\frac{\alpha^2}{\gamma^2}\frac{t^2}{w^2}} e^{-j\frac{k}{2\gamma^2}\left(\frac{\alpha^2}{R} + \frac{f_1 - d_2 A_1}{f_1 d_1}\right) t^2} F_c(t) \right\}. \tag{2.19}$$

Here, $F_c(t)$ represents the complex fiber mode, with an amplitude variation due to the finite size of the fiber and a quadratic temporal phase due to the position of the pulse shaping lens as in Eq. 2.17. Mathematically, this complex fiber mode is given by

$$F_c(t) = e^{-\frac{k^2 w_o^2}{4\gamma^2 f_1^2} A_1^2 \left\{ \frac{1}{1+\frac{k^2 w_o^2 (1-d_1 A_1)^2}{4 d_2^2 f_1^2}} - j\frac{k w_o^2}{2}\left[\frac{f_1 d_2 (f_1 - d_1 A_1)}{4 d_2^2 f_1^2 + k^2 w_o^2 (f_1 - d_1 A_1)^2}\right]\right\} t^2}. \tag{2.20}$$

Grouping amplitude and phase terms together, the pulse shaper output is given by

$$E_{DST}(x,t) = \frac{C_{DST}}{\gamma} e^{-\frac{x^2}{w_o^2}} e(t) * \left\{ m\left(-\frac{\alpha}{\gamma} t\right) W_{DST}(t) P_{DST}(t) \right\} \tag{2.21}$$

The terms $W_{DST}(t)$ and $P_{DST}(t)$ are

$$W_{DST}(t) = e^{-\frac{1}{\gamma^2}\left\{ \frac{\alpha^2}{w^2} + \frac{k^2 w_o^2}{4 f_1^2} A_1^2 \left[\frac{1}{1+\frac{k^2 w_o^2 (1-d_1 A_1)^2}{4 d_2^2 f_1^2}}\right]\right\} t^2} \tag{2.22}$$

and

$$P_{DST}(t) = e^{-j\frac{k}{2\gamma^2}\left\{ \frac{\alpha^2}{R} + \frac{f_1 - d_2 A_1}{f_1 d_1} + \frac{k w_o^2}{2}\left[\frac{f_1 d_2 (f_1 - d_1 A_1)}{4 d_2^2 f_1^2 + k^2 w_o^4 (f_1 - d_1 A_1)^2}\right]\right\} t^2}. \tag{2.23}$$

These terms give rise to the pulse shaping temporal window and a frequency modulation of the pulse shaper output, respectively. These effects will be discussed later in this chapter.

The space-to-time conversion constant [8], which gives the mapping from spatial size at the pulse shaper input to temporal duration at the pulse shaper output, is defined as

$$\frac{\gamma}{\alpha} = \frac{\lambda}{cd\cos\theta_i} \text{ (ps/mm)}, \tag{2.24}$$

and can be chosen by setting the grating period and the incident angle (θ_i). The mapping from space to time is evident from the temporal evaluation of the spatial pattern $m\left(-\frac{\alpha}{\gamma} t\right)$. This term controls the basic, user-defined form of the temporal waveform generated by the DST shaper. The following sections will discuss the effects of the fiber coupling and spatial pattern size at the grating included in $W_{DST}(t)$ and the quadratic temporal phase given by $P_{DST}(t)$ on the output waveform.

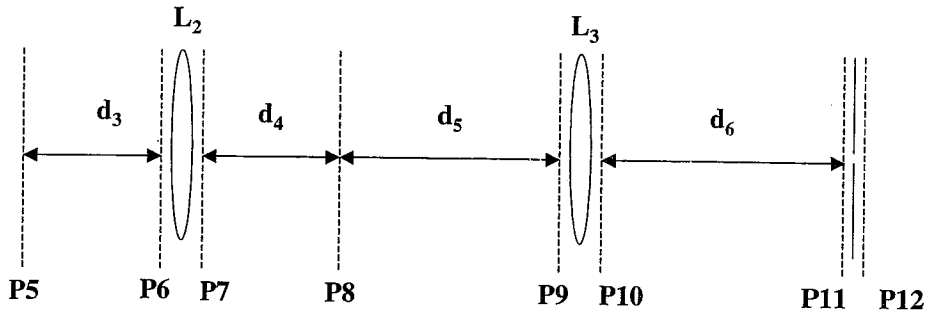

Fig. 2.3. Plane definitions for the diffraction analysis of the telescope following the DST shaper.

Thus far, only the basic (grating-lens-fiber) pulse shaper has been analyzed. To determine the behavior of the actual pulse shaping apparatus, the telescope which has been added between the basic shaper and the output fiber must be included in the diffraction analysis. Figure 2.3 shows the various plane definitions used for this analysis. If the field at plane $\mathbf{P_5}$ is propagated through the telescope to plane $\mathbf{P_{11}}$ and coupled to the output fiber ($\mathbf{P_{12}}$), the telescopic pulse shaper output is given by

$$E_T(x,t) = \frac{C_T}{\gamma} e^{-\frac{x^2}{w_o^2}} e(t) * \left\{ m\left(-\frac{\alpha}{\gamma}t\right) W_T(t) P_T(t) \right\}. \tag{2.25}$$

We again define a temporal window and phase term (W_T and P_T) as given below:

$$W_T = e^{-\frac{1}{\gamma^2}\left[\frac{\alpha^2}{w^2}+\frac{k^2 w_o^2}{4f_1^2}\frac{f_2^2}{f_3^2}\frac{A_3^2}{A_2^2}A_1^2\left(\frac{1}{1+\frac{k^2}{4f_3^4}A_3^4 w_o^4 \mathbf{B_2}^2}\right)\right]t^2} \tag{2.26}$$

$$P_T = e^{-j\frac{k}{2\gamma^2}\left[\frac{\alpha^2}{R}+\frac{f_1-d_2A_1}{f_1 d_1}+\frac{f_1^2}{f_2^2}\frac{A_2^2}{A_1^2}\left(\frac{f_2-d_3A_2}{f_2 d_4}+\frac{f_3-d_6A_3}{f_3 d_5}\right)+\frac{k^2 w_o^2}{4f_1^2}\frac{f_2^2}{f_3^2}\frac{A_3^2}{A_2^2}A_1^2\left(\frac{w_o^2 A_3^2 \mathbf{B_2}}{f_3^2+\frac{k^2}{4f_3^2}A_3^4 w_o^4 \mathbf{B_2}^2}\right)\right]t^2} \tag{2.27}$$

$$A_2 = \frac{f_2^2}{f_2 d_3 + f_2 d_4 - d_3 d_4} \tag{2.28}$$

$$A_3 = \frac{f_3^2}{f_3 d_5 + f_3 d_6 - d_5 d_6} \tag{2.29}$$

$$\tag{2.30}$$

Similar to A_1, A_2 and A_3 are unitless scaling factors relating to the positions of the telescope lenses and output fiber. Again, these have a maximum value of 1 for $\mathbf{d_3}$

and / or $\mathbf{d_4} = \mathbf{f_2}$ and $\mathbf{d_5}$ and / or $\mathbf{d_6} = \mathbf{f_3}$. The term $\mathbf{B_2}$ is given in the Appendix by Eq. A.85. In the output of the telescopic DST pulse shaper, it is interesting to note that the space-to-time conversion constant is not changed. Thus, the spatial pattern $m(x)$ applied at the grating results in the same underlying temporal output waveform as the basic grating-lens-fiber implementation of the shaper. There are, however, changes in the pulse shaping temporal window and frequency modulation behavior as the expressions for W_T and P_T illustrate. Discussions of the pulse shaping temporal window and frequency modulation behavior of the pulse shaper, in both the basic and telescopic configurations, will be discussed in the following sections.

2.3 Temporal Window of the Telescopic Direct Space-to-Time Pulse Shaper

The achievable pulse shaping temporal window in the DST pulse shaper is determined by several parameters, which are defined both by the user and the pulse shaping apparatus. Both the user defined temporal waveform, $m\left(-\alpha t/\gamma\right)$ and the finite size of the single-mode optical fiber used to sample the pulse shaper output affect the temporal duration of waveforms from the shaper. Achieving a temporal window, for our purposes defined as the intensity full-width at half-maximum (FWHM) of the measured intensity profile of the waveform, in excess of $\sim$100 ps is one specific goal of our pulse shaping apparatus. The temporal window of the basic DST shaper and the motivation to move to a telescopic configuration will now be discussed.

In the previous section, the exponential term W_{DST} (Eq. 2.22) contains information on both of the above contributions to the pulse shaping temporal window. Before beginning the discussion of the temporal window in the DST shaper, it should be noted that the spatial pattern applied to the pulse shaper input is assumed to be generated from a spatially patterned Gaussian beam, as given by Eqs. 2.5-2.8. This assumes spatial patterning is achieved as in [7, 8, 13], where a Gaussian beam is cylindrically focused and passed through an amplitude mask to achieve the desired spatial pattern. Though spatial patterning is achieved via other methods in our system, the convention of assuming a spatially patterned Gaussian beam is retained in

the mathematical treatment and does not significantly affect the results presented here.

From Eq. 2.22, the pulse shaping temporal window is determined by the expression

$$W_{DST}(t) = e^{-\frac{1}{\gamma^2}\left\{\frac{\alpha^2}{w^2}+\frac{k^2 w_o^2}{4f_1^2}A_1^2\left[\frac{1}{1+\frac{k^2 w_o^2(1-d_1A_1)^2}{4d_2^2 f_1^2}}\right]\right\}t^2} \tag{2.31}$$

- a Gaussian exhibiting a width determined, in part, by the size of the spatial pattern applied at the pulse shaper input (w) as well as the finite mode size of the output fiber (w_o). We can separate this term into the product of the constituent Gaussian windows arising from the applied spatial pattern,

$$e^{-\frac{\alpha^2}{\gamma^2}\frac{t^2}{w^2}}, \tag{2.32}$$

and the finite mode size of the output fiber

$$e^{-\frac{k^2 w_o^2}{4\gamma^2 f_1^2}A_1^2\left[\frac{1}{1+\frac{k^2 w_o^2(1-d_1A_1)^2}{4d_2^2 f_1^2}}\right]t^2}. \tag{2.33}$$

While both terms affect the overall duration of the temporal output from the shaper, the duration of the user-defined waveform (Eq. 2.32) can be viewed as the time aperture that is to be achieved from the shaper. Specifically, for applications such as optical packet generation, nearly equal-amplitude pulse sequences are required from the shaper. Thus, the sequence duration is regarded as the desired time aperture. For these applications, provided equal intensity features are applied to the pulse shaper input, the temporal window arising from the finite fiber mode size becomes the factor which limits the achievable temporal window of the pulse shaper. This factor will be the focus of the following discussion.

The quantity we are interested in is the intensity FWHM of the output temporal waveform. For the Gaussian of Eq. 2.33, this quantity is given by

$$T_{DST} = \sqrt{2ln(2)}\frac{\lambda\gamma f_1}{\pi w_o A_1}(1+\Delta)^{\frac{1}{2}}, \tag{2.34}$$

where

$$\Delta = \frac{k^2 w_o^4}{4d_2^2 f_1^2}(f_1 - d_1A_1)^2. \tag{2.35}$$

The Δ term stems from the constraint in our pulse shaper of $\mathbf{d_1} + \mathbf{d_2} = 2\mathbf{f_1}$ (please refer to Fig. 2.2), which was not the case in previous work [7, 8, 13]. In general, $\Delta \lll 1$ and can be ignored with negligible loss in accuracy of Eq. 2.34. Given the form of A_1, this term is identically zero for the case $\mathbf{d_1} = \mathbf{d_2} = \mathbf{f_1}$. Ignoring Δ in Eq. 2.34, the intensity FWHM temporal window defined by the output fiber is now

$$T_{DST} = \sqrt{2ln(2)}\frac{\lambda\gamma f_1}{\pi w_o A_1}. \tag{2.36}$$

In the case where $\mathbf{d_1} = \mathbf{d_2} = \mathbf{f_1}$, $A_1 = 1$ and the predicted intensity FWHM temporal window is ~76 ps. To illustrate the effect of this window, a series of 12 equal-intensity spots is applied to the pulse shaper input. This pattern, after space-to-time conversion, yields a series of 12 pulses at a rate of ~100 GHz that span a ~120 ps time aperture. Given the equal intensity spatial features at the pulse shaper input, the optical pulse sequence from the shaper should exhibit equal-amplitude features in the absence of any windowing effects. As Figure 2.4 clearly illustrates, this series of equal-amplitude pulses is, in fact, windowed temporally by the finite fiber mode size. The measured FWHM (~68 ps) of the intensity cross-correlation trace of the pulse sequence is seen to agree quite well with the predicted ~76 ps Gaussian temporal window (dashed line) arising from the fiber mode size.

For our intended application of optical packet generation, equal-amplitude optical pulse sequences are a requirement. Thus, the windowing effect of the finite fiber mode size must be minimized. It was determined early in our pulse shaping experiments that the contribution of the fiber mode to the temporal window of the DST shaper was one limiting factor in attaining our desired temporal window defined by the size of the spatial pattern used as the input to the pulse shaper. To illustrate this, consider the DST pulse shaper as a generalized spectrometer with a short pulse input [8]. The spectral resolution for such a spectrometer is set by the relation of the focused spectral feature size and the dimension of the slit used to sample the spectrum. For a fixed beam size on the grating, the spectral resolution will increase with decreasing slit size. For a short pulse input, the pulse out of the spectrometer will increase in duration due to the spectral filtering effect of the slit. As the slit is broadened and the spectral

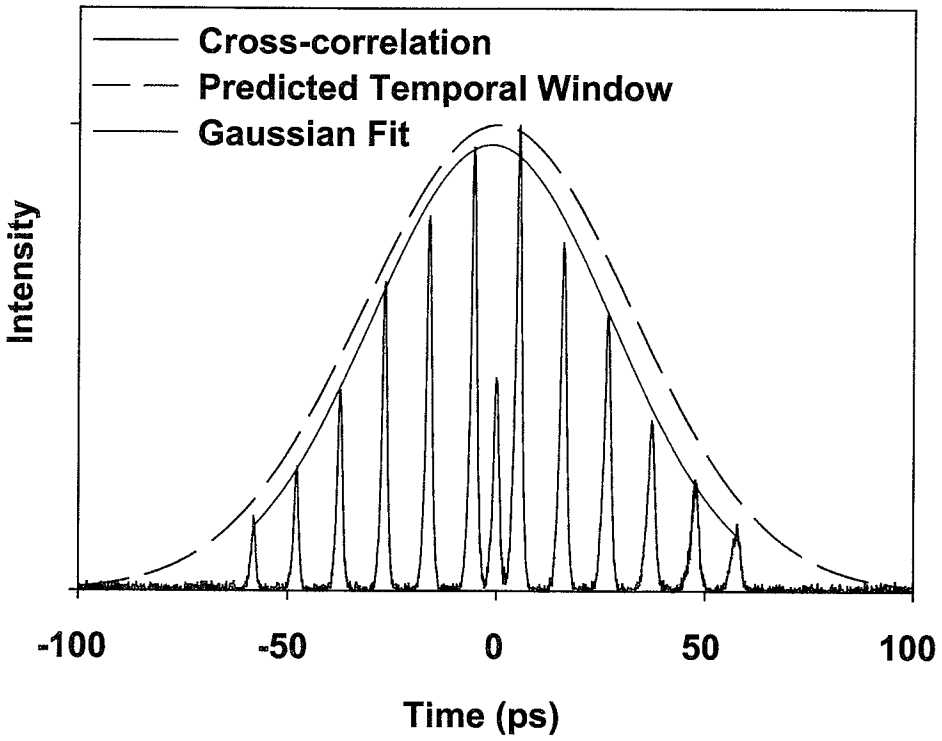

Fig. 2.4. Temporal window of the DST pulse shaper. With distances $\mathbf{d_1}$ and $\mathbf{d_2}$ set equal to $\mathbf{f_1} = 15$ cm in Fig. 2.2 the predicted pulse shaping temporal window is ~76 ps (dashed line). This value is determined from Eq. 2.36 with $\mathbf{f_1} = 15$ cm, the fiber mode-field radius $w_o \approx 5.25$ μm, and γ as given by equation 2.12. The measured temporal window (red line), with an intensity FWHM of ~68 ps, shows good agreement with the predicted window.

resolution is decreased, the filtering effect of the slit is also decreased, resulting in a temporal output which is shorter in duration than that of the case of a narrow slit. In the case of the fiber-coupled DST pulse shaper, the pattern size on the grating is determined by the overall pulse sequence duration we wish to attain, and is hence fixed at a size determined by the space-to-time conversion constant (Eq. 2.24) of the pulse shaper. Since the output "slit" of the pulse shaper is a single-mode fiber, the effective slit dimension is also fixed at a size determined by the core radius of the fiber. In order to increase the spectral resolution of this spectrometer, and hence increase the temporal window, the DST shaper was built in a telescopic configuration, where the telescope is used to magnify the pulse shaper output relative to the fiber size. This is equivalent to reducing the fiber size, bringing the effective fiber mode closer to the ideal δ function slit [8] where the temporal window is completely determined by the spatial pattern applied to the pulse shaper input. The same result could be achieved by simply replacing the pulse shaping lens with one of a longer focal length. This option is impractical, however, in that the pulse shaper length is increased. With limited space, inclusion of a telescope allows the necessary increase in spectral feature size without an equivalent increase in the size of the pulse shaper.

To illustrate the effect of the telescope, consider the temporal window term of the telescopic DST given by Eq. 2.26,

$$W_T = e^{-\frac{1}{\gamma^2}\left[\frac{\alpha^2}{w^2}+\frac{k^2 w_o^2}{4f_1^2}\frac{f_2^2}{f_3^2}\frac{A_3^2}{A_2^2}A_1^2\left(\frac{1}{1+\frac{k^2}{4f_3^4}A_3^4 w_o^4 \mathbf{B_2}^2}\right)\right]t^2}. \tag{2.37}$$

Here, the temporal window can again be expressed as the product of the window defined by the applied spatial pattern at the pulse shaper input (identical to Eq. 2.32) and the temporal window due to the fiber mode

$$e^{-\left[\frac{k^2 w_o^2}{4\gamma^2 f_1^2}\frac{f_2^2}{f_3^2}\frac{A_3^2}{A_2^2}A_1^2\left(\frac{1}{1+\frac{k^2}{4f_3^4}A_3^4 w_o^4 \mathbf{B_2}^2}\right)\right]t^2}. \tag{2.38}$$

The intensity FWHM of this Gaussian window is given by

$$T_T = \sqrt{2ln(2)}\frac{f_3}{f_2}\frac{A_2}{A_3}\frac{\lambda\gamma f_1}{\pi w_o A_1}(1+\Delta)^{\frac{1}{2}}, \tag{2.39}$$

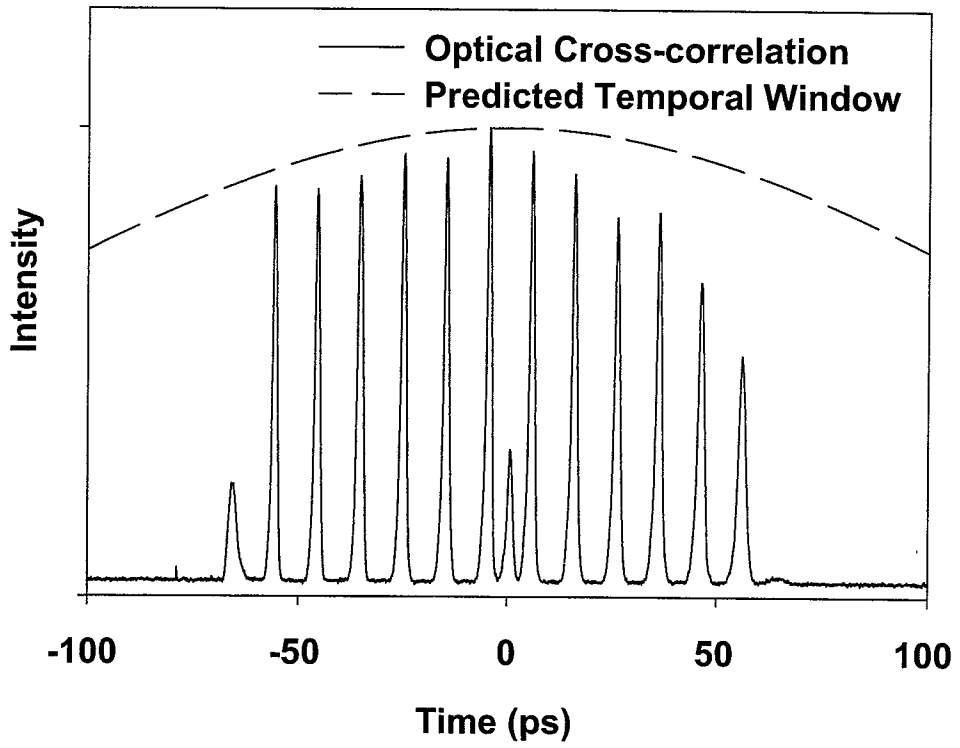

Fig. 2.5. Temporal window of the telescopic DST pulse shaper. With a perfectly aligned telescope positioned between the DST pulse shaper and output fiber, the pulse shaping temporal window is broadened by a factor of the telescope magnification of 4 to ~303 ps. For the specifics of the telescope, consult Fig. 2.13 and Section 2.6.

where

$$\Delta = \frac{k^2 w_o^4}{4 f_3^4} A_3^4 \mathbf{B_2}^2. \tag{2.40}$$

Again, $\Delta \lll 1$, leaving the intensity FWHM of the fiber mode after the telescope to be

$$T_T = \sqrt{2ln\,(2)} \frac{f_3}{f_2} \frac{A_2}{A_3} \frac{\lambda \gamma f_1}{\pi w_o A_1}. \tag{2.41}$$

Comparing this expression to the temporal window of the basic DST shaper (Eq. 2.34), the temporal window is now clearly broadened by a factor of the telescope magnification f_3/f_2 as desired.

To illustrate the effect of the telescope, we consider the case where all distances

are set to the appropriate focal length, i.e. $\mathbf{d_1} = \mathbf{d_2} = \mathbf{f_1}$, $\mathbf{d_3} = |\mathbf{f_2}|$, $\mathbf{d_4} + \mathbf{d_5} = \mathbf{f_2} + \mathbf{f_3}$ and $\mathbf{d_6} = \mathbf{f_3}$ (please refer to Figs. 2.2, 2.3). In this case, the scaling factors $A_1 = A_2 = A_3 = 1$. The optical pulse sequence of Figure 2.4 is again generated in the pulse shaper. As Figure 2.5 clearly illustrates, the temporal window is indeed broadened as expected. This is easily seen by comparing the amplitudes of pulses at the extremes of the sequence ($\pm$55 ps) to those near the center of the sequence. The predicted temporal window (T_T ~303 ps) is again shown by the dashed line. While the temporal window has been noticeably broadened, some distortion is present in the optical pulse sequence - the pulses later in time exhibit decreased amplitude and a slight broadening in time. This is believed to be related to the fact that the entire diffraction grating (pulse shaper input plane) is not exactly a focal distance away from the pulse shaping lens $\mathbf{L_1}$.

This section illustrates the functionality of the telescopic DST configuration to broaden the achievable pulse shaping temporal window. There is an additional predicted broadening which was not previously known, however; this is related to frequency modulation in the shaper. This behavior will be discussed along with frequency modulation effects in the shaper later in this chapter.

2.4 Frequency Modulation in the Telescopic DST Pulse Shaper

Previous work [13] has shown that direct space-to-time pulse shaping not only maps an applied spatial amplitude pattern to an output temporal waveform, but that the shaper also converts spatial phases to temporal phases as well. Compensation of the effects from converging or diverging inputs to the pulse shaper is possible through correct positioning of the pulse shaping lens [13]. This removes any spatial phase curvature and, hence, any temporal quadratic phase at the pulse shaper output. The purpose of this section is to review the chirp (or frequency modulation as it will be refereed to from here on) behavior of the DST shaper and to discuss additional temporal phase control in the telescopic DST shaper configuration. In addition, previously undocumented contributions to the quadratic temporal phase imparted by the telescopic DST shaper will be discussed.

To elaborate, the instantaneous phase of the basic DST shaper output (from Eqs. 2.22, 2.23) has contributions from the input pulse $e(t)$ at frequency ω_0, the phase curvature of the incident beam (R), the grating - pulse shaping lens separation $\mathbf{d_1}$, and the pulse shaping lens - fiber separation $\mathbf{d_2}$ in the pulse shaper, such that

$$\phi_{inst} = \omega_0 t - \frac{k}{2\gamma^2}\left(\frac{\alpha^2}{R} + \frac{f_1 - d_2 A_1}{f_1 d_1} + \Delta\right) t^2, \tag{2.42}$$

where

$$\Delta = \frac{k w_o^2}{2}\left[\frac{f_1 d_2 (f_1 - d_1 A_1)}{4 d_2^2 f_1^2 + k^2 w_o^4 (f_1 - d_1 A_1)^2}\right]. \tag{2.43}$$

Similar to the discussion of the pulse shaping temporal window, the term Δ arises in the diffraction analysis from allowing the distance $\mathbf{d_1}$ to vary. This term is generally multiple orders of magnitude smaller than other terms in the instantaneous phase equation and may be dropped from the expression without significantly changing the remaining derivation. After dropping this term, the instantaneous frequency, $\omega_{inst} = \partial\phi_{inst}/\partial t$ is then

$$\omega_{inst} = \omega_0 - \frac{k}{\gamma^2}\left(\frac{\alpha^2}{R} + \frac{f_1 - d_2 A_1}{f_1 d_1}\right) t. \tag{2.44}$$

As a result, the frequency modulation (chirp), defined as the time derivative of the instantaneous frequency, is now

$$\frac{\partial \omega_{inst}}{\partial t} = -\frac{k}{\gamma^2}\left(\frac{\alpha^2}{R} + \frac{f_1 - d_2 A_1}{f_1 d_1}\right). \tag{2.45}$$

It is more useful for our application to work in terms of wavelength, so the resulting frequency modulation in terms of wavelength is given by

$$\frac{\partial \lambda}{\partial t} = \frac{\lambda}{c\gamma^2}\left(\frac{\alpha^2}{R} + A_1 \frac{f_1 - d_2}{f_1^2}\right), \tag{2.46}$$

where the simplification

$$\frac{f_1 - d_2 A_1}{f_1 d_1} = A_1 \frac{f_1 - d_2}{f_1^2} \tag{2.47}$$

has been used.

From 2.45, 2.46 it is clear that the quadratic spatial phase due to the non-flat phase front of the DST input pattern is converted to a quadratic temporal phase and,

hence, a linear frequency modulation in the DST shaper. This frequency modulation can be eliminated by choosing the lens-fiber separation d_2 such that

$$\frac{f_1 - d_2 A_1}{f_1 d_1} = -\frac{\alpha^2}{R}, \tag{2.48}$$

effectively cancelling any effects due to a non-flat phase front in the DST input.

Since frequency modulation in the pulse shaper arises from spatial phase curvature, one would predict the addition of a telescope to the system would allow several more degrees of freedom in controlling the system frequency modulation. Following a derivation similar to the one above, the system frequency modulation, including the effects of the telescope, is given by

$$\frac{\partial \lambda}{\partial t} = \frac{\lambda}{c\gamma^2}\left[\frac{\alpha^2}{R} + A_1\frac{f_1 - d_2}{f_1^2} + \frac{A_1^2}{A_2}\frac{f_2 - d_3}{f_1^2} + A_3\frac{A_1^2}{A_2^2}\frac{f_2^2}{f_3^2}\frac{f_3 - d_6}{f_1^2}\right]. \tag{2.49}$$

From this expression, it is clear that the frequency modulation in the shaper can be controlled through positioning not only the pulse shaping lens, but also the first telescope lens ($\mathbf{d_3}$) as well as the output fiber position $\mathbf{d_6}$. Figure 2.6 illustrates the imposed frequency modulation as a function of pulse shaping lens and output fiber position. This measurement was performed by generating two pulses, separated by ~90 ps in the DST shaper and measuring the difference in center wavelength ($\Delta\lambda$) of these pulses as a function of pulse shaping lens or output fiber position. The imposed frequency modulation, in nm/ps, is then calculated from $\Delta\lambda$ / 90 ps. In this figure, the abscissa is the distance which is varied divided by the respective "zero frequency modulation", or chirp-free position. For example, the solid curve illustrates the imposed frequency modulation as a function of the grating - pulse shaping lens position $\mathbf{d_1}$ divided by the pulse shaping lens focal length $\mathbf{f_1}$. For this curve, the distance $\mathbf{d_2}$ is subject to the constraint $\mathbf{d_2} = 2\mathbf{f_1} - \mathbf{d_1}$ and the telescope lenses are positioned such that $\mathbf{d_3} = |\mathbf{f_2}|$, $\mathbf{d_4} + \mathbf{d_5} = \mathbf{f_2} + \mathbf{f_3}$, and $\mathbf{d_6} = \mathbf{f_3}$. In words, the telescope is perfectly aligned with the output fiber positioned in the telescope output plane and the pulse shaping lens is moved longitudinally between the diffraction grating and telescope input plane. The dashed line shows the imposed frequency

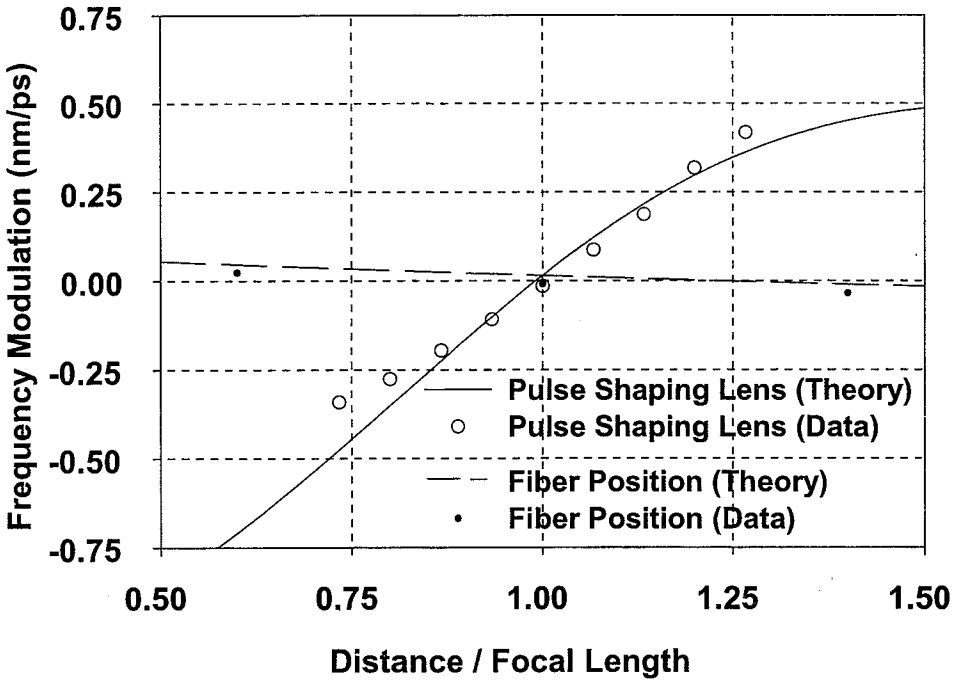

Fig. 2.6. Frequency modulation in the telescopic DST pulse shaper. The solid curve shows the frequency modulation imparted by the pulse shaper as a function of the grating-lens separation $\mathbf{d_1}$. In this case, the abscissa is $\mathbf{d_1/f_1}$ and the system is aligned such that $\mathbf{d_2 = 2f_1 - d_1}$, $\mathbf{d_3 = |f_2|}$, $\mathbf{d_4 + d_5 = f_2 + f_3}$, and $\mathbf{d_6 = f_3}$. The dashed curve illustrates the imposed frequency modulation as a function of the output fiber position $\mathbf{d_6}$. For this curve, the abscissa represents $\mathbf{d_6/f_3}$ and the pulse shaper is aligned with $\mathbf{d_1 = d_2 = f_1}$, $\mathbf{d_3 = |f_2|}$, and $\mathbf{d_4 + d_5 = f_2 + f_3}$.

modulation as a function of the output fiber position $\mathbf{d_6}$ divided by the focal length of the second telescope lens $\mathbf{f_3}$. For this measurement, the pulse shaper is aligned with $\mathbf{d_1 = d_2 = f_1}$, $\mathbf{d_3 = |f_2|}$, and $\mathbf{d_4 + d_5 = f_2 + f_3}$. The imposed frequency modulation due to movement of the pulse shaping lens is found to vary much more rapidly than that due to movement of the output fiber, as is consistent with the inclusion of the telescope. The form of the imposed frequency modulation due to the pulse shaping lens position agrees with that demonstrated previously [13], however, there is now the more slowly varying modulation controlled by the output fiber position which may be utilized to fine-tune the imposed frequency modulation. The small offset from zero when the pulse shaper is in the chirp-free configuration is due to a finite radius of curvature on the phase front of the applied spatial pattern. This residual frequency modulation of $\sim$.015 nm/ps predicts a value of $R = \sim$ -94 cm in Eq. 2.49. This represents a relatively slowly converging input to the pulse shaper.

2.5 Frequency Modulation Effects in the Direct Space-to-Time Pulse Shaper

Frequency modulation in the DST pulse shaper can be either a useful tool, or a hindrance, depending on the intended application. The intent of this section is to illustrate the effects of frequency modulation in the shaper and to discuss new predicted temporal window effects which appear when the pulse shaper is arranged to impose a frequency modulation on the pulse shaper output.

To illustrate the frequency modulation imposed by either a converging / diverging spatial input to the pulse shaper, or by intentional positioning of the lenses in the system, consider Figure 2.7. This shows the optical spectrum of the pulse shaper output in the large frequency modulation regime. Here, the modulation arises from a spatial phase curvature present at the input to the shaper; the result is that each pulse in the 10 pulse sequence from the shaper exhibits a different center wavelength. Figure 2.7 shows the spectra for 8 of the 10 pulses in the sequence - the spectra for the other two pulses in the sequence are significantly lower in power and are not shown here. Thus, each spectral feature in the optical spectrum of Figure 2.7 is due to a different

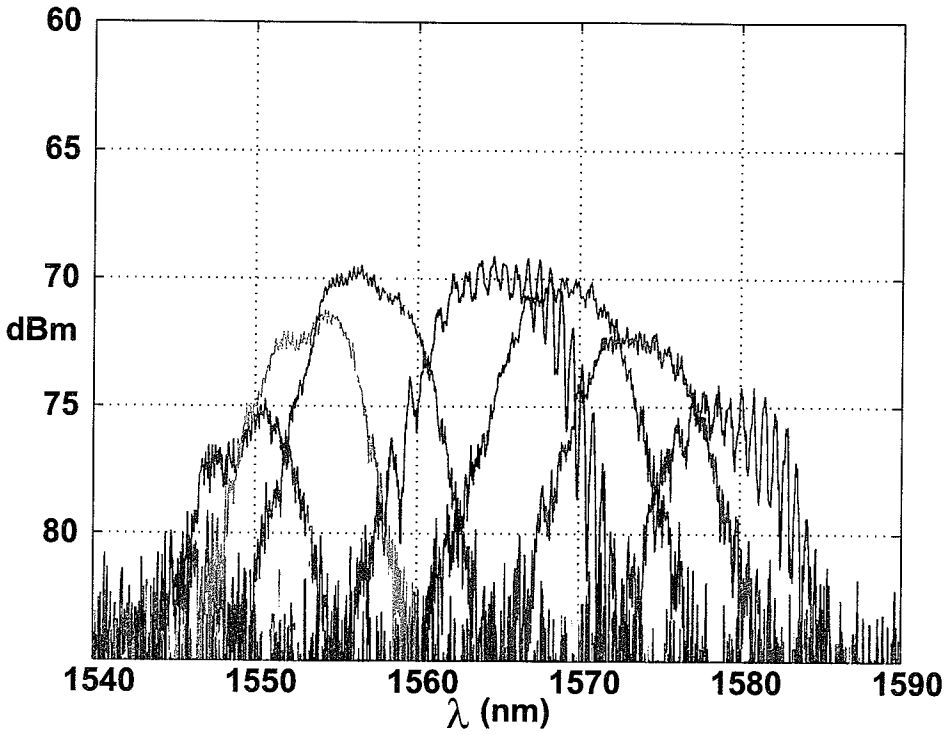

Fig. 2.7. Optical spectra illustrating the effect of frequency modulation in the DST pulse shaper. Here, each pulse in the 10 pulse sequence from the shaper exhibits a different center wavelength. This effect leads to time-aperture effects due to the shape of the input optical power spectrum.

pulse in the output sequence. Though this behavior is desirable, in fact useful, in some cases as will be discussed in Chapter 4, often it causes distortion in the optical pulse sequence generated by the pulse shaper. When the imposed frequency modulation is sufficiently large, it is possible to modulate individual pulses in the sequence outside of the input source bandwidth. In this regime, there is a temporal windowing effect due to the finite optical bandwidth of the short pulse input to the apparatus. Figure 2.8 presents the optical intensity cross-correlation measurement of the optical pulse sequence corresponding to the optical spectrum of Figure 2.7. Here, only seven of the expected 10 pulses in the sequence appear in the measurement; the other three pulses have been modulated outside of the ~5 nm source bandwidth. When the

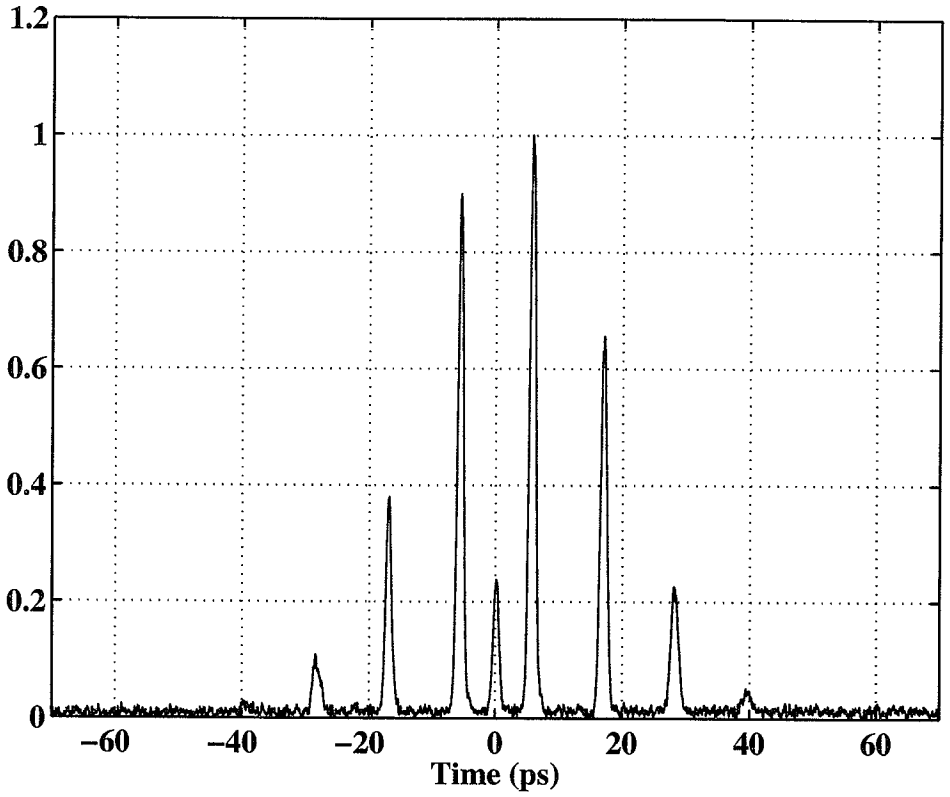

Fig. 2.8. Measured temporal output of the DST shaper illustrating the effects of chirp in the optical system.

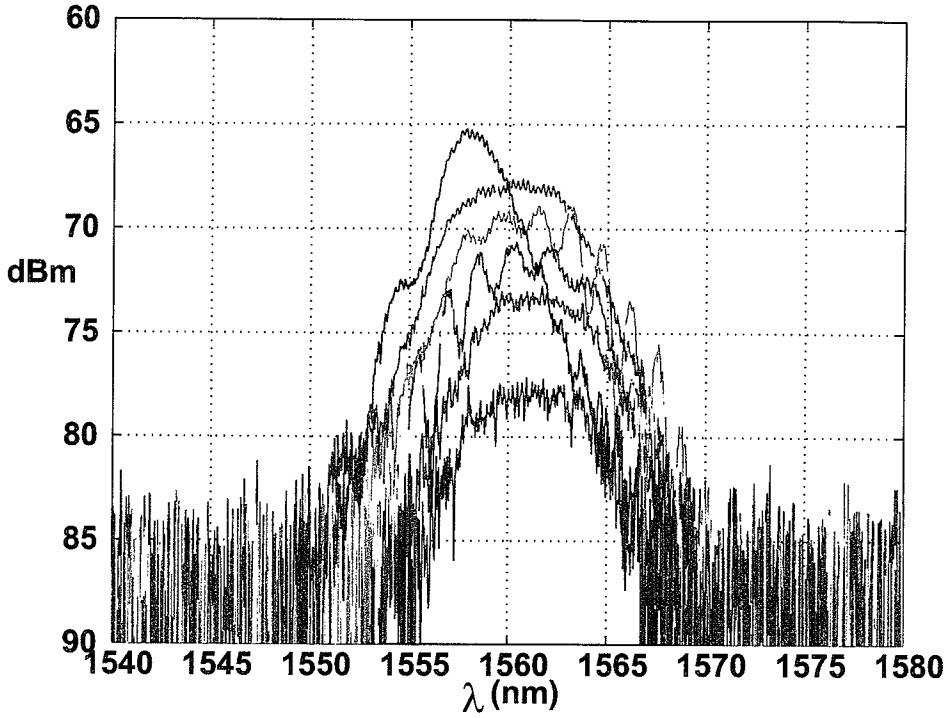

Fig. 2.9. Optical spectra in the absence of frequency modulation. When the frequency modulation is removed, all pulses in the pulse shaper output have the same center wavelength, removing spectral time-aperture effects.

output fiber position is set to nullify the finite phase-front radius of curvature of the pulse shaper input, this frequency modulation is removed. This is illustrated nicely in Figure 2.9, where all 10 pulses (of which the spectra for a representative 7 are shown) in the output pulse sequence exhibit the same center wavelength. As a result of all 10 pulses residing within the source bandwidth, the output sequence contains all ten pulses as shown in Figure 2.8. While this frequency modulation is detrimental for some applications, specifically optical pulse sequence generation from a limited-bandwidth short pulse input, frequency-modulated optical pulse sequences also prove to be quite useful. An application of these sequences will be discussed in Chapter 4.

As mentioned in Section 2.3, when the pulse shaper is aligned to impose a frequency modulation on the shaper output, the pulse shaping temporal window is pre-

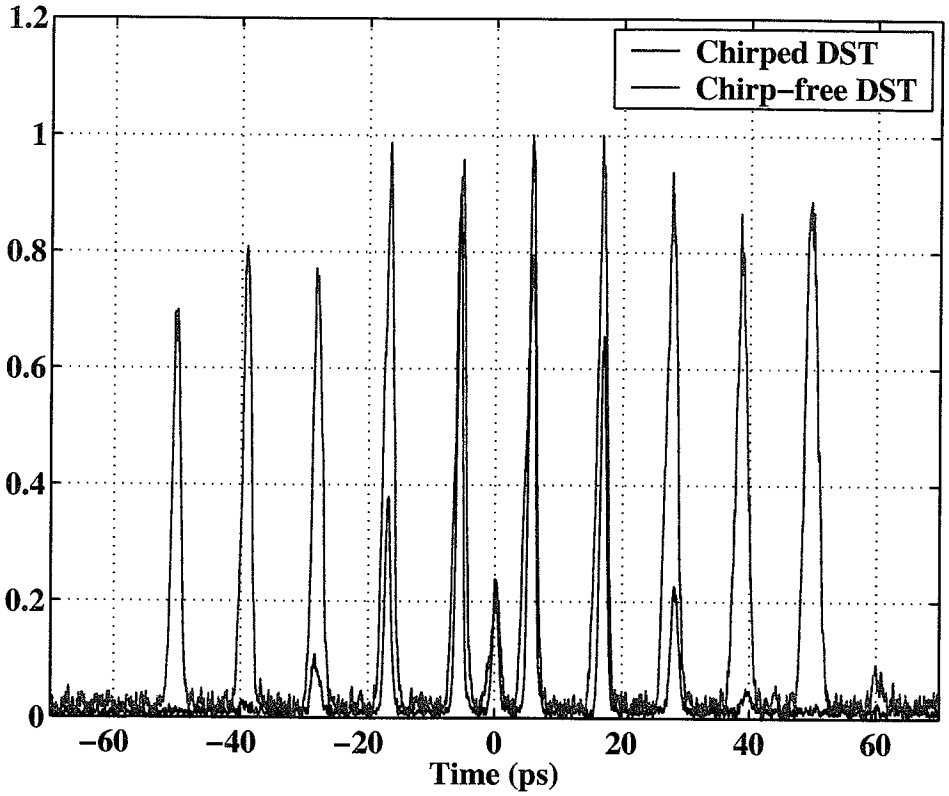

Fig. 2.10. Comparison of chirped / chirp-free operation of the DST shaper. The chirp-free (red) trace clearly shows ten, nearly equal amplitude, pulses as expected from the use of a DOE to perform the input spatial patterning. The output from the chirped configuration (blue) is repeated here for comparison.

dicted to broaden. Consider the intensity FWHM of the basic DST pulse temporal window (Eq. 2.36)

$$T_{DST} = \sqrt{2ln(2)}\frac{\lambda\gamma f_1}{\pi w_o A_1}. \tag{2.50}$$

Here, the scaling factor A_1 appearing in the denominator varies as a function of the pulse shaping lens position as shown in Eq. 2.3. As the pulse shaping lens is moved in either direction from the chirp-free position of $\mathbf{d_1} = \mathbf{d_2} = \mathbf{f_1}$, A_1 decreases from it's maximum value of 1 leading to an increase in the width of the achievable temporal window. As the pulse shaping lens position $\mathbf{d_1}$ is numerically varied over a range of $.5\mathbf{f_1} \leq \mathbf{d_1} \leq 1.5\mathbf{f_1}$ with $\mathbf{d_2} = 2\mathbf{f_1} - \mathbf{d_1}$, while holding all other distances fixed at the appropriate chirp-free position, the temporal window is predicted to vary from $\sim$76 ps to $\sim$95 ps FWHM as illustrated in Figure 2.11. Conceptually, this is once again explained using the aforementioned spectrometer analogy. As the pulse shaping lens position is varied, the spectral features at the pulse shaper output are no longer focused at the output fiber; the spectral feature size is now larger. Therefore, the output fiber appears smaller (closer to the ideal δ function slit) and the temporal window is accordingly broadened.

While this behavior is clearly predicted from the diffraction analysis of the system, measurement of this phenomena in our apparatus is quite difficult. The simplest measurement of this broadening would be to impose a large frequency modulation to the shaper output and perform a numerical Gaussian fit to the optical cross-correlation measurement of the resulting optical pulse sequence. This is non-ideal however, in that the use of an optical pulse sequence spanning a $\sim$100 ps time aperture results in significant spectral broadening. The optical bandwidth in our system is limited to $\sim$30 nm by our erbium-doped fiber amplifiers. Over the specified range of pulse shaping lens position, the imposed frequency modulation varies between $\sim \pm .3$ nm/ps. The result is that pulses in this sequence are modulated near the edge of the optical spectrum and the entire sequence is temporally-apertured by the optical spectrum of the amplifiers. In the end, this effect is quite difficult to separate from the predicted broadening of the pulse shaping temporal window. One could also

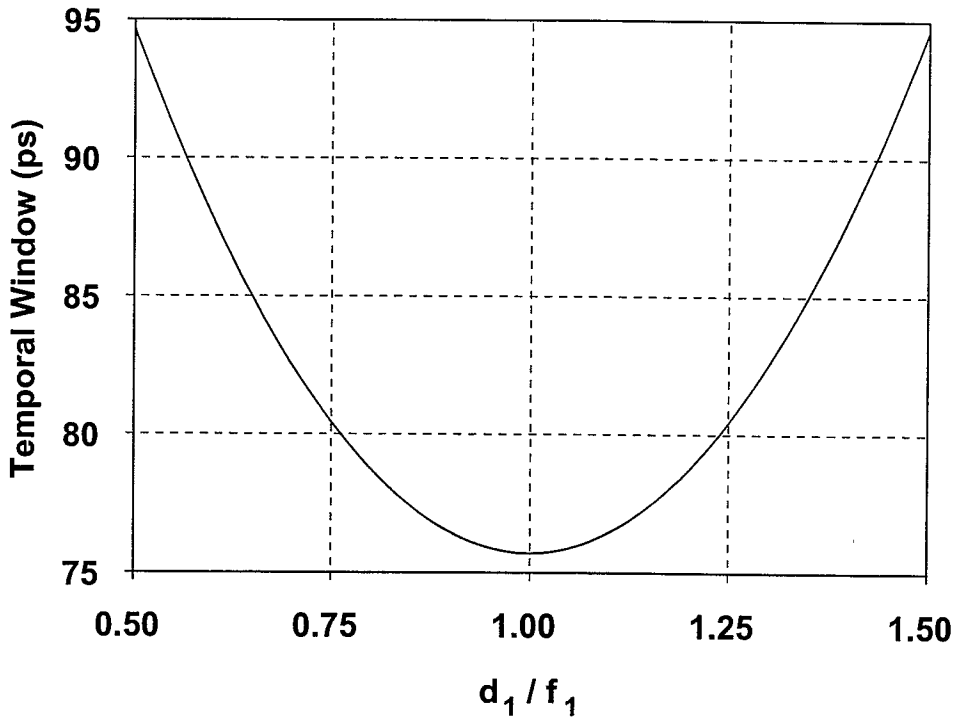

Fig. 2.11. Predicted broadening of the pulse shaping temporal window as a function of pulse shaping lens position.

envision performing the same measurement for a small imposed frequency modulation; however, the broadening effect is quite small in this regime, which again frustrates the fitting process. The Gaussian fits to the temporal window exhibit no significant broadening in practice. Thus, this phenomena stands as a prediction. Should one desire to measure this effect in the future, broadband, gain-flattened amplifiers could be employed to remove spectral time-aperture effects.

2.6 Implementation of the 1.5 μm DST Pulse Shaper and Burst Optical Packet Generation

The goal of DST pulse shaping is generation of high-rate optical pulse sequences. Fourier transform pulse shaping [1] is a commonly accepted method for generating nearly arbitrarily shaped optical waveforms, including high-rate pulse sequences. Despite the success of FT shaping, however, the method suffers from the complexity of calculating the requisite Fourier transform when generating high-rate pulse sequences in real time. This complexity is removed in DST pulse shaping where there exists a direct mapping from a spatially-patterned short pulse input to the time-domain optical waveform. Functionally, the DST shaper acts as an optical parallel-to-serial converter for a spatially-patterned short pulse input as illustrated schematically in Figure 2.1. The temporal output of the shaper is controlled through simple manipulation of the applied spatial pattern at the pulse shaper input.

In this work, we demonstrate significant improvements upon the basic grating - lens - slit implementation of the DST pulse shaper. In previous work, the temporal window is limited by the finite size of the slit used to sample the pulse shaper output and the free-space system is not easily compatible with optical fiber-based systems. Additionally, the use of an amplitude mask and cylindrically focused input beam led to roll-off effects in the measured temporal output of the pulse shaper. We have included several novel features in our current DST pulse shaper to address these concerns. We have moved this work to the 1.5 μm optical communication wavelength band, where a variety of fiber-based sources are available to be used as the input to our pulse shaper. Specifically, we aim for an apparatus compatible with high repetition-rate

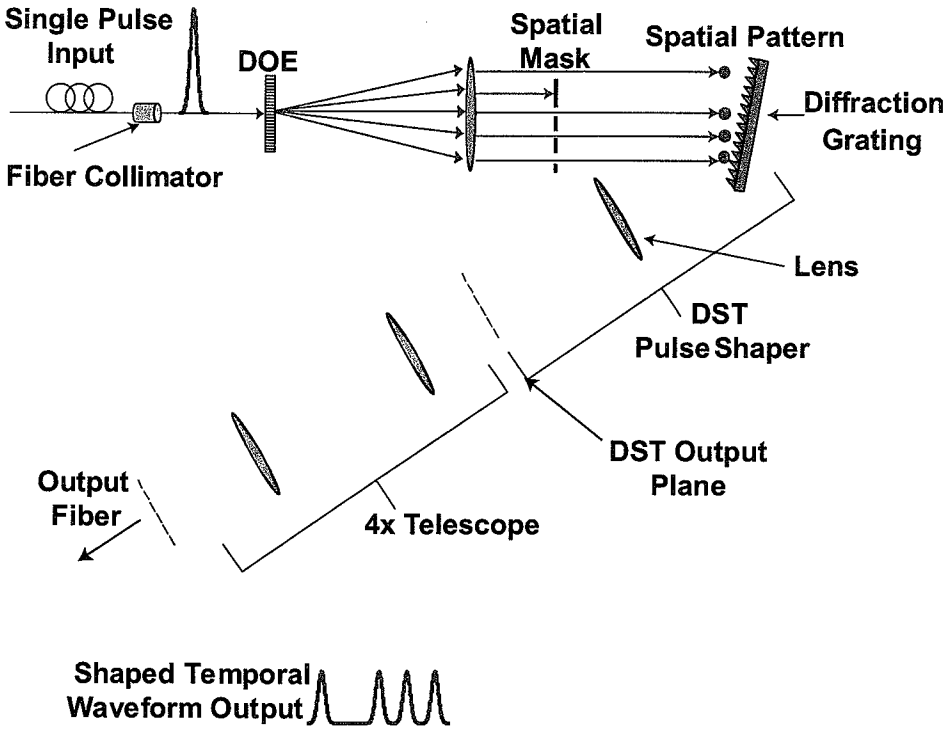

Fig. 2.12. Experimental setup for our 1.5μm pulse shaping experiments.

sources, such as picosecond sources operating at 10 GHz, which will allow generation of continuous optical pulse sequences at rates in the 100 GHz range. To this end, we demonstrate the apparatus illustrated in Figure 2.12.

The output from a passively modelocked Erbium fiber laser [25], providing 100 fs pulses at a 50 MHz repetition-rate, is amplified in an erbium-doped fiber amplifier (EDFA), collimated with a fiber-pigtailed collimating lens, and used as the input to our system. After collimation, the short pulse input beam is spatially patterned via a diffractive optical element and subsequent spatial mask and the resulting spatial pattern is used as the pulse shaper input. A 600 l/mm low polarization-dependent loss (PDL) diffraction grating, which reduces the system PDL to $\sim$.1dB, and 15cm focal length achromat lens form the basis for the pulse shaper. A 4x telescope, consisting of -2.5 cm and 10 cm focal length lenses, is inserted between the output plane of the basic DST shaper and the single-mode optical fiber (Corning SMF-28), which replaces the thin slit used in previous work [7, 8, 13], and serves as the fiber-coupled output of our system. The output from the pulse shaper is subsequently amplified by another EDFA and the output optical pulse sequences are measured via intensity cross-correlation with an ultrashort reference pulse from the source laser. For our apparatus, the space-to-time conversion constant is $\sim$3.1 ps/nm, as determined by the 600 l/mm diffraction grating, 12° incident angle, and a center wavelength of $\sim$1558 nm. For a detailed schematic of the apparatus, including all relevant distances and focal lengths, please reference Figure 2.13.

One very significant difference in the current pulse shaper implementation, compared to that of previous work, is the manner in which the requisite spatial patterning is achieved. Since the temporal output of the shaper is a directly scaled version of the applied spatial pattern at the input to the pulse shaper, any variation in the applied input pattern is exhibited by the output temporal waveform. When an amplitude mask is used to pattern a cylindrically focused Gaussian beam [7, 8, 13], the temporal waveform from the pulse shaper clearly shows a Gaussian roll-off due to the Gaussian nature of the illuminating input beam. In addition, any portion of the

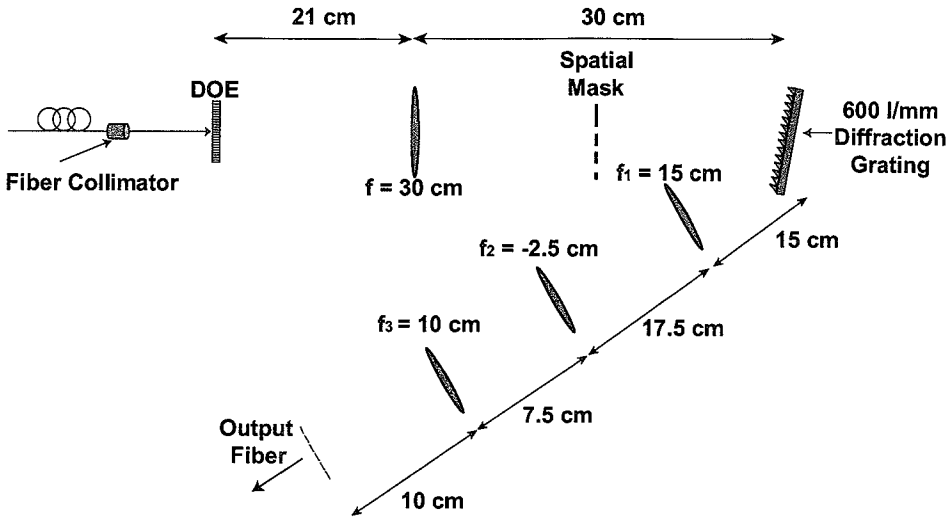

Fig. 2.13. Detailed schematic of the 1.5 μm DST pulse shaper.

input beam which is blocked by the mask results in decreased system throughput. To achieve nearly equal-amplitude temporal features and increase the patterning efficiency of our pulse shaper, spatial patterning is now accomplished using diffractive optical elements (DOEs) [26, 27]. These devices provide periodic spatial patterns which are further manipulated using an amplitude mask, allowing either periodic optical pulse sequences or optical data to be generated in the pulse shaper.

Our DOEs (custom devices, INO, Quebec, Canada) are binary, phase-only masks designed to divide the power from a single input beam equally into multiple output beams. These DOEs function as 1-D spot generators and produce patterns ranging from 8 - 21 spots, providing a variety of input patterns for our pulse shaper. Examples of several odd-order patterns are shown in Figure 2.14. These patterns were taken by a spatial profilometer and represent the patterns just prior to the diffraction grating. Note the small zero-order diffraction spots at $x = 0$ in the traces. These are most likely due to an error in phase step in our elements, which causes decreased diffraction out of the zero-order (incident) beam and can be blocked from the DST shaper input if so desired. Alternatively, patterns using the even-order diffraction spots may be used,

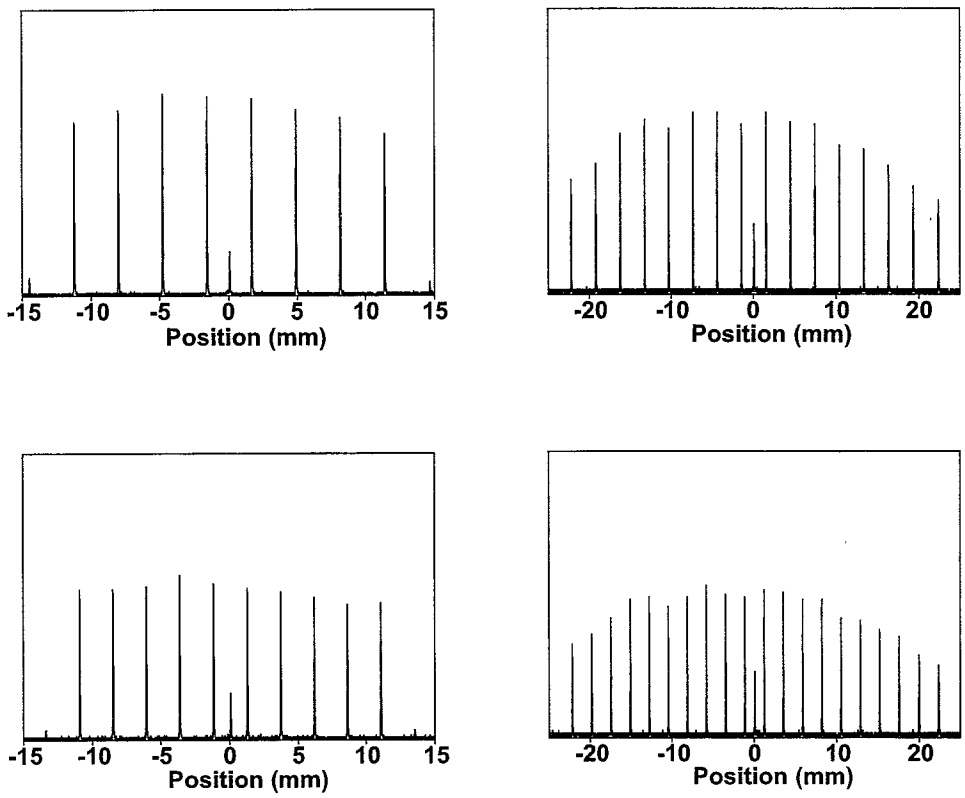

Fig. 2.14. Spatial profilometer measurements of representative DOE patterns. Clockwise from the top left : 8, 16, 20, and 10 spot patterns.

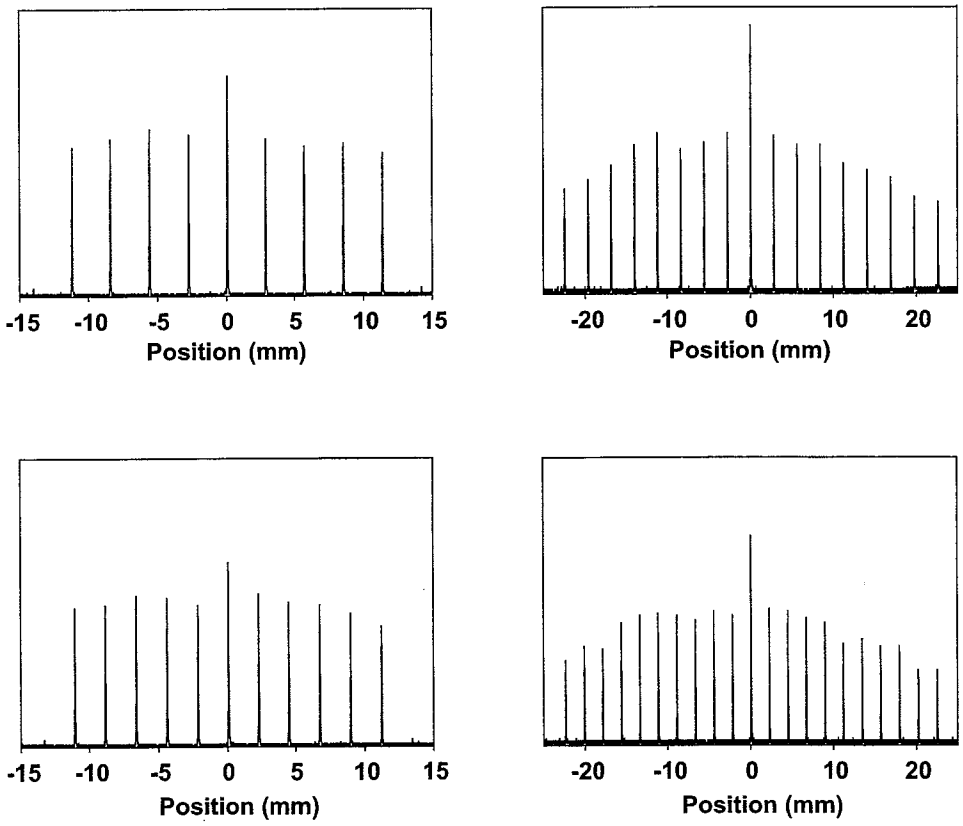

Fig. 2.15. Spatial profilometer measurements of representative DOE patterns. Clockwise from the top left : 9, 17, 21, and 11 spot patterns.

in which case there is a slight amplitude difference in the zero order diffraction spot. Spatial profilometer measurements of several even-order patterns are shown in Figure 2.15. When using an even-order pattern as the pulse shaper input, the central zero-order spot can be attenuated if so desired. As is clearly illustrated, the DST shaper input consists of a series of nearly equal intensity spots, effectively removing the time-aperture effect. Subsequent to the DOE, individual spots in the periodic patterns may be blocked to create optical data packets or otherwise desirable input patterns. Figure 2.16 clearly illustrates the mapping from space to time. The bottom trace shows the pulse shaper output as measured by optical intensity cross-correlation with a ultrashort reference pulse from the source laser. The pulse shaper output consists of a series of ten pulses at ~92 GHz as determined by the space-to-time conversion constant of ~3.1 ps/mm and the ~3.5mm spot spacing in the input pattern. The temporal output is found to exhibit nearly equal amplitude pulses enabled by the use of a DOE for pattern generation. Our new spatial patterning technique clearly removes time-aperture effects stemming from Gaussian illumination of an amplitude mask in previous work and increases the system patterning efficiency.

As mentioned previously, the intended application of our DST pulse shaping apparatus is generation of high-rate optical data packets in the 1.5 μm wavelength band. Specifically, we aim to utilize the shaper, in conjunction with a high repetition-rate laser source, to generate continuous optical data at rates of ~100 GHz. To illustrate the optical packet generation concept, as a prelude to our work in continuous optical pulse sequence generation, consider Figure 2.17. As discussed earlier in this section, the DOEs used as the bases for our spatial patterns produce periodic spatial patterns ranging from 8-21 spots. By design, several of these patterns occupy the same spatial extent at the grating, but exhibit different spatial periods. The resulting optical packets, after space-to-time conversion, then all span a time aperture of ~104 ps, but exhibit different pulse rates. The time aperture of ~104 ps is determined by the ~33.6 mm pattern size at the grating and the space-to-time conversion constant of ~3.1 ps/mm. In (a), the 8 spot spatial pattern, with a period of ~4.8 mm, results

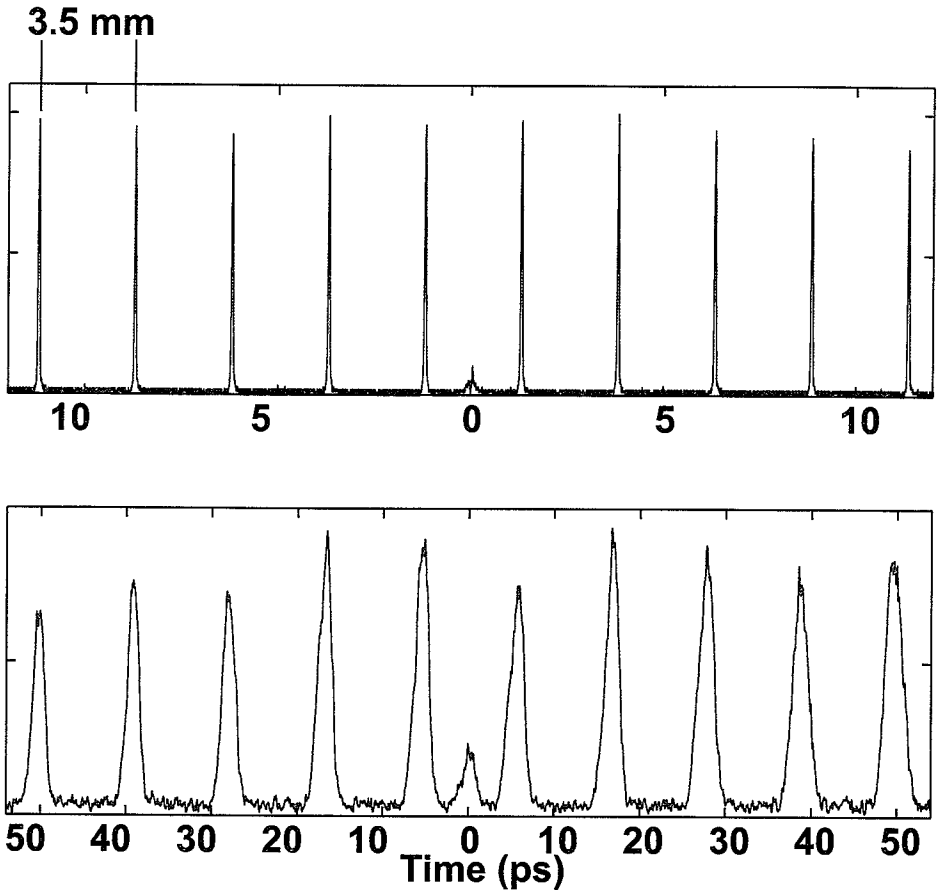

Fig. 2.16. Example of space-to-time mapping. (a) 10 spot spatial pattern just prior to the diffraction grating. The spot-to-spot spacing is ~3.5 mm. (b) Optical cross-correlation of the DST output for the pattern shown in (a). Given the space-to-time conversion constant of ~3.1 ps/mm and the spatial pattern above, the result is a ~92 GHz optical pulse sequence.

in an 8 pulse sequence with a pulse rate of ~67 GHz after space-to-time conversion. Similarly, the 9 pulse, ~76 GHz sequence of (b) results from a 9 spot pattern, with a spatial period of ~4.2 mm, applied to the pulse shaper input. The 10 and 11 pulse sequences shown in (c) and (d), with pulse rates of ~85 and ~96 GHz, are generated from spatial patterns with spatial periods of 3.73 and 3.36 mm, respectively. These pulse sequences also illustrate the difference in even- and odd-order diffraction patterns generated by our DOEs. As in Figure 2.16, the pulse sequences of (a) and (c)

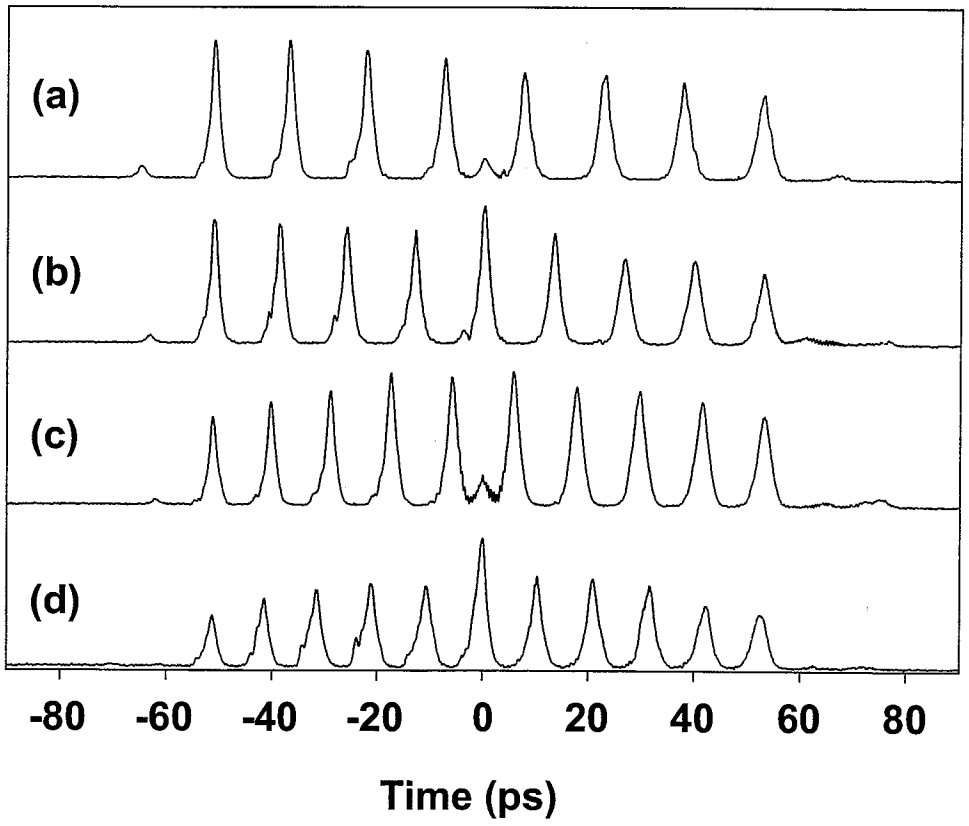

Fig. 2.17. Burst periodic pulse sequences from the DST pulse shaper.(a) - 8 pulses at ~67 GHz. (b) - 9 pulses at ~76 GHz. (c) - 10 pulses at ~85 GHz. (d) - 11 pulses at ~96 GHz.

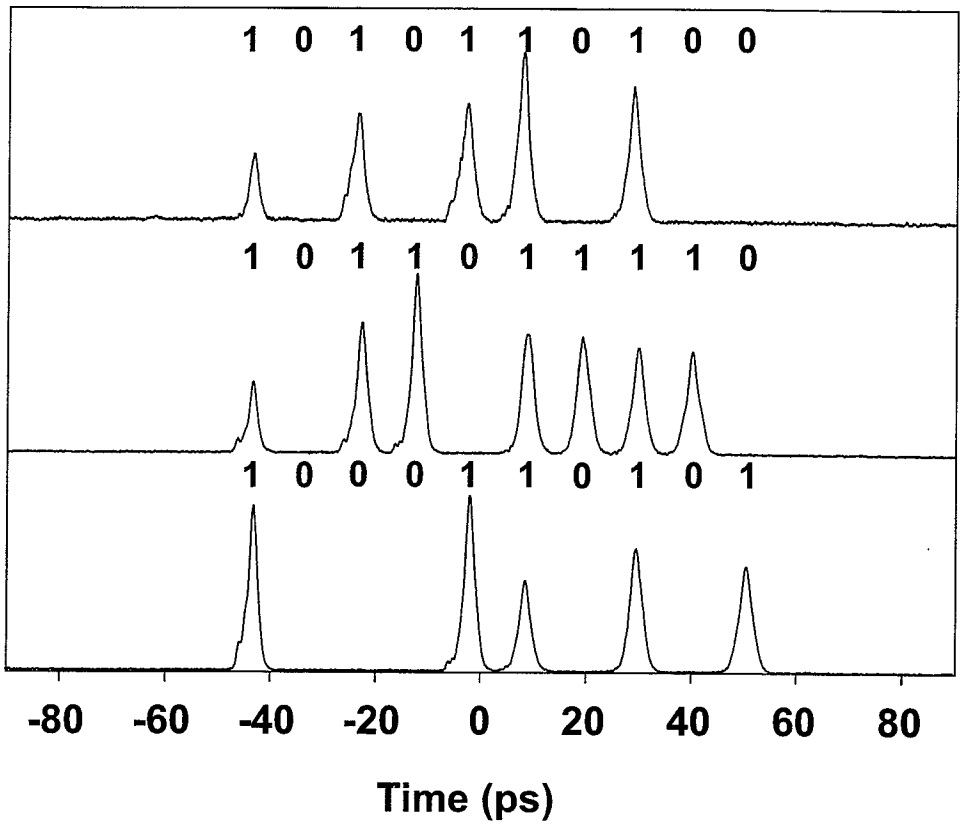

Fig. 2.18. Burst ~100 GHz data. By blocking individual spots from the optical pulse sequence of Figure 2.17 burst optical data packets are generated in the DST.

are generated from DOEs which utilize the odd diffraction orders ($\pm 1, \pm 3, \pm 5$, etc) to generate the spatial pattern. For these patterns, the slight error in phase step, along with the binary nature of the phase gratings, leave a residual amount of the incident power in the zero-order (undiffracted) spot. After space-to-time conversion, this results in a small pulse at time $t = 0$ in the measured optical pulse sequences. This effect is also present in the patterns based on the even-order diffraction spots ($0, \pm 2, \pm 4$, etc), however, since the zero-order is actually part of the desired pattern, this spot exhibits slightly higher intensity than the other orders. The result is that the optical pulse generated from this spot in the pulse shaper exhibits a slightly larger amplitude than others in the sequence, as illustrated in (b) and (d).

To generate optical "data" packets from these periodic optical pulse sequences, we need to remove individual pulses in the sequence to encode the optical data. Given the straight-forward mapping from space to time in the pulse shaper, this is easily accomplished by blocking individual spots in the periodic spatial input patterns. Three optical data packets generated in this manner are shown in Figure 2.18. To generate these optical data packets, individual spots in the spatial pattern used to generate the ~96 GHz sequence of Figure 2.17 (d) were blocked, subsequent to the DOE, with a fixed amplitude mask. While a fixed mask has been utilized here, a spatial light modulator (such as the liquid crystal modulators frequently used in FT pulse shaping [28]) could be used to dynamically change the input spatial pattern via computer control. High-speed optoelectronic modulator arrays could also find application here and will be discussed further in the following section.

We have demonstrated generation of high-rate, amplitude-equalized optical pulse sequences over a time aperture in excess of 100 ps and at rates approaching 100 GHz. This is accomplished through a novel direct space-to-time pulse shaper, constructed for the first time in the 1.5 μm optical communications wavelength band. Novelties in our pulse shaping apparatus, including a telescopic configuration and the use of diffractive optical elements for spatial pattern generation, have enabled this operation through minimization of several time-aperture effects. These optical pulse sequences are, however, burst sequences. Each pulse sequence, spanning a ~100 ps time aperture, is generated from one source pulse and these sequences then repeat at the source repetition rate of 50 MHz. Thus, the bursts are effectively isolated in time. These burst optical pulse sequences are of fundamental importance for continuous optical pulse sequence generation. Generation of such sequences will be discussed in the following section.

2.7 Continuous 100 GHz Optical Pulse Sequence Generation

The intended application for our system is optical packet generation at rates in excess of the current commercial state-of-the-art of 40 GB/s. Several techniques with this aim have been demonstrated, for example the interleaving of identical lower-rate (i.e. 10Gb/s) data streams common in OTDM systems experiments [29, 30] and the use of fiber Bragg gratings [31, 32] to generate high-rate fixed pulse sequences. These techniques, however, suffer from strict synchronism requirements and lack reprogrammability, respectively, when considered for real systems. Generation of optical data packets spanning 100 ps frame through DST pulse shaping, when combined with a source of comparable pulse period and high-speed modulator arrays avoids both of these concerns. Reprogrammability is addressed through simple changes in the applied spatial pattern to the pulse shaper while synchronous operation is ensured through the physics of the pulse shaping apparatus. In this section we present our work on generation of continuous optical pulse sequences at rates of 100 GHz, aimed at reprogrammable optical packet generation.

In this work, we replace the passively modelocked erbium fiber laser[25] ($\sim$100fs pulses, 50MHz) with an actively modelocked telecom source [10] which provides $\sim$1 ps pulses at a rate of 10 GHz. The goal here is to generate pulse sequences, spanning a 100 ps frame, from each source pulse and stitch these frames together to form continuous optical data. In the simplest case, this amounts to rate-multiplying our 10 GHz source up to 100 GHz. To illustrate this concept, consider Figure 2.19 which shows an optical cross-correlation measurement of an series of $\sim$88 GHz optical pulse bursts. Here, each frame of eight pulses is generated from a single source pulse, with the boundaries between adjacent frames delineated by a dashed line. The frames then repeat at the source repetition-rate of 10 GHz. To achieve the goal of a continuous 100 GHz pulse train, there are several items which need to be addressed given the data of Fig. 2.19. First, there is an obvious stitching error between adjacent frames - for a continuous 100 GHz train we need the pulse-to-pulse spacing within a single frame to be 10 ps and the frame duration (as well as the laser pulse period) to be 100

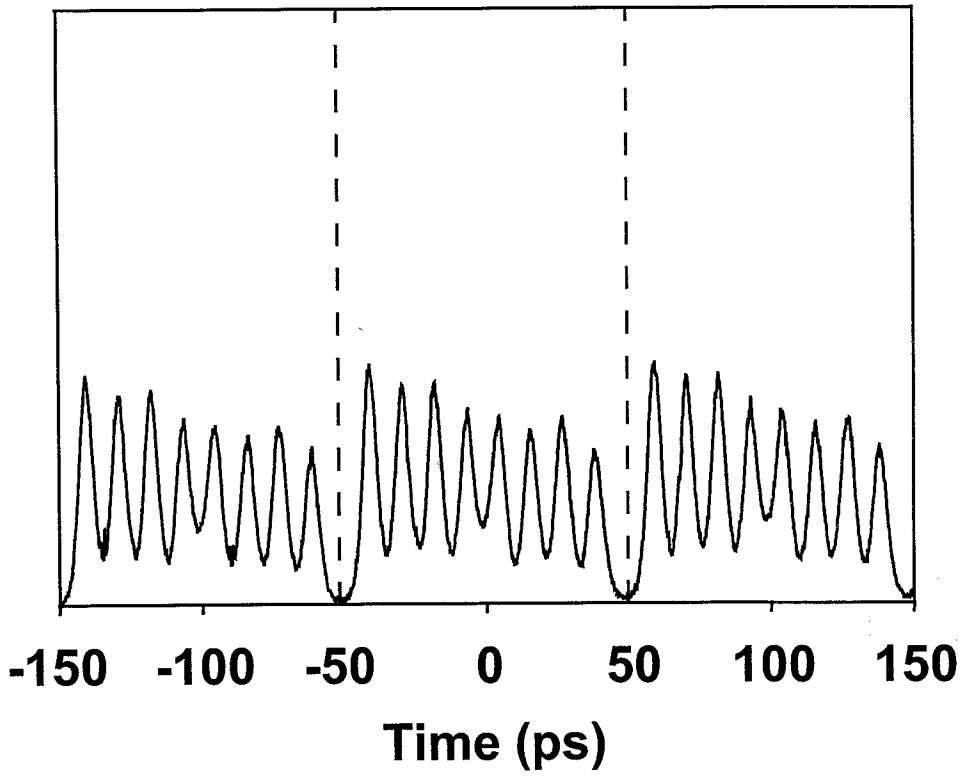

Fig. 2.19. ~88 GHz optical pulse sequences. Here, each burst of eight pulses is generated from one source pulse, arriving each 100 ps. The stitching error at the frame boundaries (dashed lines) is a result of the mismatch between the source pulse period and the duration of the optical pulse sequence. Timing jitter in the source laser is seen to degrade the extinction between neighboring pulses in the optical cross-correlation measurement.

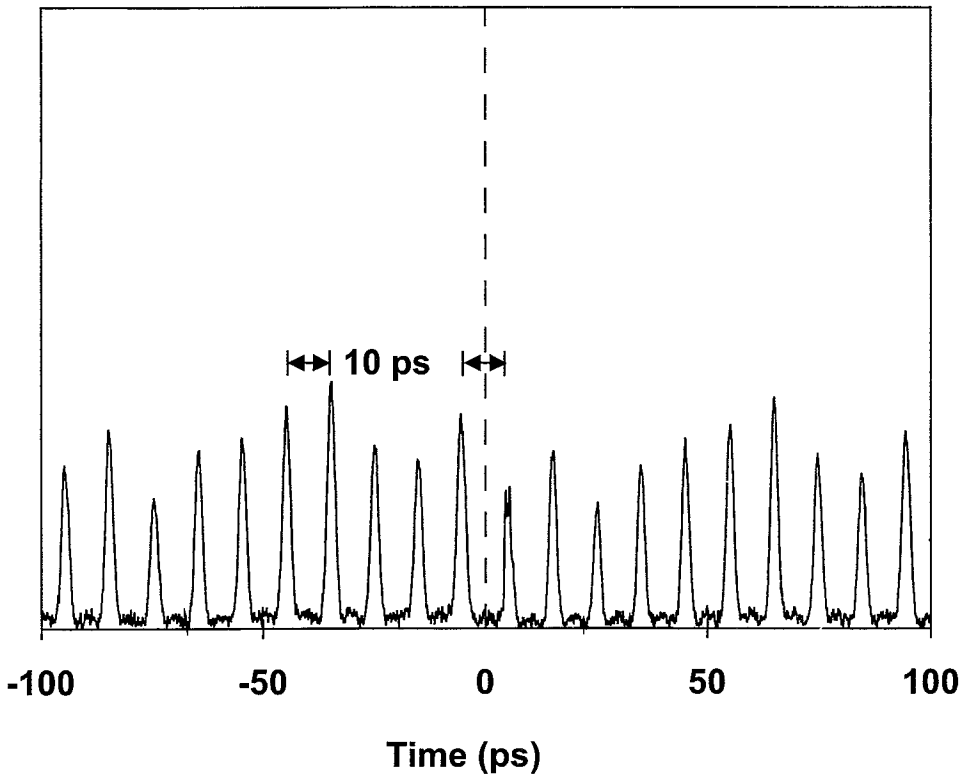

Fig. 2.20. Continuous 100 GHz pulse train. Compared to the pulse bursts illustrated in Fig. 2.19, the stitching error between frames has been minimized through proper choice of the optical pulse sequence duration. Additionally, reduction in the source timing jitter (<200 ps from ~1.4 ps) gives 100 % extinction between pulses.

ps. Additionally, the extinction between pulses is observed to be less than optimal. Appropriate choice of spatial input pattern to the DST shaper alleviates stitching concerns. By replacing the spatial pattern used to generate the above pulse sequence with one giving pulse sequences exhibiting 10 ps pulse spacing after space-to-time conversion, we obtain a continuous 100 GHz optical pulse train as shown in Figure 2.20. The extinction is also observed to be 100%, due to minimization of timing jitter in our 10 GHz source, which has been reduced from ~1.4 ps to less than 200 fs.

To encode optical data onto this pulse train, we need only alter the spatial pattern applied to the pulse shaper input. To keep the overall pulse rate, we block

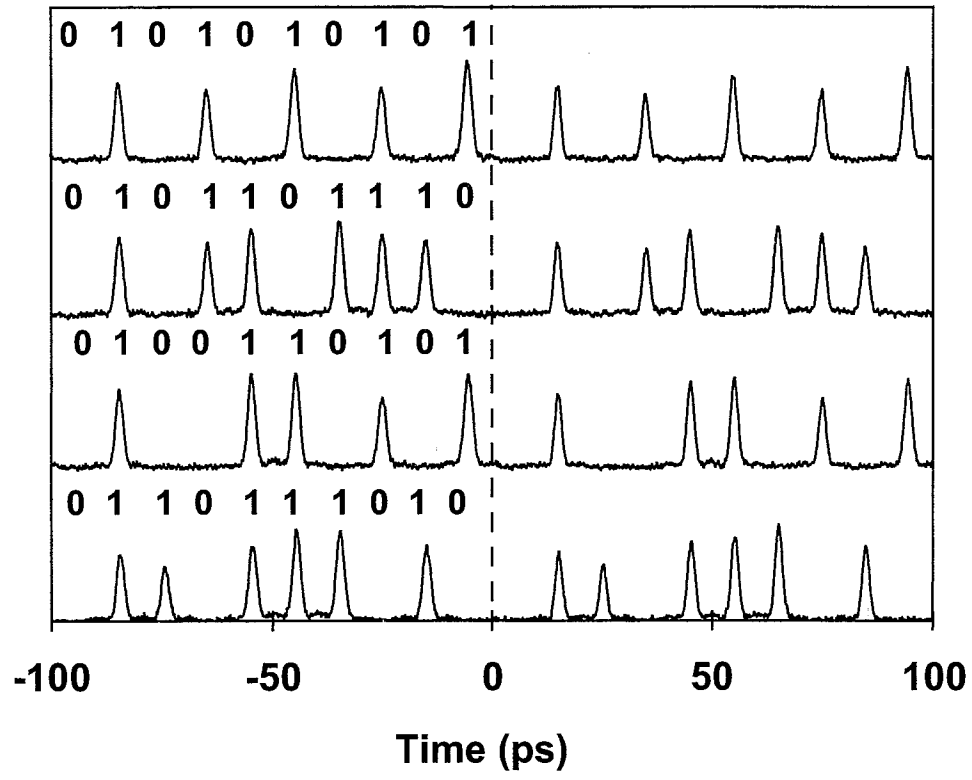

Fig. 2.21. 100 GHz optical data. Data packets spanning 100 ps, with pulse rates of 100 GHz, are generated from each source pulse. The optical data is arbitrary within each frame (dashed lines) and is repeated at the source repetition-rate. Incorporation of a high-speed optoelectronic modulator array would allow reprogramming on a frame-by-frame basis.

individual spots in the input spatial pattern used to generate the pulse train of Fig. 2.20. Examples of optical data generated in this manner are shown in Figure 2.21. The data within a single frame, again separated by the dashed lines, is arbitrary and repeats at the source repetition-rate. To achieve electronic control over the data within a frame we note the fixed mask could be replaced with a spatial light modulator, such as a liquid crystal modulator frequently employed in Fourier pulse shaping experiments[1], allowing the spatial pattern and, hence, pulse shaper output to be altered via computer control. With the inclusion of high-speed optoelectronic modulator arrays operating at the source repetition-rate of 10 GHz, optical data could be reprogrammed on a frame-by-frame basis enabling generation of truly independent optical data at rates of 100 Gb/s.

3. PHOTONICALLY ASSISTED GENERATION OF ARBITRARY MILLIMETER-WAVE ELECTROMAGNETIC WAVEFORMS VIA DIRECT SPACE-TO-TIME OPTICAL PULSE SHAPING

3.1 Introduction and Motivation

The emerging area of microwave photonics, which exploits optical techniques to generate, measure, and transmit microwave and millimeter-wave analog data, has seen much growth over the past several years. Various methods for photonic analog-to-digital conversion have been demonstrated utilizing several optical time-division demultiplexing schemes [33, 34] in addition to time-stretching techniques [35] with the goal of measuring electronic signals in the microwave and millimeter-wave range. Fiber-wireless systems [36, 37] have also been demonstrated for optical transmission of electrical signals in the millimeter-wave band. Optical generation of electromagnetic waveforms in the GHz and multiple tens of GHz range, specifically arbitrarily shaped waveforms, is an area which warrants further exploration.

Arbitrarily shaped millimeter and microwave waveforms could find applications in a variety of radio-frequency (RF) communications systems, including ultrawide-bandwidth (UWB) [38], secure, and multiple-access systems, in addition to other areas such as electronic countermeasures and pulsed radar [39]. Current commercial electromagnetic arbitrary waveform generation (AWG) technology is, however, limited to the range below $\sim$ 2 GHz. Novel optical techniques for generation of arbitrarily shaped electromagnetic waveforms could remarkably improve the current state-of-the-art in millimeter-wave and microwave AWG. Recently, several techniques have been demonstrated for generation of narrow-band electromagnetic signals in the

1 - 10 GHz range. A system employing a tunable laser diode source, electro-optic modulator and fiber delay lines has been demonstrated to produce tunable RF radiation from 550 MHz - 9 GHz through RF interference [40]. In addition, a modelocked laser diode, combined with a wavelength division de-multiplexing technique has been demonstrated to produce narrow-band electromagnetic signals, in the 12.4 - 37.2 GHz range, through beating of different longitudinal laser modes. This techniques also allows individual longitudinal modes of the laser to be independently phase- or amplitude-modulated allowing arbitrarily shaped beat signals to be generated [41]. Another optical heterodyne scheme, based on microchip lasers has also been demonstrated to produce electromagnetic radiation at $\sim$8 GHz, with possible extension into the millimeter-wave range [42]. Various other techniques for generation of millimeter-wave electromagnetic signals, including subharmonic injection locking [43, 44] and fiber Bragg grating based techniques [45], have been demonstrated. Additionally, novel techniques such as optical rectification in a nonlinear photonic crystal [46] have been proposed for coherent microwave and millimeter-wave signal generation. These techniques, while producing spectrally pure electromagnetic radiation, are narrow-band techniques, allowing modulation of the GHz waveforms over many cycles of the underlying periodic signal. Recently, a wide-band phase-modulated waveform in the low ($\sim$6) GHz range has been demonstrated through a wavelength-division multiplexing scheme combined with a series of optical delay lines used to create an optical pulse sequence to drive a photodiode [47]. This technique, while demonstrating cycle-by-cycle generation of electromagnetic waveforms, suffers from the need to tailor the fiber delay lines to each specific waveform. Consequently, reprogrammability is not easily achieved.

In this chapter, an overview of our work in photonically-assisted generation of broadband electromagnetic waveforms is presented. Our technique, based on direct space-to-time optical pulse shaping [48], enables generation of arbitrarily shaped, phase-, and frequency-modulated waveforms at center frequencies up to $\sim$50 GHz. The focus of this work is generation of these millimeter waveforms on a cycle-by-cycle

basis instead of through narrowband modulation techniques [40, 41]. In contrast to other cycle-by-cycle techniques [47], our technique is inherently reprogrammable given our direct space-to-time pulse shaper, with waveform alterations induced through simple changes in the pulse shaper input. Generation of arbitrary burst [11] and continuous [12] electromagnetic waveforms in the 30 - 50 GHz range will now be discussed.

3.2 Experimental Concept

The concept of our experiment is to exploit our direct space-to-time pulse shaping apparatus which enables generation of optical pulse sequences at rates approaching ~100 GHz [49]. Through high-speed optical-to-electrical (O/E) conversion, the pulse sequences from our pulse shaper are converted to millimeter-wave electromagnetic waveforms. The concept of using shaped optical pulses to generate electromagnetic waveforms has previously been demonstrated in our group, where freely propagating THz waveforms were generated from photoconductive antennae driven by optical pulses shaped in a Fourier transform (FT) shaper [50]. To extend this concept to generation of waveforms in the multiple tens of GHz range, we replace the FT shaper with our novel DST pulse shaper, which provides the 100+ ps temporal window necessary for generation of multi-cycle waveforms in the GHz range. Additionally, O/E conversion is now accomplished through a high-speed photodiode which replaces the photoconductive antennae used previously. These changes enable cycle-by-cycle generation of electromagnetic waveforms which effectively fill the frequency void in previous results [47, 50].

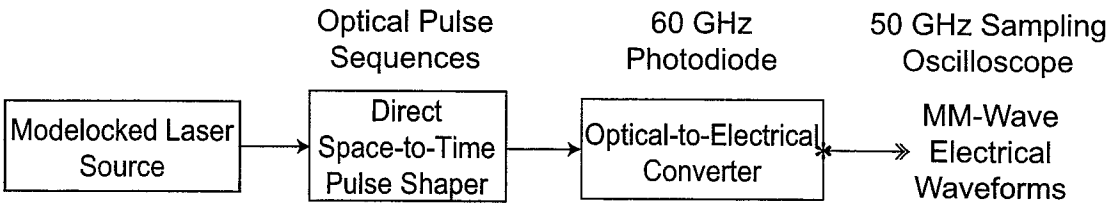

Fig. 3.1. Schematic diagram of our millimeter-wave AWG experiments.

A general block diagram of our experiment is shown in Figure 3.2. The short-pulse output from one of several modelocked erbium fiber lasers (the specifics of which will be discussed in the following sections) is converted into arbitrary optical pulse sequences in the DST pulse shaper. These optical pulse sequences are then down-converted to millimeter electromagnetic waveforms through O/E conversion in a 60 GHz photodiode. The resulting waveforms are measured on a 50 GHz sampling oscilloscope. Here, the limited bandwidth of the electrical system suppresses harmonics in the optical pulse sequences - effectively converting isolated optical pulse sequences into smooth millimeter-wave sinusoids.

3.3 Burst Arbitrary Millimeter Waveform Generation

This section discusses generation of burst millimeter waveforms at center frequencies approaching 50 GHz [11]. In these experiments, the source laser is a passively modelocked Erbium fiber laser [25] which provides ~300 fs pulses at a rate of 40 MHz. Each source pulse is converted to an optical pulse sequence spanning a time aperture $\geq$100 ps in the DST shaper which is subsequently converted into an electromagnetic waveform by the high-speed photodiode.

For these experiments, periodic spatial patterns (similar to the one shown in Fig. 2.16) consisting of 20 and 16 spots are used as the DST input. The choice of patterns is based on the desired pulse repetition-rate out of the pulse shaper. Our electrical system bandwidth is limited by the speed of the 60 GHz photodetector and 50 GHz sampling oscilloscope, so it is desirable to generate pulse sequences with center frequencies below 50 GHz to remain in the bandwidth of the electrical system. A spatial mask is now used to manipulate the periodic patterns created by the DOE. This mask is designed to manipulate the pulse position and / or spacing depending upon the output millimeter waveform which is desired. For the first set of measurements, every second input spot was blocked in these 20 and 16 spot patterns, yielding periodic spatial patterns with periods of 7 mm and 8.75 mm, respectively, at the diffraction grating. The space-to-time conversion constant of $\gamma/\alpha \sim 3.1$ ps/mm of our pulse shaper predicts output pulse sequences with repetition rates of ~48 and ~38 GHz, respectively, for these spatial input patterns. When these pulse sequences are measured with our electrical system, the millimeter-wave electrical output waveforms are found to be good sinusoids, as illustrated in Figure 3.2. Agreement with 48 / 38 GHz sinusoidal fits is found to be quite good, and the waveforms are quite smooth in nature, which is in stark contrast to the driving optical pulse sequences (bottom trace).

Our method provides not only the ability to synthesize periodic millimeter waveforms, but also enables us to introduce a phase-shift in these waveforms by controlling the temporal position of pulses in the driving optical pulse sequence. Figure 3.3 shows

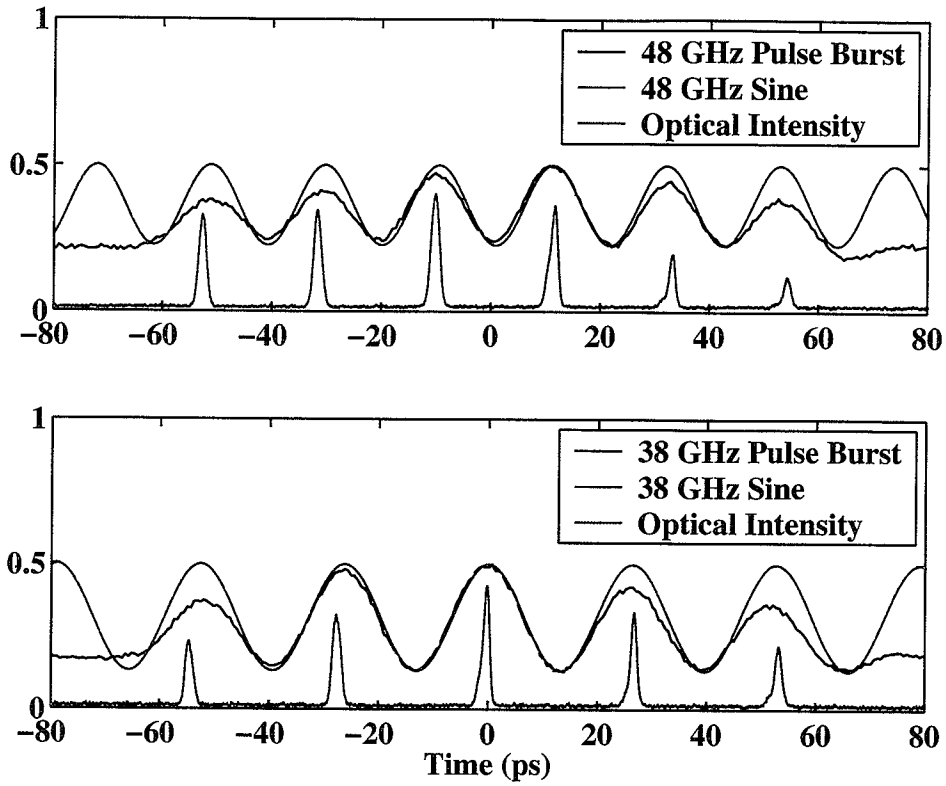

Fig. 3.2. (a) 48 GHz and (b) 38 GHz sinusoidal millimeter waveforms. The shape of these waveforms is found to be a good sinusoid, in contrast to the driving optical pulse sequence (bottom trace).

examples of millimeter-wave phase modulation. The top waveform is the same 48 GHz signal shown in Fig. 3.2(a). For the subsequent traces, a π phase shift is induced by changing the temporal position of pulses in the driving optical pulse sequence. These phase shifts can be seen quite clearly by comparing the relative positions of the peaks and nulls of each waveform. Relative to the first peak in the waveform, the phase shift occurs after 1, 1.5, and 2 complete 48 GHz cycles. For example, in the second trace the optical pulses driving the photodetector occur at approximately -60, -40, -10, 10, 30, and 50 ps respectively. The extra 10 ps temporal shift between pulses 2 and 3 induces a π phase shift in the output millimeter waveform.

We have shown that we are able to achieve phase modulation by controlling the

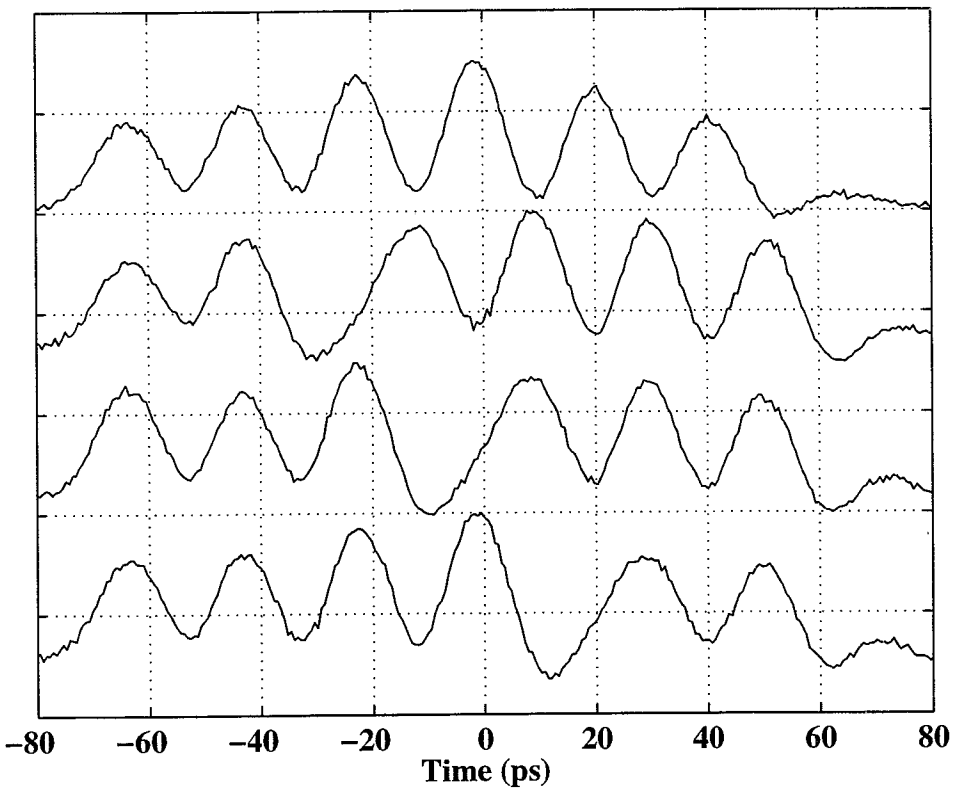

Fig. 3.3. Examples of millimeter-wave phase modulation. A phase shift can be introduced in the millimeter-wave electrical signal by controlling the *position* of pulses in the driving optical waveform.

temporal *position* of pulses in the driving optical pulse sequence from our DST shaper. We now illustrate that by controlling the temporal *spacing* of pulses in our driving optical pulse sequence, we are able to achieve frequency modulation of the output millimeter waveform. Here we exploit the limited bandwidth of the electrical system and the ability to control the pulse spacing in our driving optical pulse sequence to achieve frequency modulation in the 20 - 50 GHz range. An example of our frequency modulation data is shown in Figure 3.4. The top trace (a) is a measured millimeter electrical waveform with a center frequency of 48 GHz which then abruptly shifts to 24 GHz for the last several cycles. This waveform is found to agree quite well with a sinusoidal fit exhibiting the same frequency modulation. The key to obtaining

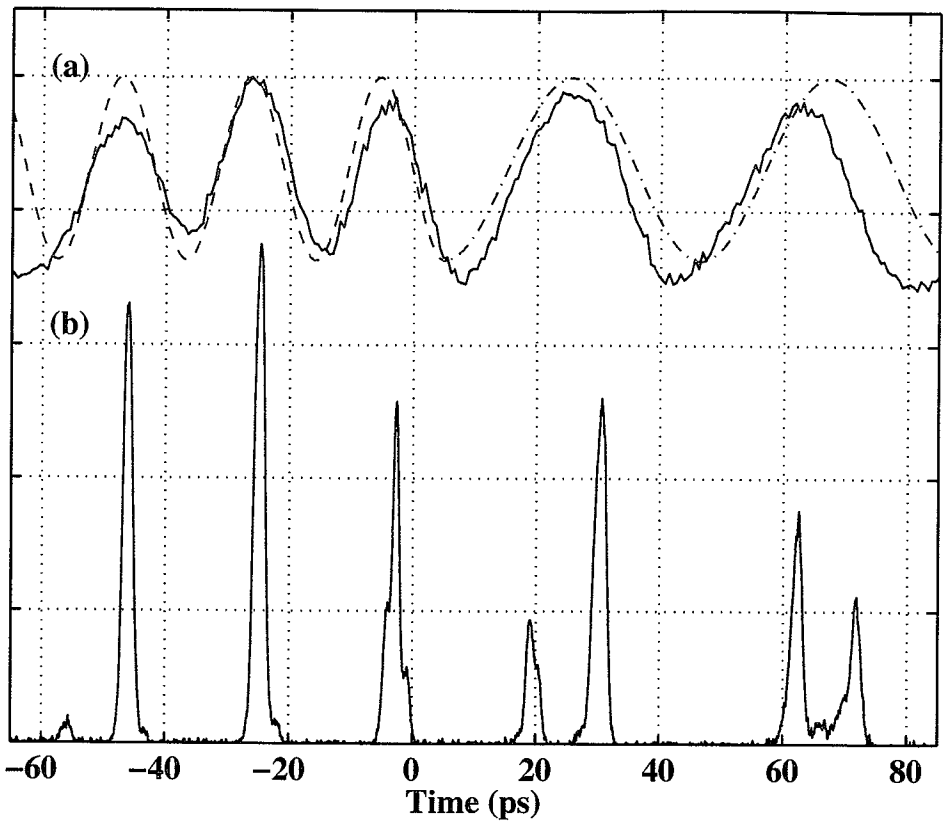

Fig. 3.4. Example of millimeter-wave frequency modulation. The frequency of the electrical waveform can be controlled by controlling the *spacing* of pulses in the driving optical pulse sequence. (a) Measured millimeter-wave signal (red) and 48 / 24 GHz sinusoidal fits (green). (b) Optical cross-correlation of the driving optical pulse sequence.

frequency modulation in our experiments is to use pulses which are spaced too closely to be individually resolved by the photodiode. The optical waveform used to drive the photodiode is shown in trace (b). Here the first three pulses occur at 48 GHz and are followed by two pulse pairs. These pulse pairs repeat at 24 GHz, however, the pulse spacing within the pairs is $\sim$ 10 ps ($\sim$100 GHz), which is too close for the individual pulses to be resolved by the detector. It is clear from the driving optical pulse sequence shown in Fig. 3.4(b) that these pulses pairs have a smaller pulse amplitude than the individual pulses driving the 48 GHz portion of the waveform.

We observe that when the pulse pairs are of the same amplitude as the preceding single pulses, the 24 GHz cycles of the waveform exhibit a larger amplitude than the preceding high frequency cycles. This can be explained in part by the electrical system response which is greater at 24 GHz and that the detector is responding to roughly twice the energy as for a single pulse. These pulse pairs are therefore purposely attenuated to attain lower frequency cycles of the same amplitude as the preceding higher frequency cycles. For comparison, Figure 3.5 shows the driving optical pulse sequence and output electrical waveform without (a) and with (b) manipulation of the optical pulse sequence. The equalization operation is shown schematically in Figure 3.6. In this manner, the shape of the electrical waveform may be tailored as desired, for example equalized, by appropriate pre-distortion of the driving optical pulse sequence based on the electrical measurement.

To illustrate the broadband nature of our burst waveforms, we present RF power spectra for several of these waveforms in Figure 3.7, calculated by performing a Fourier transform of the time domain data. The spectrum for the 48 GHz sinusoidal burst of Fig. 3.2 is shown in (a). The spectrum is found to have a center frequency of $\sim$48 GHz and a bandwidth of $\sim$7 GHz, as determined by the approximately 130 ps duration of the waveform. In (b), the spectrum of the frequency-modulated waveform of Fig. 3.4(b) is presented. Here, the spectrum shows features at 24 and 48 GHz as expected and dramatically illustrates the broad bandwidth of our waveforms, with non-zero spectral content over the range of $\sim$15 - 60 GHz.

The output millimeter-wave signal from our system can be predicted from convolving the measured electrical impulse response shown in Figure 3.8 with the measured optical cross-correlation of the driving optical pulse sequence. Figure 3.9 shows several examples of these predictions. In Fig 3.9(a) the measured 48 GHz signal (red) shows excellent agreement with the signal predicted by the convolution of the electrical system impulse response and the optical cross correlation data (bottom trace Fig. 3.2(a)) for the pulse sequence used to generate this signal. Similarly, the frequency modulated waveform predicted in this manner (blue) also agrees quite well with the

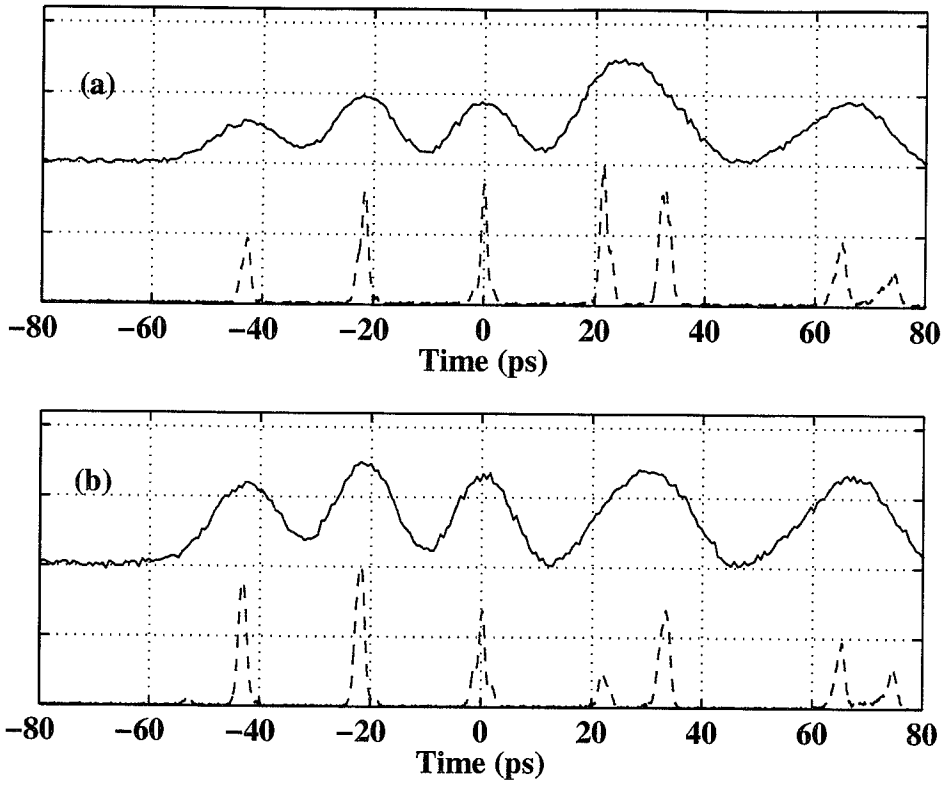

Fig. 3.5. Effect of pre-distortion of the optical pulse sequence on the measured electrical waveform. By purposely attenuating the pulse pairs in the optical waveform we obtain frequency modulated waveforms with equalized amplitude features.

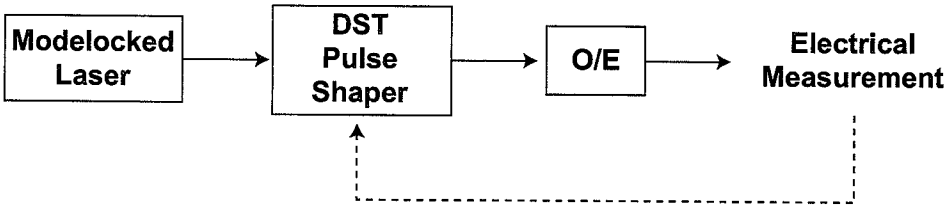

Fig. 3.6. Tailoring of the electrical waveform. Predistortion of the driving optical pulse sequence based on the electrical measurement allows the electrical waveforms to be shaped as desired.

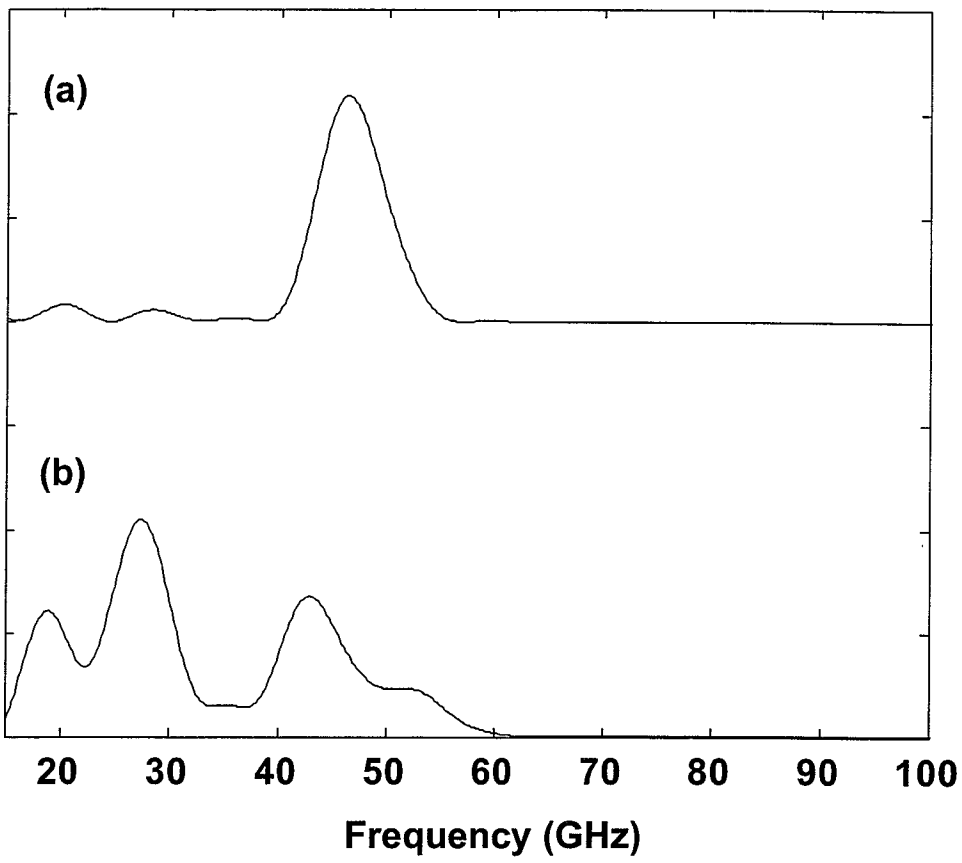

Fig. 3.7. Calculated RF power spectra for (a) 48 GHz sinusoidal burst and (b) 48 / 24 GHz frequency-modulated burst waveform.

waveform which is experimentally measured. This prediction method would also work if the optical pulse sequence is simulated by a series of δ functions whose amplitudes are weighted by the energy in each pulse of the driving optical waveform.

The waveforms generated in this experiment exhibit amplitudes of roughly 3mV peak-to-peak, which is determined by the optical excitation power and the efficiency of the 60 GHz photodiode. For these experiments, the average input optical power to the system is approximately 1 mW (0 dBm). The average output power from the system is approximately -46 dBm. From previous work [8], we expect a loss of $\sim$30 dB in the shaper arising from the $\sim$300 ps output temporal window and $\sim$300 fs input pulse

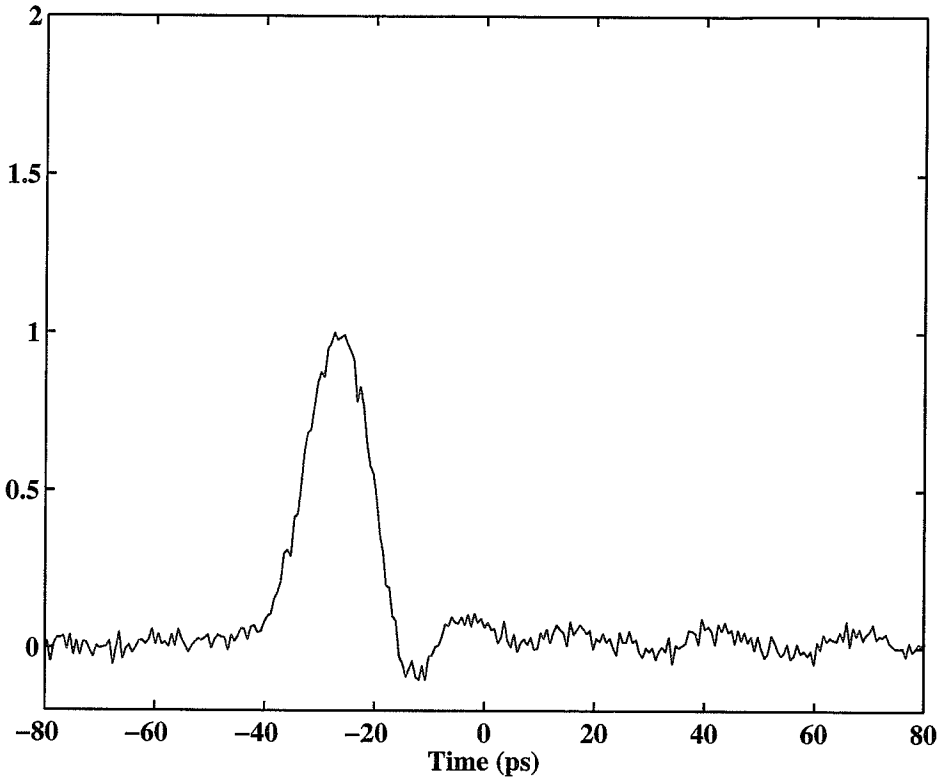

Fig. 3.8. Electrical system impulse response.

width - the additional loss in our system is due mostly to non-optimized coupling to the output fiber in the vertical (non-shaped) direction and optimization of the spatial pattern in the shaper. The pulse shaper output is amplified by approximately 13 dB in an erbium-doped fiber amplifier prior to measurement with the photodiode. The average incident power on the photodiode is then $\sim$ -33 dBm ($\sim$0.5 μW). Since the energy is generally distributed over a 6 optical pulse sequence that repeats at the 40 MHz repetition rate of our source laser, the average energy per pulse is $\sim$2.0 fJ. The electrical impulse response is approximately 13 ps FWHM and the responsivity of the photodiode is $\sim$0.3 A/W. As a result, the measured electrical waveforms show peak voltages in the $\sim$3 mV range when measured on our sampling oscilloscope (50 Ω impedance). If applications require larger amplitude signals, either increased optical

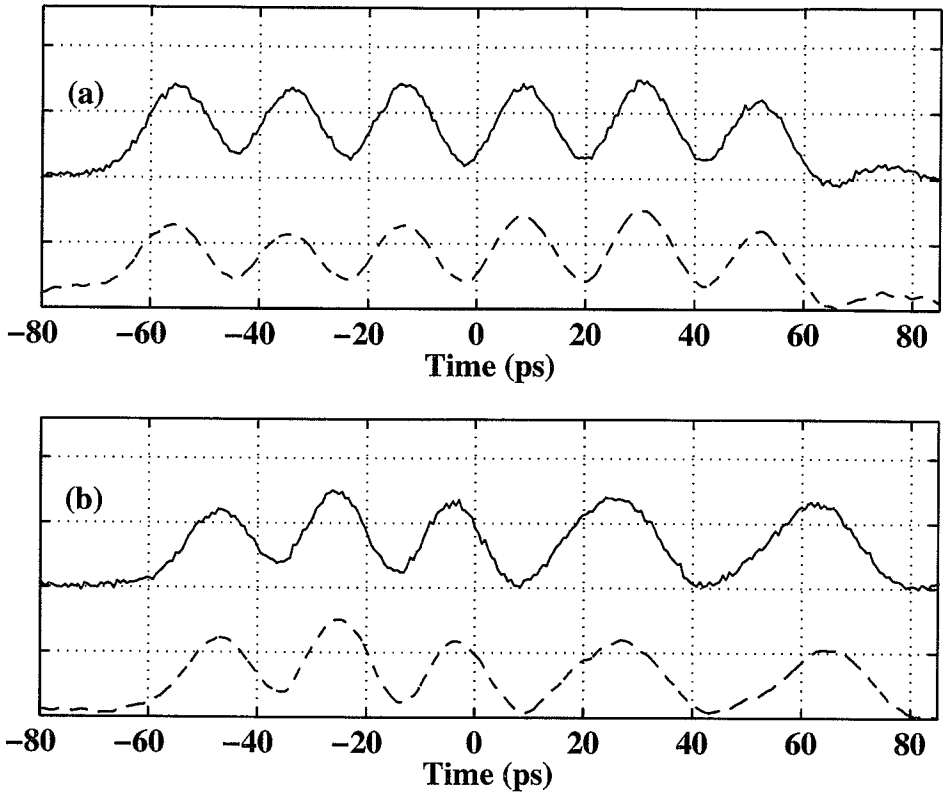

Fig. 3.9. Predicted waveforms based on the convolution of the electrical system impulse response (Fig. 2.6) and the measured optical pulse sequence. (a) Measured (red) and predicted (blue) 48 GHz sinusoidal signal. (b) Measured (red) and predicted (blue) frequency-modulated millimeter waveform.

excitation power or wideband electrical amplification could be used to increase the electrical signal level.

The following section will discuss generation of continuous millimeter waveforms enable by the inclusion of a high rep-rate telecom source laser.

3.4 Continuous Periodic Arbitrary Millimeter Waveform Generation

The preceding section details the generation of arbitrarily phase- and frequency-modulated burst waveforms in the multiple tens of GHz range. The burst nature of these waveforms is determined by the laser source used as the input to our system. Thus far, our waveforms span a time aperture in excess of 100 ps and repeat at the source repetition-rate of 40 MHz, so they are essentially isolated in time. For applications requiring higher data rates, it is desirable to have waveforms which are continuous in nature, i.e., shaped electromagnetic waveforms which repeat at period approaching the pulse shaping window. Generation of continuous millimeter-wave signals [12] will now be discussed.

To move towards generation of continuous waveforms, we have replaced the passively modelocked fiber laser with an actively modelocked fiber source [10] which provides $\sim$1 ps pulses at a repetition-rate of 10 GHz. The goal here is to combine our ability to generate electromagnetic waveforms over a $\sim$100 ps frame with a source of comparable pulse period to generate continuous millimeter waveforms. The idea is to create an arbitrarily shaped millimeter waveform, spanning this frame, from each source pulse and then stitch these waveforms together to form a continuous signal. To illustrate this concept, consider Figures 3.10 and 3.11. Here, the pulse sequences of Figure 3.10 generate the electrical waveforms of Figure 3.11 after O/E conversion. In Fig 3.10 (a), a frame consisting of 4 pulses at $\sim$40 GHz is generated in the DST shaper from each pulse from the source. The boundary between adjacent frames is delineated by the dashed line. After O/E conversion, the $\sim$40 GHz electrical waveform of Fig. 3.11 (a) results. Similarly, the phase modulated waveforms of Fig. 3.11 (b), (c) are generated from the pulse sequences of Fig. 3.10 (b), (c). In (b), an extra $\sim$12.5 ps delay is added after the second pulse in the driving optical pulse sequence. This extra delay results in a π phase shift following the second cycle of the electrical waveform. Similarly, the shift in (c) is generated by driving the third electrical cycle with a single 80 GHz pulse pair. The concept of stitching together frames is clearly demonstrated here; however, the need to match the waveform duration and

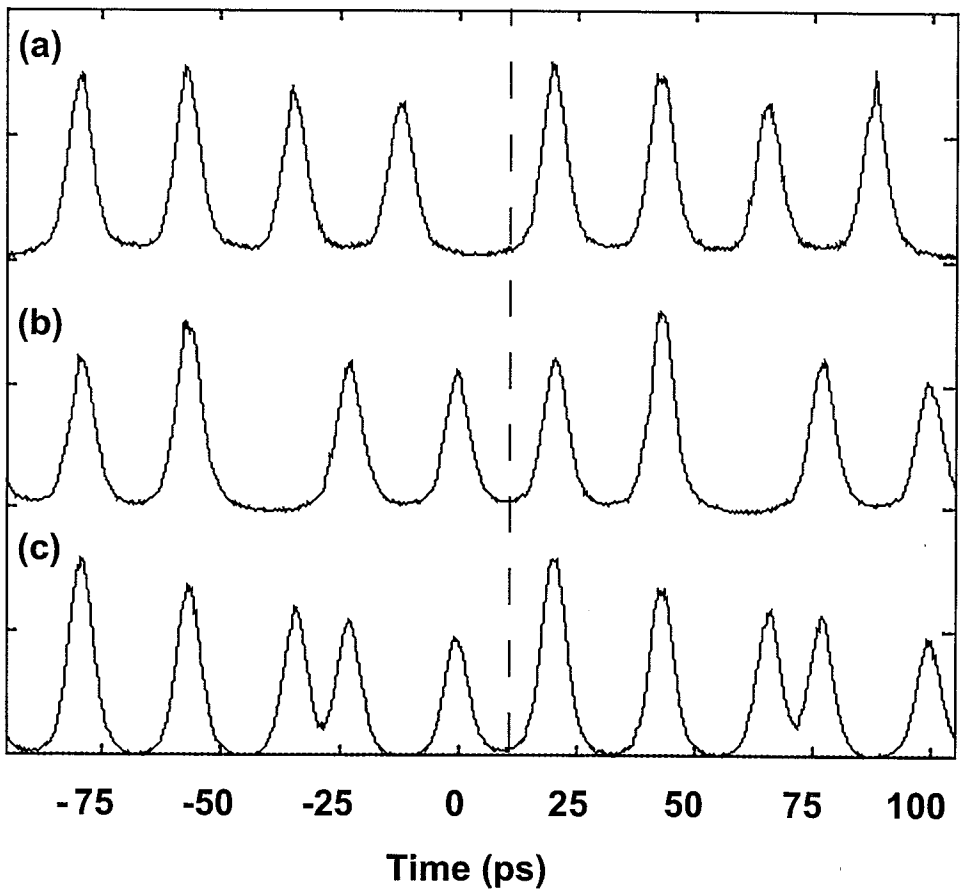

Fig. 3.10. Optical cross-correlation traces of $\sim$ 40 GHz optical pulse sequences used to generate nearly continuous electrical waveforms. Each frame of pulses (separated by the dashed line) is generated from a single source pulse every 100 ps. (a) 40 GHz periodic sequence. (b) 40 GHz sequence with an extra $\sim$12.5 ps delay introduced after the second pulse in each frame. (c) 40 GHz sequence with a 80 GHz pulse pair introduced following the second pulse in the sequence.

the source repetition rate is also illustrated. If we wish to achieve continuous waveforms, the pulse sequence duration from the DST shaper and, hence, the duration of the electrical waveform must be chosen such that the frames join appropriately at the frame boundary. For example, consider the pulse sequence and electrical waveform of (a). There is an obvious stitching error at the frame boundary which results from a mismatch in frame duration and the source pulse period. This leads to a small

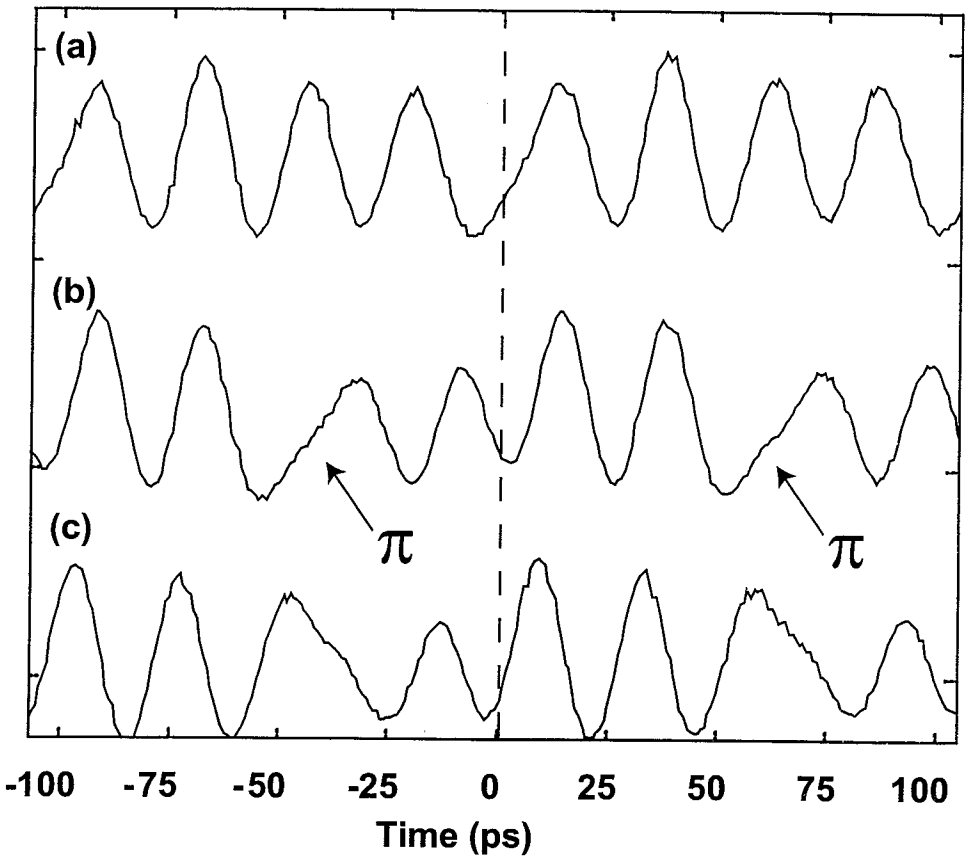

Fig. 3.11. Electrical waveforms resulting from O/E conversion of the pulse sequences of Fig. 3.10. (a) Nearly continuous 40 GHz sinusoid. (b) 40 GHz phase-modulated waveform exhibiting a π phase shift after the second cycle in each frame. (c) Modulated waveform showing a phase shift midway through the third cycle.

phase shift at the frame boundary in the electrical waveform. To match the electrical waveforms at the frame boundaries and remove this error, the duration of the driving optical pulse sequence must be chosen appropriately. To change the duration of the optical pulse sequence, we simply change the periodic spatial pattern applied to the pulse shaper input. One proper choice of spatial pattern leads to a pulse sequence from the DST where the pulse-to-pulse spacing is 20 ps and the frame duration is 100 ps, resulting in a continuous 50 GHz optical pulse sequence with negligible stitching error between adjacent frames. This continuous pulse sequence is illustrated in Fig-

ure 3.12 (a). After O/E conversion, the measured electrical waveform is seen to be a smooth ~50 GHz sinusoid, as illustrated in Fig. 3.13 (a). Here, the stitching error apparent in Fig. 3.11 (a) has been effectively eliminated.

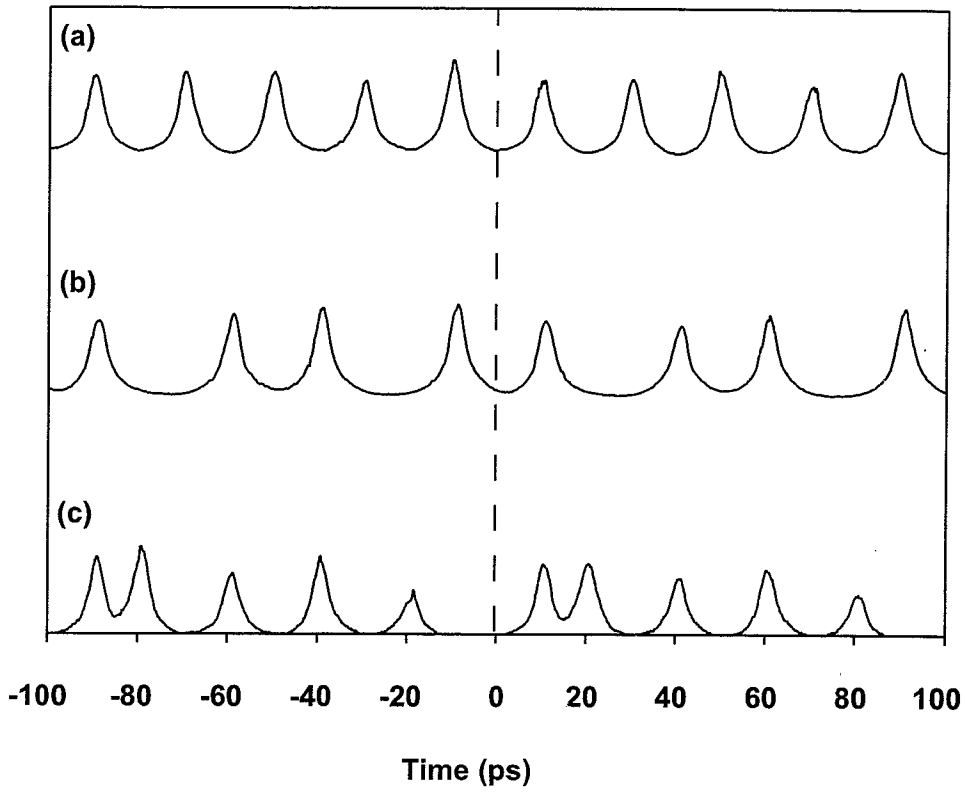

Fig. 3.12. Driving optical pulse sequences used to generate continuous millimeter waveforms. (a) 50GHz optical pulse sequence. (b) Pulse sequence exhibiting an extra 10 ps delay after the first and third pulse in each frame. (c) 100 GHz pulse pair followed by three pulses at 50 GHz, which repeats every 100ps.

We are also able to achieve phase and frequency modulation in the same manner as previously demonstrated with burst waveforms. For example, an extra 10 ps delay is introduced after the first and third pulses in the optical pulse sequence of Fig. 3.12(b) which results in a 50 GHz sinusoid exhibiting a π phase shift after the first and third cycles in the electrical waveform (Fig. 3.13(b)). Similarly, by introducing a single ~100 GHz pulse pair (Fig. 3.12(c)), a single 25 GHz cycle precedes three 50

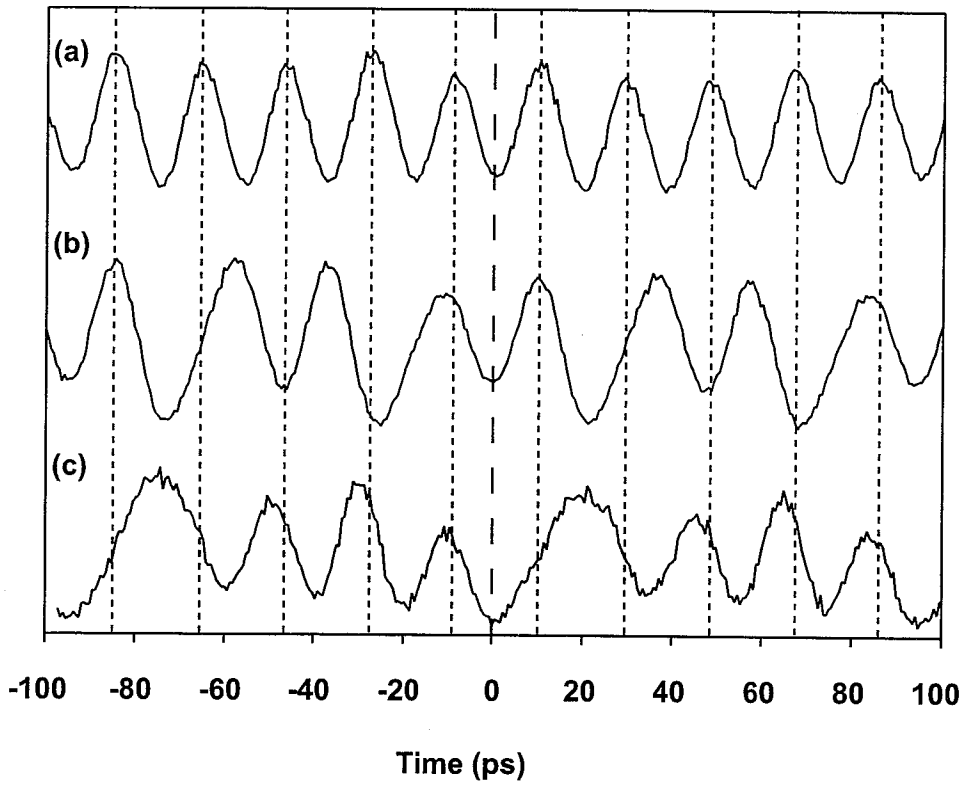

Fig. 3.13. Continuous millimeter waveforms. Individual waveforms, spanning a 100ps frame as delineated by the dashed line, are stitched together to form continuously periodic millimeter waveforms. (a) Continuous 50GHz sinusoid. (b) Periodically phase-modulated waveform exhibiting a π phase shift after the first and third electrical cycles within each frame. (c) 25/50GHz frequency-modulated waveform. A single 25GHz cycle is induced by a 100 GHz pulse pair (Fig. 3.12(c)) followed by three $\sim$50 GHz cycles.

GHz cycles as shown in Figure 3.13(c).

By matching the ability to form optical pulse sequences over a time aperture $\geq$100 ps with a high repetition-rate source, we are able to generate continuous arbitrary electromagnetic waveforms at center frequencies of $\sim$50 GHz. These waveforms, due to increased optical excitation power, exhibit peak-to-peak amplitudes of approximately 20 mV. Again, wideband electronic amplification or a further increase in optical excitation could be used to increase the amplitudes of these signals. We note

the modulation is arbitrary within one frame and is repeated at the source repetition rate. Incorporation of a high-speed optoelectronic modulator array for rapid reprogramming of the spatial pattern at the input of the DST pulse shaper would allow reprogramming of the optical pulse sequences on a frame-by-frame basis. This ability would allow generation of arbitrarily shaped millimeter waveforms where the modulation varies independently from frame-to-frame.

4. GHZ ELECTROMAGNETIC WAVEFORM GENERATION VIA DST PULSE SHAPING AND DISPERSIVE STRETCHING

For certain applications, particularly UWB RF communications [38], it is desirable to obtain arbitrarily shaped electromagnetic waveforms in the GHz range. Given the February 2002 ruling by the FCC, a particular frequency range of interest is the approved UWB 3.1 - 10.6 GHz band. With reaching this particular frequency range in mind, we now show how to move our electromagnetic waveform generation technique from the tens of GHz range into the GHz range.

While both FT and DST pulse shaping techniques are capable of generating optical waveforms which span a several hundred picosecond time aperture, achieving waveforms with nanosecond durations directly from either pulse shaper is not feasible. Inclusion of a fixed amount of chromatic dispersion after either shaper, however, can easily stretch the temporal durations into the nanosecond regime. Recently, a group at UCLA [51] demonstrated a Fourier pulse shaping technique, combined with dispersive stretching, to generate RF waveforms in the 1 - 12 GHz range. In this method, the optical spectrum of a supercontinuum source is amplitude modulated in a FT pulse shaper [1]. Following the pulse shaper, a length of single-mode optical fiber dispersively stretches the temporal output of the pulse shaper. For large dispersion, the measured optical waveform after stretching is a scaled version of the amplitude modulation applied to the optical spectrum. This is equivalent to the Fourier transform of the pulse shaper temporal output. After O/E conversion, the measured temporal electrical waveform exhibits the shape of the optical spectrum.

While conceptually similar, the fundamental difference between the FT technique

[51] and our DST shaping technique [14, 15] is the manner by which the optical spectrum is modulated and the relation between the pulse shaper temporal output and the measured electrical waveform. In contrast to direct modulation of the optical spectrum via a spatial light modulator (SLM) in an FT shaper, the optical spectrum in our apparatus is modulated by the applied spatial pattern and the physics of the DST pulse shaping apparatus.

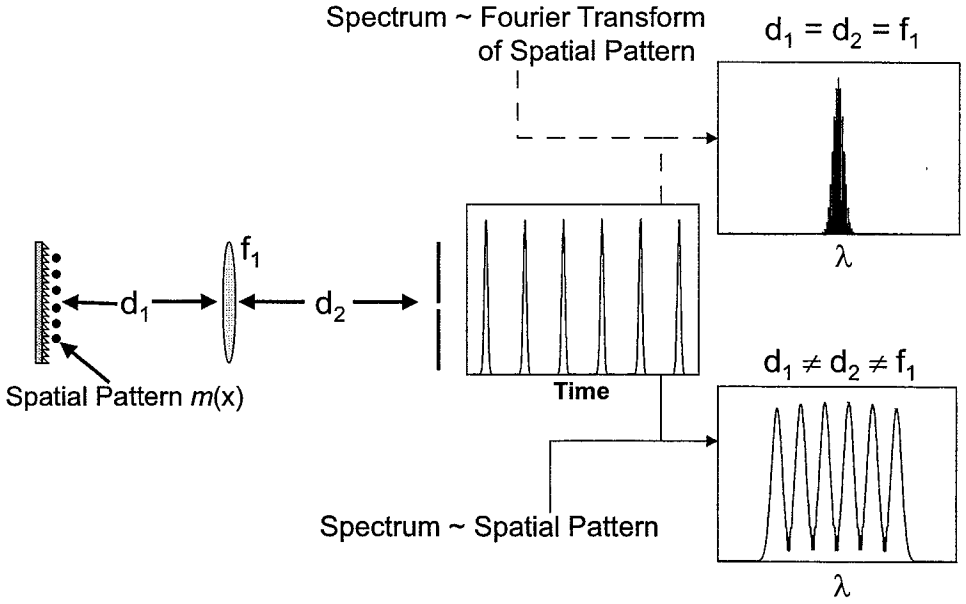

Fig. 4.1. Frequency modulation in the DST shaper. A quadratic temporal phase is imparted to the pulse shaper output when $d_1, d_2 \neq f_1$. For large enough frequency modulation, the applied spatial pattern is mapped to the optical spectrum at the output of the DST shaper. This frequency modulation capability, combined with dispersive stretching, allows the ~100ps optical pulse sequences from the DST to be stretched to several nanoseconds in duration.

In a DST pulse shaper, the intensity of the output temporal waveform is always a scaled version of the applied spatial pattern. It has been shown, however, that a quadratic temporal phase may be imparted to the DST shaper temporal output when the apparatus is configured appropriately [13] (as in Section 2.4). To illustrate this concept, consider Figure 4.1. If we assume a perfectly collimated spatial input to the

pulse shaper, the apparatus contributes no quadratic spatial phase when configured in a "chirp-free", i.e., $d_1 = d_2 = f_1$, configuration. In this particular case, the phase fronts of both the spatial pattern applied to the grating and the spectrum prior to the output fiber are flat and the DST shaper does not impart any quadratic phase, or frequency-modulation to the temporal output waveform. The result is that the optical spectrum of the pulse shaper output is related to the Fourier transform of the temporal output as is expected. When the pulse shaping lens is moved from the chirp-free position i.e., $d_1 \neq d_2 \neq f_1$, however, the phase-front at the output fiber now has a curvature, and hence a quadratic spatial phase. Through the physics of the pulse shaper, this quadratic spatial phase maps to a quadratic temporal phase in the DST output which is now expressed as

$$E_{DST}(t) \propto e_{in}(t) * \left[m\left(-\frac{\alpha}{\gamma}t\right) e^{-j\mathbf{A}t^2} \right], \tag{4.1}$$

where

$$\mathbf{A}(d_1, d_2) = \frac{\pi}{\lambda\gamma^2}\left(\frac{f_1 - d_2}{f_1 d_1 + f_1 d_2 - d_1 d_2}\right). \tag{4.2}$$

This quadratic temporal phase gives rise to a frequency modulation (FM, in nm/ps) which, when sufficiently large, maps the applied spatial pattern onto the optical spectrum. In this case, both the temporal waveform and the optical spectrum are scaled versions of the applied spatial pattern. Thus, when the DST shaper is followed by a fixed amount of dispersion as illustrated in Figure 4.2, the optical waveform after stretching is still a directly scaled version of the pulse shaper temporal output. After O/E conversion, the electrical waveform is now a stretched version of the pulse shaper output. The stretching factor is determined by the magnitude of FM imparted by the pulse shaper and the amount of fixed dispersion. For our system, which employs $L \sim$ 5.5 km of Corning SMF-28 ($D = 17$ ps/nm-km), the stretching factor is approximately given by

$$\text{Stretching Factor} \sim |FM| \cdot D \cdot L. \tag{4.3}$$

In our apparatus, a variety of stretching factors are attainable. As the pulse shaping lens is displaced from the chirp-free position of $d_1 = 15$ cm $= f_1$ to $d_1 = 11.25$ cm, the

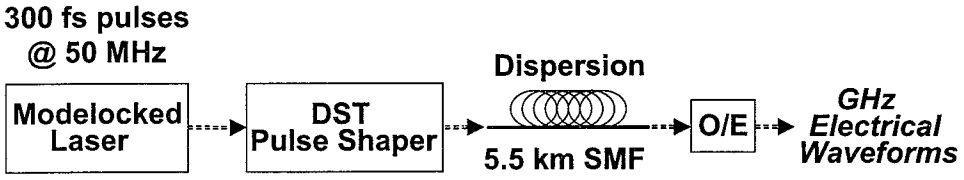

Fig. 4.2. Experimental schematic for GHz waveform generation. Optical pulse sequences from the DST shaper are temporally stretched by ~5.5 km of single-mode optical fiber prior to O/E conversion, enabling generation of electrical waveforms spanning several nanoseconds.

induced frequency modulation is continuously tuned from 0 nm/ps to −0.3 nm/ps. This variation in chirp gives a stretching factor which varies from 0 to ~28 over this small range of lens position. For these experiments, an extra telescope (magnification = 1.1 / 1.5 = ~.147) has been added to the system, prior to spatial patterning. This broadens the individual features in the pulse shaper output, $m(-\alpha t/\gamma)$, roughly by a factor of 7, while keeping the periodicity the same. This can also be viewed as reducing the bandwidth of individual features by a factor of ~7. This reduces the broadening of individual pulses in the stretching operation and, hence increases the extinction between features in the measured electrical waveforms.

It is interesting to compare our GHz waveform generation concept with that of temporal imaging [52]. Temporal imaging is accomplished through the combination of dispersion, quadratic temporal phase modulation, and a second dispersion applied to an input optical waveform [53]. When the dispersion and phase modulation are chosen appropriately, the input optical waveform is mapped to an output waveform which is either temporally expanded or compressed. The key element in these systems is the quadratic phase modulator, or time lens [54]. Our DST shaper operates as just such a lens - where the temporal focal length is easily tuned through longitudinal displacement of the pulse shaping lens.

We now present several examples of GHz waveform generation in our system. As a first example, the DST lens is positioned to give a FM of ~ -0.22 nm/ps, yielding

a predicted stretching factor of ~20.57. Experimentally, when a four-pulse sequence which is 70 ps in duration and has a center frequency of ~50 GHz is generated in the DST shaper, we expect the optical spectrum to be stretched over approximately 15 nm as determined by the magnitude of FM and the 70 ps pulse sequence duration. The measured optical spectrum is shown in Figure 4.3. The measured spectrum

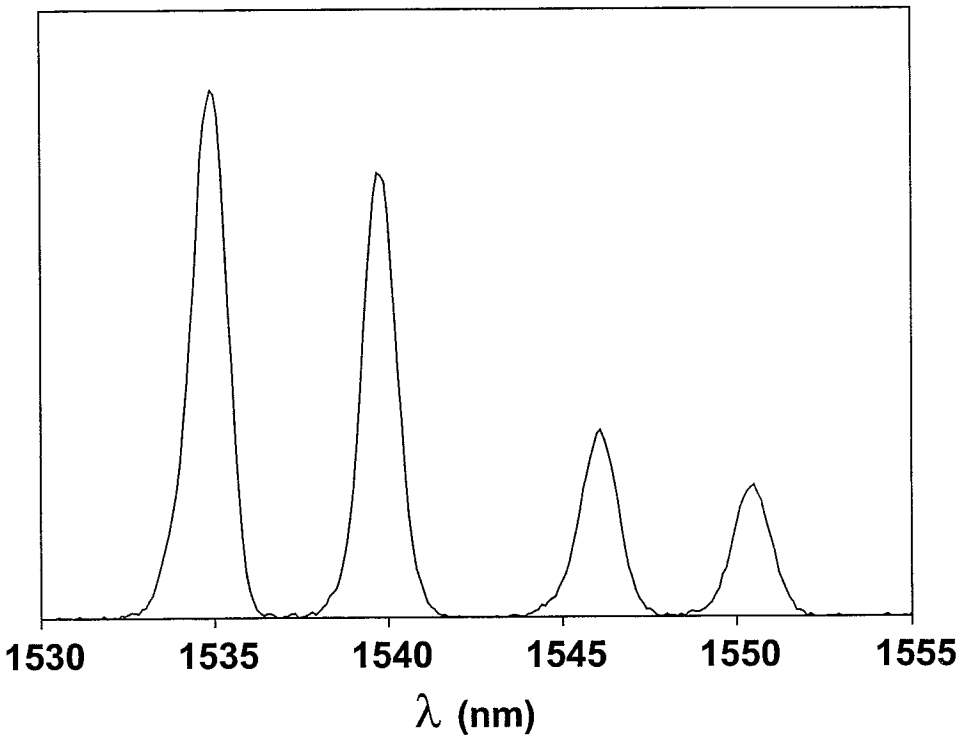

Fig. 4.3. Mapping of DST input pattern to the optical spectrum. The 4 pulse, 70 ps duration pulse sequence from the DST is mapped to a 4-feature optical spectrum. The ~15 nm span shows excellent agreement with that predicted by the imposed FM of ~-0.22 nm/ps and the 70 ps pulse sequence duration.

spans roughly 15 nm and shows excellent agreement with the predicted value. In this figure, the applied spatial input to the shaper (and, hence, the pulse shaper output) is clearly mapped to the optical spectrum. The measured stretched electrical waveform is found to have a duration of ~1.34 ns - approximately 20x the duration of the initial waveform. This waveform is presented in Figure 4.4. The duration of

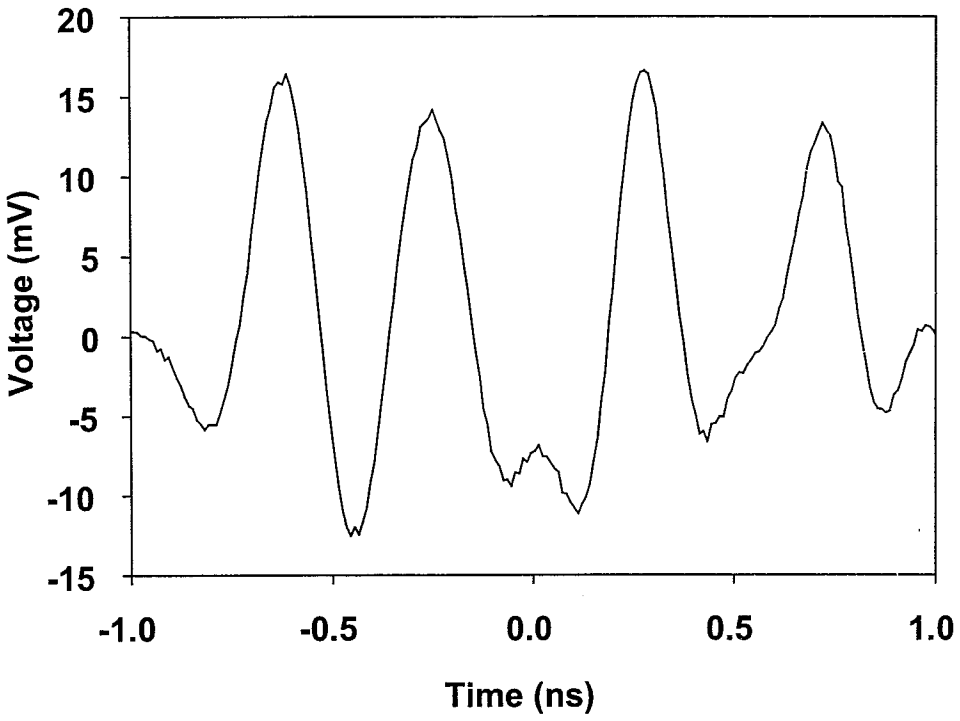

Fig. 4.4. GHz waveform generation. After passing through ~5.5 km SMF, the ~70 ps four-pulse 50 GHz sequence from the DST shaper is stretched ~20x. After O/E conversion, the measured four-cycle electrical waveform has a duration of ~1.34 ns and a center frequency of ~2.6 GHz.

the measured waveform shows excellent agreement with the predicted duration, with the slight discrepancy most likely due to uncertainty in the length of the stretching fiber.

For a fixed amount of dispersion, in our case $D \cdot L \approx 93.5\ ps/nm$, the stretching factor may be tuned simply by changing the position of the pulse shaping lens. For small changes in lens position, $\pm 10\%$ changes in temporal duration are easily attainable. To illustrate this tunability of the electrical waveform duration a four-pulse, 100 ps pulse sequence is generated in the DST shaper. This sequence can be represented as "1 0 0 1 1 1", with "1" representing a pulse in the sequence. In this sequence, each pulse occupies a 20 ps frame, resulting in a center frequency of ~50

GHz. The optical spectrum of this waveform, for several different values of frequency modulation is shown in Figure 4.5. Again, the 4-pulse sequence mentioned above is clearly mapped to the optical spectrum and the spectral content again shows excellent agreement with that predicted by the applied FM (as shown above) and the 100 ps pulse sequence duration. This waveform, after stretching and O/E conversion, is

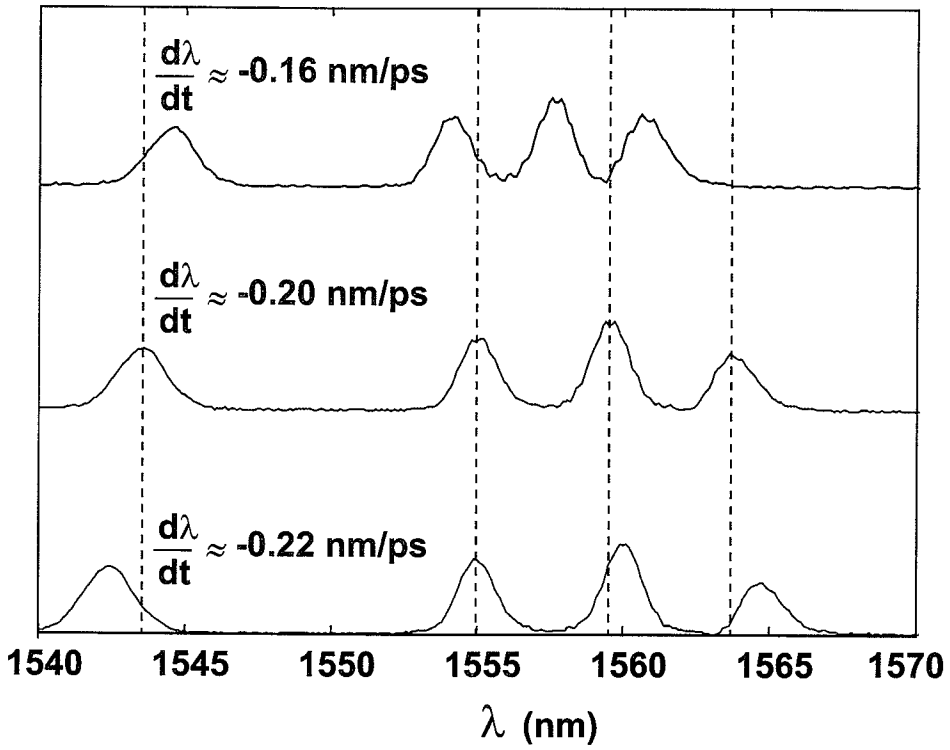

Fig. 4.5. Tunable scaling of the optical spectrum. When a 100 ps optical pulse sequence is generated in the DST shaper, the optical spectrum after the shaper is scaled to occupy from 16 - 23 nm of bandwidth. This is accomplished through FM imposed by simple movement of the pulse shaping lens.

shown for several stretching factors in Figure 4.6. The center waveform, exhibiting a duration of ~1.8 ns, as measured from the separation of the first and last peak in the waveform, will be used as the reference. Dividing this sequence duration into five 360 ps frames, the waveform exhibits a center frequency of ~2.77 GHz. To achieve this waveform, the pulse shaping lens is positioned with $d_1 = 13.25$ cm and $d_2 = 16.75$

cm (please reference Fig. 4.1), resulting in a frequency modulation of ~-0.20 nm/ps in the pulse shaper. For this value of frequency modulation, the predicted stretching factor as given by Eq. (4.3) is approximately 18.7. The measured 1.8 ns waveform shows excellent agreement with this predicted value. Now, by repositioning the pulse shaping lens, this waveform may be contracted or dilated in time. For example, when the pulse shaping lens is positioned 5 mm from the reference position (d_1 = 13.75 cm, d_2 = 16.25 cm), the top electrical waveform results. The waveform is contracted from 1.8 ns to approximately 1.5 ns which again shows excellent agreement with the predicted duration of ~1.49 ns. Again, dividing the waveform duration into five equal frames, this waveform exhibits a ~ 3.33 GHz center frequency. To dilate the waveform, the lens is displaced -2.5 mm from the reference position (d_1 = 13 cm, d_2 = 17 cm). In this position, the applied frequency modulation increases in magnitude to approximately -0.22 nm/ps, yielding a stretching factor of ~20.5. The measured ~2 ns (~2.5 GHz) electrical waveform is shown in the bottom trace. Though we focus on time-domain waveforms here, it should be noted that the entire broadband RF spectrum is, in fact, tuned in frequency space. This clearly illustrates how, through very small adjustments to the pulse shaper, the temporal duration and broadband RF spectrum of arbitrarily shaped waveforms can easily be tuned over a range greater than ±10%.

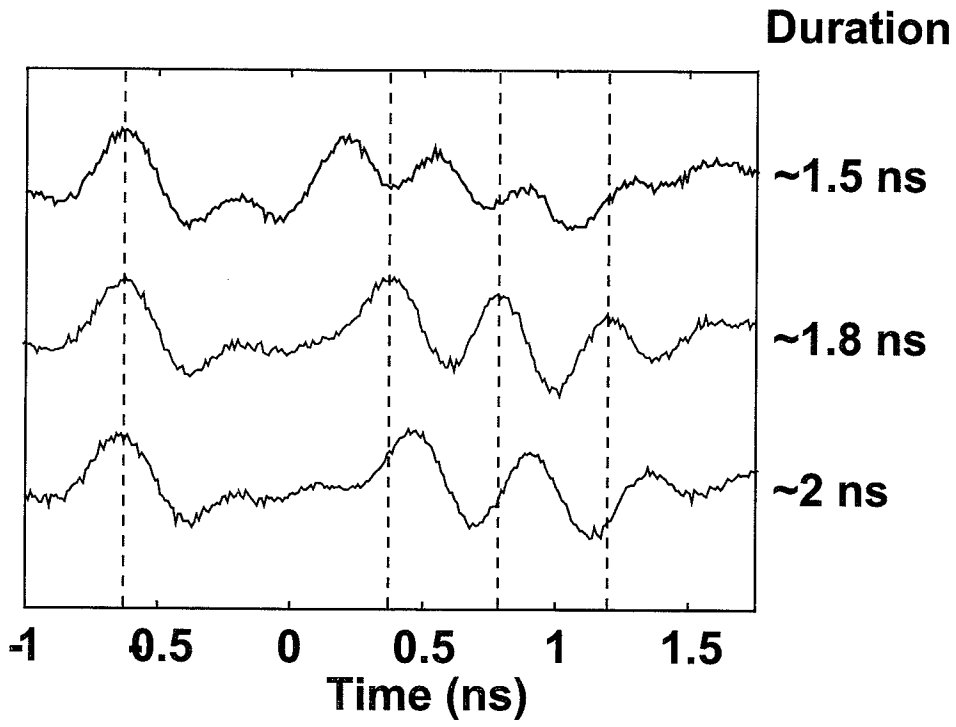

Fig. 4.6. Tunability of electrical waveform duration. For small changes in pulse shaping lens position, ± 10 % changes in waveform duration are easily attained. Above, the electrical waveform is scaled from 1.5 - 2 ns, amounting to a center frequency variation over the range of $\sim$ 3.3 - 2.5 GHz, for a change in lens position of 7.5 mm.

5. SUMMARY AND FUTURE RESEARCH DIRECTIONS

We have demonstrated a novel, direct space-to-time pulse shaper operating for the first time in the 1.5 μm optical communications band. Through the use of a diffractive optical element for spatial pattern generation and a telescopic, fiber-coupled configuration, we demonstrate, for the first time to our knowledge, pulse shaping over a temporal window in excess of 100 ps. High-rate, equal amplitude burst optical data packets, as well as continuous 100 GHz optical pulse sequences generated with this pulse shaping apparatus could find application in high-speed optical communications systems.

We also demonstrate this pulse shaping apparatus to be an enabling technology for generation of arbitrary electromagnetic waveforms in the microwave and millimeter-wave frequency range. By driving a high-speed optical-to-electrical converter with appropriately tailored optical pulse sequences from our DST pulse shaper, we obtain amplitude-equalized broadband burst and continuous millimeter electrical waveforms at center frequencies approaching 50 GHz. By controlling the position and spacing of pulses in the driving optical pulse sequence, we demonstrate arbitrary phase- and frequency-modulation of the output millimeter-wave signals. Additionally, by exploiting the physics of the pulse shaping apparatus and dispersive stretching of the pulse shaper output, we extend our electromagnetic waveform generation technique to arbitrary waveforms in the GHz range. We predict our technique, which allows reprogrammable cycle-by-cycle electrical waveform synthesis, could find application in a number of RF communication schemes, as well as pulse radar and electronic countermeasures.

While many novelties have been implemented in our current 1.5 μm direct space-to-time pulse shaper, other additional improvements could further increase the system

performance for potential applications. In the near term, inclusion of a spatial light modulator (specifically, an available liquid crystal modulator) will enable the input spatial patterns, and hence, the output optical pulse sequences to be altered via computer control. This will also enable more thorough equalization of the optical pulse sequences through finer control of the intensity of the applied spatial pattern. In the longer term, high-speed optoelectronic modulator arrays, specifically one operating at a rate of $\sim$10 GHz, will enable the continuous 100 GHz optical pulse sequences to be reprogrammed on a frame-by-frame basis. This will not only allow generation of truly independent high-rate optical data, but will allow generation of continuous arbitrary millimeter waveforms exhibiting independent modulation from frame to frame. For electromagnetic waveform generation applications, the overall system efficiency could be improved through the use of high-speed, free-space travelling wave photodetectors [55]. This would allow the multi-wavelength output capabilities of the pulse shaper to be used to increase the optical-to-electrical conversion efficiency through use of multiple output channels driving the same photodiode.

Regarding future applications, there are several specifically in the area of microwave photonics. Millimeter-wave / microwave generation through the use of photonic crystals, as proposed in [46], could take advantage of both periodic and aperiodic tailored optical pulse sequences. Also, high-rate photonic A/D applications could be demonstrated using high-rate pulse sequences generated in our system.

LIST OF REFERENCES

[1] A. M. Weiner, "Femtosecond pulse shaping using spatial light modulators," *Rev. Sci. Instrum.*, vol. 71, p. 1929, 2000.

[2] B. Colombeau, M. Vampouille, and C. Froehly, "Shaping of short laser pulses by passive optical fourier techniques," *Opt. Commun.*, vol. 19, pp. 201–204, 1976.

[3] C. Dorrer, E. M. Kosik, and I. A. Walmsley, "Direct space-time characterization of the electric fields of ultrashort optical pulses," *Opt. Lett.*, vol. 27, pp. 548–550, 2002.

[4] C. Dorrer and I. A. Walmsley, "Simple linear technique for the measurement of space-time coupling in ultrashort optical pulses," *Opt. Lett.*, vol. 27, pp. 1947–1949, 2002.

[5] M. M. Wefers and K. A. Nelson, "Space-time profiles of shaped ultrafast optical waveforms," *IEEE J. Quantum Electron.*, vol. 32, pp. 161–172, 1996.

[6] R. Piestun and D. A. B. Miller, "Spatiotemporal control of ultrashort optical pulses by refractive-diffractive-dispersive structured optical elements," *Opt. Lett.*, vol. 26, pp. 1373–1375, 2001.

[7] D. E. Leaird and A. M. Weiner, "Femtosecond optical packet generation by a direct space-to-time pulse shaper," *Opt. Lett.*, vol. 24, pp. 853–855, 1999.

[8] D. E. Leaird and A. M. Weiner, "Femtosecond direct space-to-time pulse shaping," *IEEE J. Quantum Electron.*, vol. 37, pp. 494–504, 2001.

[9] J. D. McKinney, D. E. Leaird, and A. M. Weiner, "1.5 μm direct space-to-time pulse shaper utilizing a diffractive optical element for pattern generation," in *Conference on Lasers and Electro-Optics (CLEO), OSA Technical Digest, Postconference Edition*, vol. 73 of *OSA Trends in Optics and Photonics (TOPS)*, pp. 115–116, Optical Society of America, 2002.

[10] T. F. Carruthers and I. N. D. III, "10-ghz, 1.3-ps erbium fiber laser employing soliton pulse shortening," *Opt. Lett.*, vol. 21, pp. 1927–1929, 1996.

[11] J. D. McKinney, D. E. Leaird, and A. M. Weiner, "Millimeter-wave arbitrary waveform generation with a direct space-to-time pulse shaper," *Opt. Lett.*, vol. 27, pp. 1345–1347, 2002.

[12] J. D. McKinney, D. S. Seo, and A. M. Weiner, "Photonically assisted generation of continuous arbitrary millimetre electromagnetic waveforms," *Electron. Lett.*, vol. 39, pp. 309–311, 2003.

[13] D. E. Leaird and A. M. Weiner, "Chirp control in the direct space-to-time pulse shaper," *Opt. Lett.*, vol. 25, pp. 850–852, 2000.

[14] J. D. McKinney, D. S. Seo, D. E. Leaird, and A. M. Weiner, "Photonically assisted burst and continuous arbitrary millimeter waveform generation via direct space-to-time pulse shaping," in *Ultrafast Electronics and Optoelectronics*, OSA Technical Digest, pp. 109–112, Optical Society of America, 2003. [INVITED].

[15] J. D. McKinney, D. S. Seo, D. E. Leaird, and A. M. Weiner, "Photonically assisted generation of arbitrary millimeter-wave and microwave electromagnetic waveforms via direct space-to-time optical pulse shaping," *Submitted to IEEE J. Lightwave Technol. Microwave Photonics Special Issue*, 2003.

[16] P. Emplit, J. P. Hamaide, F. R. ad C. Froehly, and A. Barthelemy, "Picosecond steps and dark pulses through nonlinear single mode fibers," *Opt. Commun.*, vol. 62, pp. 374–379, 1987.

[17] P. Emplit, M. Haelterman, and J. P. Hamaide, "Picosecond dark soliton over a 1-km fiber at 850 nm," *Opt. Lett.*, vol. 18, pp. 1047–1049, 1993.

[18] R. N. Thurston, J. P. Heritage, A. M. Weiner, and W. J. Tomlinson, "Analysis of picosecond pulse shape synthesis by spectral masking in a grating pulse compressor," *IEEE J. Quantum Electron.*, vol. 22, pp. 682–696, 1986.

[19] O. E. Martinez, "Pulse distortions in tilted pulse schemes for ultrashort pulses," *Opt. Commun.*, vol. 59, pp. 229–232, 1986.

[20] D. E. Leaird, *Direct space-to-time pulse shaping for ultrafast optical waveform generation.* PhD thesis, Purdue University, December 2000.

[21] O. E. Martinez, "Grating and prism compressors in the case of finite beam size," *J. Opt. Soc. Am. B*, vol. 3, pp. 929–934, 1986.

[22] C.-L. Chen, *Elements of Optoelectronics & Fiber Optics.* Chicago: Richard D. Irwin, a Times Mirror Higher Education Group, Inc. company, 1996.

[23] J. T. Verdeyen, *Laser Electronics.* New Jersey: Prentice-Hall, Inc., third ed., 1995.

[24] D. E. Leaird, A. M. Weiner, S. Shen, A. Sugita, S. Kamei, M. Ishii, and K. Okamoto, "High repetition rate femtosecond wdm pulse generation using direct space-to-time pulse shapers and arrayed waveguide gratings," *Opt. Quantum Electron.*, vol. 33, pp. 811–826, 2001.

[25] K. Tamura, H. A. Haus, and E. P. Ippen, "Self-starting additive pulse modelocking erbium fiber ring laser," *Electron. Lett.*, vol. 28, pp. 2226–2228, 1992.

[26] J. N. Mait, "Design of binary-phase and multiphase fourier gratings for array generation," *J. Opt. Soc. Am. A*, vol. 7, pp. 1514–1528, 1990.

[27] U. Krackhardt and N. Streibl, "Design of damman-gratings for array generation," *Opt. Commun.*, vol. 74, pp. 31–36, 1989.

[28] A. M. Weiner, D. E. Leaird, J. S. Patel, and J. R. Wullert-II, "Programmable shaping of femtosecond optical pulses by use of 128-element liquid crystal phase modulator," *IEEE J. Quantum Electron.*, vol. 28, pp. 908–920, 1992.

[29] S. Kawanishi, "Ultrahigh-speed optical time-division-multiplexed transmission technology based on optical signal processing," *IEEE J. Quantum Electron.*, vol. 34, pp. 2064–2079, 1998.

[30] M. Nakazawa, T. Yamamoto, and K. R. Tamura, "Ultrahigh-speed otdm transmission beyond 1 terabit-per-second using a femtosecond pulse train," *IEICE Transactions on Electronics*, vol. E85-C, pp. 117–125, 2002.

[31] P. Petropoulos, M. Ibsen, M. N. Zervas, and D. Richardson, "Generation of a 40-ghz pulse stream by pulse multiplication with a sampled fiber bragg grating," *Opt. Lett.*, vol. 25, pp. 521–523, 2000.

[32] J. Lee, P. The, Z. Yusoff, M. Ibsen, W. Belardi, T. Munro, and D. Richardson, "A holey fiber-based nonlinear thresholding device for optical cdma receiver performance enhancement," *IEEE Photon. Technol. Lett.*, vol. 14, p. 876, 2002.

[33] J. C. Twichell, J. L. Wasserman, P. W. Juodawlkis, G. E. Betts, and R. C. Williamson, "High-linearity 208-ms/s photonic analog-to-digital converter using 1-to-4 optical time-division demultiplexers," *IEEE Photon. Technol. Lett.*, vol. 13, pp. 714–716, 2001.

[34] T. R. Clark and M. L. Dennis, "Toward a 100-gsample/s photonic a-d converter," *IEEE Photon. Technol. Lett.*, vol. 13, pp. 236–238, 2001.

[35] A. S. Bhushan, P. V. Kelkar, B. Jalali, O. Boyraz, and M. Islam, "130-gsa/s photonic analog-to-digital converter with time stretch preprocessor," *IEEE Photon. Technol. Lett.*, vol. 14, pp. 684–686, 2002.

[36] C. Lim, A. Nirmalathas, D. Novak, R. Waterhouse, and G. Yoffe, "Millimeter-wave broad-band fiber-wireless system incorporating baseband data transmission over fiber and remote lo delivery," *J. Lightwave Technol.*, vol. 18, pp. 1355–1363, 2000.

[37] R. A. Griffin, H. M. Salgado, P. M. Lane, and J. J. O'Reilly, "System capacity for millimeter-wave radio-over-fiber distribution employing an optically supported pll," *J. Lightwave Technol.*, vol. 17, pp. 2480–2487, 1999.

[38] M. Z. Win and R. A. Scholtz, "Ultra-wide bandwidth time-hopping spread-spectrum impulse radio for wireless multiple-access communications," *IEEE Trans. Commun.*, vol. 48, pp. 679–691, 2000.

[39] G. Morris and L. Harkness, eds., *Airborne Pulsed Doppler Radar.* Artech House, Inc., 2nd ed., 1996.

[40] S. Poinsot, H. Porte, J.-P. Goedgebuer, W. T. Rhodes, and B. Boussert, "Contiuous radio-frequency tuning of an optoelectronic oscillator with dispersive feedback," *Opt. Lett.*, vol. 27, pp. 1300–1302, 2002.

[41] T. Yilmaz, C. M. DePriest, T. Turpin, J. H. Abeles, and P. J. Delfyett, "Toward a photonic arbitrary wavefrm generator using a modelocked external cavity semiconductor laser," *IEEE Photon. Technol. Lett.*, vol. 14, pp. 1608–1610, 2002.

[42] Y. Li, S. M. G. Amarildo J. C. Viera, and P. R. Herczfeld, "Rapidly tunable millimeter-wave optical transmitter for lidar-radar," *IEEE Trans. Microwave Theory Tech.*, vol. 49, pp. 2048–2054, 01.

[43] Y. J. Wen, H. F. Liu, D. Novak, and Y. Ogawa, "Millimeter-wave signal generation from a monolithic semiconductor laser via subharmonic optical injection," *IEEE Photon. Technol. Lett.*, vol. 12, pp. 1058–1060, 2000.

[44] J. Hong and R. Hui, "Tunable millimeter-wave generation with subharmonic injection locking in two-section strongly gain-coupled dfb lasers," *IEEE Photon. Technol. Lett.*, vol. 12, pp. 543–545, 2000.

[45] T. Kawanishi, S. Oikawa, and M. Izutsu, "Reciprocating optical modulation for millimeter-wave generation by using a dual-section fiber bragg grating," *J. Lightwave Technol.*, vol. 20, pp. 1408–1415, 2002.

[46] Y. qing Lu, M. Xiao, and G. J. Salamo, "Coherent microwave generation in a nonlinear photonic crystal," *IEEE J. Quantum Electron.*, vol. 38, pp. 481–485, 2002.

[47] B. Jalali, P. Kelkar, and V. Saxena, "Photonic arbitrary waveform generator," in *Proceedings of the 14th Annual Meeting of the IEEE*, vol. 1, 2001.

[48] J. D. McKinney, D. E. Leaird, and A. M. Weiner, "Microwave arbitrary waveform generation using a direct space-to-time optical pulse shaper," in *The Thirteenth International Conference on Ultrafast Phenomena, OSA Technical Digest, Post-conference Edition*, vol. 72 of *OSA Trends in Optics and Photonics (TOPS)*, pp. 205–207, Optical Society of America, 2002.

[49] J. D. McKinney, D. S. Seo, and A. M. Weiner, "100 ghz pulse sequence generation from a 1.5 μm direct space-to-time pulse shaper," in *Ultrafast Electronics and Optoelectronics*, OSA Technical Digest, pp. 25–28, Optical Society of America, 2003.

[50] Y. Liu, S. G. Park, and A. M. Weiner, "Terahertz waveform synthesis via optical pulse shaping," *IEEE J. Select. Topics Quantum Electron.*, vol. 2, p. 709, 1996.

[51] J. Chou, Y. Han, and B. Jalali, "Adaptive rf-photonic arbitrary waveform generator," *IEEE Photon. Technol. Lett.*, vol. 15, pp. 581–583, 2003.

[52] C. V. Bennet and B. H. Kolner, "Upconversion time microscope demonstrating 103x magnification of femtosecond waveforms," *Opt. Lett.*, vol. 24, pp. 783–785, 1999.

[53] B. H. Kolner and M. Nazarathy, "Temporal imaging with a time lens," *Opt. Lett.*, vol. 14, pp. 630–632, 1989.

[54] B. H. Kolner, "Generalization of the concepts of focal length and f-number to space and time," *J. Opt. Soc. Am. A*, vol. 11, pp. 3229–3234, 1994.

[55] T. Merlet, D. Dolfi, P. Collot, J. Nagle, and J. P. Huignard, "A high-speed free-space traveling wave photodetector," *Appl. Phys. Lett.*, vol. 72, pp. 1134–1136, 1998.

[56] J. W. Goodman, *Introduction to Fourier Optics.* New York: The McGraw-Hill Companies, Inc., second ed., 1996.

[57] S. Ramo, J. R. Whinnery, and T. VanDuzer, *Fields and Waves in Communication Electronics.* New York: John Wiley and Sons, Inc., third ed., 1994.

A. DIFFRACTION ANALYSIS OF THE TELESCOPIC DIRECT SPACE-TO-TIME PULSE SHAPER

A.1 Mathematical Relations

This section includes the relevant Fresnel diffraction integrals and lens effects, Fourier transform definitions, and relations.

A.1.1 Fourier Relations

The Fourier transform definitions used in the diffraction analysis are shown below. These were chosen given the convention of $e^{j(\omega t - kx)}$.

$$F(\omega) = \frac{1}{\sqrt{2\pi}} \int_{-\infty}^{\infty} dt\ f(t)\ e^{-j\omega t} \tag{A.1}$$

$$f(t) = \frac{1}{\sqrt{2\pi}} \int_{-\infty}^{\infty} d\omega\ F(\omega)\ e^{j\omega t} \tag{A.2}$$

$$S(\xi) = \frac{1}{\sqrt{2\pi}} \int_{-\infty}^{\infty} dx\ s(x)\ e^{j\xi x} \tag{A.3}$$

$$s(x) = \frac{1}{\sqrt{2\pi}} \int_{-\infty}^{\infty} d\xi\ S(\xi)\, e^{-j\xi x} \tag{A.4}$$

Several Fourier transform relations were also needed during the course of the diffraction analysis. These, separated by time and space, are given below.

$$x(t - t_0) \Leftrightarrow e^{-j\omega t_0} X(\omega) \tag{A.5}$$

$$e^{j\omega_0 t} x(t) \Leftrightarrow X(\omega - \omega_0) \tag{A.6}$$

$$x(at) \Leftrightarrow \frac{1}{|a|} X\left(\frac{\omega}{a}\right) \tag{A.7}$$

$$x(-t) \Leftrightarrow X(-\omega) \tag{A.8}$$

$$s(x - x_0) \Leftrightarrow e^{j\xi x_0} S(\xi) \tag{A.9}$$

$$e^{-j\xi_0 x} s(x) \Leftrightarrow S(\xi - \xi_0) \tag{A.10}$$

$$s(ax) \Leftrightarrow \frac{1}{|a|} S\left(\frac{\xi}{a}\right) \tag{A.11}$$

$$s(-x) \Leftrightarrow S(-\xi) \tag{A.12}$$

A.1.2 Fresnel Diffraction

To treat the propagation of a field from one plane in space to another, through a distance z, the Fresnel diffraction integral [56] is used. The integral is given below.

$$E(x_2) = C_z \int_{-\infty}^{\infty} dx_1 \; E(x_1) \, e^{-j\frac{k}{2z}x_1^2} e^{j\frac{k}{z}x_2 x_1} \tag{A.13}$$

where

$$C_z = \frac{e^{-jkz}}{\sqrt{j\lambda z}} e^{-j\frac{k}{2z}x_2^2} \tag{A.14}$$

$$= C_z' e^{-j\frac{k}{2z}x_2^2} \tag{A.15}$$

In addition to the diffraction integral, the lenses will be treated as thin lenses, imparting a phase of

$$t_l = e^{j\frac{k}{2f}x^2} \tag{A.16}$$

onto the incident field. The assumption of thin lenses allows the x coordinate before and after the lens to be set equal.

Also, a useful integral [57]

$$\Gamma = \int_{-\infty}^{\infty} dx \; e^{j(\alpha x^2 + \beta x)} = \sqrt{\frac{j\pi}{\alpha}} e^{-j\frac{\beta^2}{4\alpha}} \tag{A.17}$$

$$= C_\Gamma e^{-j\frac{\beta^2}{4\alpha}} \tag{A.18}$$

will be used to simplify certain integral expressions in the course of the analysis.

A.2 Diffraction Analysis of the DST shaper

Please reference Figs. 2.2, 2.3 for the relevant plane and lens definitions used during the course of this analysis. It is assumed that all distances may vary in this analysis. We begin by assuming a spatially patterned, monochromatic field $s(x)$ at plane $\mathbf{P_2}$ just after the diffraction grating. The inclusion of the short-pulse input (polychromatic field) will be treated in the following section. The notation $\mathbf{E_p}$ will be used to denote the field at plane $\mathbf{P_p}$.

Propagating this field from $\mathbf{P_2}$ to $\mathbf{P_3}$:

$$\mathbf{E_3}(x) = C_1' e^{-j\frac{k}{2d_1}x^2} \int_{-\infty}^{\infty} dx'\; s(x')\, e^{-j\frac{k}{2d_1}x'^2} e^{j\frac{k}{d_1}x'x} \tag{A.19}$$

Including the phase transformation by L_1

$$\mathbf{E_3}(x) = C_1' e^{-j\frac{k}{2}\left(\frac{1}{d_1}-\frac{1}{f_1}\right)x^2} \int_{-\infty}^{\infty} dx'\; s(x')\, e^{-j\frac{k}{2d_1}x'^2} e^{j\frac{k}{d_1}x'x}. \tag{A.20}$$

Now, propagating the field $\mathbf{E}_3$ from $\mathbf{P_4}$ to $\mathbf{P_5}$:

$$\mathbf{E_5}(x) = C_2' C_1' e^{-j\frac{k}{2d_2}x^2} \int_{-\infty}^{\infty} dx'' \left\{ e^{-j\frac{k}{2}\left(\frac{1}{d_1}-\frac{1}{f_1}\right)x''^2} \int_{-\infty}^{\infty} dx'\; s(x')\, e^{-j\frac{k}{2d_1}x'^2} e^{j\frac{k}{d_1}x'x''} \right\} e^{-j\frac{k}{2d_2}x''^2} e^{j\frac{k}{d2}x''x}. \tag{A.21}$$

Interchanging the order of integration we have

$$\mathbf{E_5}(x) = C_1' C_2' e^{-j\frac{k}{2d_2}x^2} \int_{-\infty}^{\infty} dx'\; s(x')\, e^{-j\frac{k}{2d_1}x'^2} \int_{-\infty}^{\infty} dx''\; e^{-j\frac{k}{2}\left(\frac{1}{d_1}+\frac{1}{d_2}-\frac{1}{f_1}\right)x''^2} e^{jk\left(\frac{x'}{d_1}+\frac{x}{d_2}\right)x''} \tag{A.22}$$

Performing the integral over x'' using the simplification A.18, with

$$\alpha = -\frac{k}{2}\left(\frac{1}{d_1}+\frac{1}{d_2}-\frac{1}{f_1}\right) \tag{A.23}$$

$$\beta = k\left(\frac{x'}{d_1}+\frac{x}{d_2}\right) \tag{A.24}$$

$$\mathbf{E_5}(x) = C_{\Gamma_1} C_2' C_1' e^{-j\frac{k}{2d_2}\left(\frac{f_1-d_1A_1}{f_1}\right)x^2} \int_{-\infty}^{\infty} dx'\; s'(x')\, e^{j\frac{k}{f_1}A_1x'x} \tag{A.25}$$

where

$$s'(x') = s(x')\, e^{-j\frac{k}{2d_1}\left(\frac{f_1-d_2A_1}{f_1}\right)x'^2} \tag{A.26}$$

$$A_1 = \frac{f_1^2}{f_1d_1 + f_1d_2 - d_1d_2}. \tag{A.27}$$

Given the spatial Fourier transform relation A.3, the field just before the output waveguide (slit) is

$$\mathbf{E_5}(x) = \sqrt{2\pi}C_{\Gamma_1}C_2'C_1'e^{-j\frac{k}{2d_2}\left(\frac{f_1-d_1A_1}{f_1}\right)x^2}S'\left(\frac{k}{f_1}A_1x\right) \tag{A.28}$$

$$\mathbf{E_5}(x) = C_{DST}e^{-j\frac{k}{2d_2}\left(\frac{f_1-d_1A_1}{f_1}\right)x^2}S'\left(\frac{k}{f_1}A_1x\right) \tag{A.29}$$

Now, the telescope after the DST shaper will be treated. Propagating the field $\mathbf{E_5}(x)$ from $\mathbf{P_5}$ to $\mathbf{P_6}$:

$$\mathbf{E_6}(x) = C_3'e^{-j\frac{k}{2d_3}x^2}C_{DST}\int_{-\infty}^{\infty}dx'\; S'\left(\frac{k}{f_1}A_1x'\right)e^{-j\frac{k}{2d_2}\left(\frac{f_1-d_1A_1}{f_1}\right)x'^2}e^{-j\frac{k}{2d_3}x'^2}e^{j\frac{k}{d_3}x'x} \tag{A.30}$$

Including the phase transformation by L_2

$$\mathbf{E_6}(x) = C_3'C_{DST}e^{-j\frac{k}{2}\left(\frac{1}{d_3}-\frac{1}{f_2}\right)x^2}\int_{-\infty}^{\infty}dx'\; S'\left(\frac{k}{f_1}A_1x'\right)e^{-j\frac{k}{2}\left(\frac{f_1-d_1A_1}{f_1d_2}+\frac{1}{d_3}\right)x'^2}e^{j\frac{k}{d_3}x'x} \tag{A.31}$$

Now propagating the field $\mathbf{E_6}(x)$ from $\mathbf{P_7}$ to $\mathbf{P_8}$:

$$\mathbf{E_8}(x) = C_4'C_3'C_{DST}e^{-j\frac{k}{2d_4}x^2}\int_{-\infty}^{\infty}dx''e^{-j\frac{k}{2}\left(\frac{1}{d_3}+\frac{1}{d_4}-\frac{1}{f_2}\right)x''^2}e^{j\frac{k}{d_4}x''x} \left\{\int_{-\infty}^{\infty}dx'\; S'\left(\frac{k}{f_1}A_1x'\right)e^{-j\frac{k}{2}\left(\frac{f_1-d_1A_1}{f_1d_2}+\frac{1}{d_3}\right)x'^2}e^{j\frac{k}{d_3}x'x}\right\} \tag{A.32}$$

Interchanging the order of integration we have

$$\mathbf{E_8}(x) = C_4'C_3'C_{DST}e^{-j\frac{k}{2d_4}x^2}\int_{-\infty}^{\infty}dx'\; S'\left(\frac{k}{f_1}A_1x'\right)e^{-j\frac{k}{2}\left(\frac{f_1-d_1A_1}{f_1d_2}+\frac{1}{d_3}\right)x'^2} \int_{-\infty}^{\infty}dx''\; e^{-j\frac{k}{2}\left(\frac{1}{d_3}+\frac{1}{d_4}-\frac{1}{f_2}\right)x''^2}e^{jk\left(\frac{x'}{d_3}+\frac{x}{d_4}\right)x''} \tag{A.33}$$

Performing the integral over x'' using the simplification A.18, with

$$\alpha = -\frac{k}{2}\left(\frac{1}{d_3}+\frac{1}{d_4}-\frac{1}{f_2}\right) \tag{A.34}$$

$$\beta = k\left(\frac{x'}{d_3}+\frac{x}{d_4}\right) \tag{A.35}$$

$$\mathbf{E_8}(x) = C_{\Gamma_2}C_4'C_3'C_{DST}e^{-j\frac{k}{2d_4}\left(\frac{f_2-d_3A_2}{f_2}\right)x^2} \tag{A.36}$$

$$\int_{-\infty}^{\infty} dx'\ S'\left(\frac{k}{f_1}A_1x'\right)e^{-j\frac{k}{2}\left(\frac{f_1-d_1A_1}{f_1d_2}+\frac{f_2-d_4A_2}{f_2d_3}\right)x'^2}e^{j\frac{k}{f_2}A_2x'x} \tag{A.37}$$

$$A_2 = \frac{f_2^2}{f_2d_3+f_2d_4-d_3d_4}. \tag{A.38}$$

If if the quadratic phase term above is defined to be $P_2(x)$,

$$P_2(x) = e^{-j\frac{k}{2}\left(\frac{f_1-d_1A_1}{f_1d_2}+\frac{f_2-d_4A_2}{f_2d_3}\right)x^2}, \tag{A.39}$$

$\mathbf{E_8}(x)$ is now expressed as

$$\mathbf{E_8}(x) = C_{\Gamma_2}C_4'C_3'C_{DST}e^{-j\frac{k}{2d_4}\left(\frac{f_2-d_3A_2}{f_2}\right)x^2}\int_{-\infty}^{\infty} dx'\ S'\left(\frac{k}{f_1}A_1x'\right)P_2(x')\,e^{j\frac{k}{f_2}A_2x'x}. \tag{A.40}$$

Using the spatial Fourier transform relation A.4 and the relation A.11, and the change of variables

$$\xi = -\frac{k}{f_2}A_2x',\ d\xi = -\frac{k}{f_2}A_2dx' \Rightarrow dx' = -\frac{f_2}{kA_2}d\xi \tag{A.41}$$

$$\mathbf{E_8}(x) = \frac{C_{\Gamma_2}f_2}{kA_2}C_4'C_3'C_{DST}\int_{-\infty}^{\infty} d\xi\ \left[S'\left(-\frac{f_2}{f_1}\frac{A_1}{A_2}\xi\right)P_2\left(-\frac{f_2}{kA_2}\xi\right)\right]e^{-j\xi x} \tag{A.42}$$

$$\mathbf{E_8}(x) = \frac{\sqrt{2\pi}}{kA_1}\frac{f_1}{f_2}C_{\Gamma_2}C_4'C_3'C_{DST}e^{-j\frac{k}{2d_4}\left(\frac{f_2-d_3A_2}{f_2}\right)x^2}\left[s'\left(-\frac{f_1}{f_2}\frac{A_2}{A_1}x\right)*p_2\left(-\frac{k}{f_2}A_2x\right)\right]. \tag{A.43}$$

$\mathbf{E_8}(x)$ is the field halfway through the telescope. It should be noted that the field is proportional to a scaled, spatially-reversed version of the initial field just after the

grating. Now treat the final stage of the telescope, by first propagating the field $\mathbf{E_8}(x)$ from $\mathbf{P_8}$ to $\mathbf{P_9}$:

$$\mathbf{E_9}(x) = \frac{\sqrt{2\pi}}{kA_1}\frac{f_1}{f_2}C_{\Gamma_2}C_5'C_4'C_3'C_{DST}e^{-j\frac{k}{2d_5}x^2}$$
$$\int_{-\infty}^{\infty} dx'\, e^{-j\frac{k}{2d_4}\left(\frac{f_2-d_3A_2}{f_2}\right)x'^2}\left[s'\left(-\frac{f_1}{f_2}\frac{A_2}{A_1}x'\right) * p_2\left(-\frac{k}{f_2}A_2x'\right)\right]e^{-j\frac{k}{2d_5}x'^2}e^{j\frac{k}{d_5}x'x}. \quad \text{(A.44)}$$

Accounting for the phase transformation due to lens L_3,

$$\mathbf{E_9}(x) = \frac{\sqrt{2\pi}}{kA_1}\frac{f_1}{f_2}C_{\Gamma_2}c_5'C_4'C_3'C_{DST}e^{-j\frac{k}{2}\left(\frac{1}{d_5}-\frac{1}{f_3}\right)x^2}$$
$$\int_{-\infty}^{\infty} dx'\, e^{-j\frac{k}{2}\left(\frac{f_2-d_3A_2}{f_2d_4}+\frac{1}{d_5}\right)x'^2}\left[s'\left(-\frac{f_1}{f_2}\frac{A_2}{A_1}x'\right) * p_2\left(-\frac{k}{f_2}A_2x'\right)\right]e^{j\frac{k}{d_5}x'x}. \quad \text{(A.45)}$$

Propagating the field to $\mathbf{P_{11}}$:

$$\mathbf{E_{11}}(x) = \frac{\sqrt{2\pi}}{kA_1}\frac{f_1}{f_2}C_{\Gamma_2}C_6'C_5'C_4'C_3'C_{DST}e^{-j\frac{k}{2d_6}x^2}\int_{-\infty}^{\infty} dx''e^{-j\frac{k}{2}\left(\frac{1}{d_5}+\frac{1}{d_6}-\frac{1}{f_3}\right)x''^2}e^{j\frac{k}{d_6}x''x}$$
$$\left\{\int_{-\infty}^{\infty} dx'\, \left[s'\left(-\frac{f_1}{f_2}\frac{A_2}{A_1}x'\right) * p_2\left(-\frac{k}{f_2}A_2x'\right)\right]e^{-j\frac{k}{2}\left(\frac{f_2-d_3A_2}{f_2d_4}+\frac{1}{d_5}\right)x'^2}e^{j\frac{k}{d_5}x'x}\right\}. \quad \text{(A.46)}$$

Interchanging the order of integration, performing the integral over x'' using A.18, and simplifying,

$$\alpha = -\frac{k}{2}\left(\frac{1}{d_5}+\frac{1}{d_6}-\frac{1}{f_3}\right) \quad \text{(A.47)}$$

$$\beta = k\left(\frac{x'}{d_5}+\frac{x}{d_6}\right) \quad \text{(A.48)}$$

$$\mathbf{E_{11}}(x) = \frac{\sqrt{2\pi}}{kA_1}\frac{f_1}{f_2}C_{\Gamma_3}C_{\Gamma_2}C_6'C_5'C_4'C_3'C_{DST}e^{-j\frac{k}{2d_6}\left(\frac{f_3-d_5A_3}{f_3}\right)x^2}$$
$$\int_{-\infty}^{\infty} dx'\, \left[s'\left(-\frac{f_1}{f_2}\frac{A_2}{A_1}x'\right) * p_2\left(-\frac{k}{f_2}A_2x'\right)\right]e^{-j\frac{k}{2}\left(\frac{f_2-d_3A_2}{f_2d_4}+\frac{f_3-d_6A_3}{f_3d_5}\right)x'^2}e^{j\frac{k}{f_3}A_3x'x} \quad \text{(A.49)}$$

$$A_3 = \frac{f_3^2}{f_3d_5+f_3d_6-d_5d_6} \quad \text{(A.50)}$$

To further simplify this expression, define

$$\begin{aligned} s''\left(-\frac{f_1}{f_2}\frac{A_2}{A_1}x\right) &= s'\left(-\frac{f_1}{f_2}\frac{A_2}{A_1}x\right)e^{-j\frac{k}{2}\left(\frac{f_2-d_3A_2}{f_2d_4}+\frac{f_3-d_6A_3}{f_3d_5}\right)x^2} \\ &= s\left(-\frac{f_1}{f_2}\frac{A_2}{A_1}x\right)e^{-j\frac{k}{2}\left[\frac{f_1^2}{f_2^2}\frac{A_2^2}{A_1^2}\left(\frac{f_1-d_2A_1}{f_1d_1}\right)+\frac{f_2-d_3A_2}{f_2d_4}+\frac{f_3-d_6A_3}{f_3d_5}\right]x^2} \end{aligned} \tag{A.51}$$

and

$$p_3(x) = p_2\left(-\frac{k}{f_2}A_2x\right)e^{-j\frac{k}{2}\left(\frac{f_2-d_3A_2}{f_2d_4}+\frac{f_3-d_6A_3}{f_3d_5}\right)x^2}. \tag{A.52}$$

To evaluate $p_3(x)$, an expression for $p_2\left(-kA_2x/f_2\right)$ is needed. The expression of A.39 can be written as

$$\begin{aligned} P_2(x) &= e^{-\alpha x^2} \\ \alpha &= j\frac{k}{2}\left(\frac{f_1-d_1A_1}{f_1d_2}+\frac{f_2-d_4A_2}{f_2d_3}\right) \end{aligned} \tag{A.53}$$

Using the relation for the Fourier transform of a Gaussian,

$$e^{-\alpha x^2} \overset{\mathcal{F}}{\Leftrightarrow} e^{-\frac{\xi^2}{4\alpha}} \tag{A.54}$$

and evaluating at $\xi = -kA_2x/f2$, the Fourier transform of $P_2(x)$ is given by

$$p_2\left(-\frac{k}{f_2}A_2x\right) = e^{j\frac{k}{2}A_2^2\frac{d_2d_3}{f_2^2}\left[\frac{1}{d_3\left(\frac{f_1-d_1A_1}{f_1}\right)+d_2\left(\frac{f_2-d_4A_2}{f_2}\right)}\right]x^2} \tag{A.55}$$

Inserting the above expression for $p_2\left(-kA_2x/f2\right)$ into A.52,

$$p_3(x) = e^{-j\frac{k}{2}\left[\frac{f_2-d_3A_2}{f_2d_4}+\frac{f_3-d_6A_3}{f_3d_5}-A_2^2\frac{d_2d_3}{f_2^2}\frac{1}{d_3\left(\frac{f_1-d_1A_1}{f_1}\right)+d_2\left(\frac{f_2-d_4A_2}{f_2}\right)}\right]x^2}. \tag{A.56}$$

Given these definitions, the spatial Fourier transform relation A.4, and the scaling property A.11,

$$\begin{aligned} \mathbf{E_{11}}(x) &= \frac{2\pi}{f_3}\frac{A_3}{A_2}C_{\Gamma_3}C_{\Gamma_2}C_6'C_5'C_4'C_3'C_{DST} \\ &\quad e^{-j\frac{k}{2d_6}\left(\frac{f_3-d_5A_3}{f_3}\right)x^2}S''\left(-\frac{f_2}{f_3}\frac{k}{f_1}\frac{A_3}{A_2}A_1x\right)P_3\left(\frac{k}{f_3}A_3x\right) \end{aligned} \tag{A.57}$$

$$\mathbf{E_{11}}(x) = C_Te^{-j\frac{k}{2d_6}\left(\frac{f_3-d_5A_3}{f_3}\right)x^2}S''\left(-\frac{f_2}{f_3}\frac{k}{f_1}\frac{A_3}{A_2}A_1x\right)P_3\left(\frac{k}{f_3}A_3x\right) \tag{A.58}$$

where

$$P_3\left(\frac{k}{f_3}A_3x\right) = e^{j\frac{k}{2f_3^2}A_3^2\left\{\frac{d_4d_5\left[d_3\left(\frac{f_1-d_1A_1}{f_1}\right)+d_2\left(\frac{f_2-d_4A_2}{f_2}\right)\right]}{\left[d_5\left(\frac{f_2-d_3A_2}{f_2}\right)+d_4\left(\frac{f_3-d_6A_3}{f_3}\right)\right]\left[d_3\left(\frac{f_1-d_1A_1}{f_1}\right)+d_2\left(\frac{f_2-d_4A_2}{f_2}\right)\right]-\frac{d_2d_3d_4d_5}{f_2^2}A_2^2}\right\}x^2}. \tag{A.59}$$

A.3 Spatial Patterning and Grating Effects

We wish to relate the DST / telescope output to an applied spatial pattern. Recall, the diffraction analysis assumed a spatially patterned beam just after the grating ($\mathbf{P}_2$). For a Gaussian, patterned fs ($E(\omega)$)input beam [22, 23, 8] before the grating we have,

$$\mathbf{E_1}(x,\omega) = m(x)\ e^{-\frac{x^2}{w^2}}\ e^{-j\frac{k}{2R}x^2}\ E(\omega) \tag{A.60}$$

where

$$m(x) = \text{applied spatial pattern} \tag{A.61}$$

$$e^{-\frac{x^2}{w^2}} = \text{Gaussian shape of input beam (leads to a temporal window)} \tag{A.62}$$

$$e^{-j\frac{k}{2R}x^2} = \text{radius of curvature of the Gaussian beam phase front (gives a chirp term)} \tag{A.63}$$

The field just after the grating, in now defined as

$$\mathbf{E_2}(x,\omega) = m(\alpha x)\ e^{-\frac{\alpha^2 x^2}{w^2}}\ e^{-j\frac{k}{2R}\alpha^2 x^2}\ e^{-j\gamma\omega x}\ E(\omega) \tag{A.64}$$

$$= s(x_2)\ E(\omega) \tag{A.65}$$

with

$$\alpha = \frac{\cos\theta_i}{\cos\theta_d} \tag{A.66}$$

$$\gamma = \frac{\lambda}{cd\cos\theta_d}. \tag{A.67}$$

Here, λ is the source wavelength, c is the speed of light, d is the period of the diffraction grating and θ_i, θ_d are the incident and diffracted angles of the beam off the grating. To complete the derivation of the pulse shaper output, we redefine

$$s'(\alpha x) = m(\alpha x)\, e^{-\alpha^2\frac{x^2}{w^2}} e^{-j\frac{k}{2}\left(\frac{\alpha^2}{R}+\frac{f_1-d_2A_1}{f_1 d_1}\right)x^2} \tag{A.68}$$

and set $x_2 = \alpha x$, we have

$$s(x_2) = s'(\alpha x)\ e^{-j\gamma\omega x}. \tag{A.69}$$

Inserting A.69 in to the expression for s' given by Eq. A.26, and inserting this into the integral form of the DST output A.25,

$$\mathbf{E_5}(x,\omega) = C_{\Gamma_1} C_2' C_1' e^{-j\frac{k}{2d_2}\left(\frac{f_1 - d_1 A_1}{f_1}\right)x^2} \int_{-\infty}^{\infty} dx'\; s'(\alpha x')\, e^{-j\gamma\omega x'} e^{j\frac{k}{f_1}A_1 x' x}. \tag{A.70}$$

Making the change of variables, $x'' = \alpha x'$, $dx' = 1/\alpha\; dx''$ and then taking the spatial Fourier transform using the spatial shift property A.10,

$$\mathbf{E_5}(x,\omega) = \frac{C_{DST}}{\alpha} E(\omega)\, e^{-j\frac{k}{2d_2}\left(\frac{f_1 - d_1 A_1}{f_1}\right)x^2} S'\left\{-\frac{\gamma}{\alpha}\left(\omega - \frac{k}{f_1 \gamma} A_1 x\right)\right\}, \tag{A.71}$$

which is the field just prior to the output waveguide (slit) in the DST shaper. To find the output from the telescope before the output waveguide, the grating dispersion is explicitly included and the result is substituted into A.49 to yield

$$\begin{aligned}\mathbf{E_{11}}(x) = {} & \frac{\sqrt{2\pi}}{kA_1}\frac{f_1}{f_2} C_{\Gamma_3} C_{\Gamma_2} C_6' C_5' C_4' C_3' C_{DST} e^{-j\frac{k}{2d_6}\left(\frac{f_3 - d_5 A_3}{f_3}\right)x^2} \\ & E(\omega) \int_{-\infty}^{\infty} dx' \left[s''\left(-\frac{f_1}{f_2}\frac{A_2}{A_1}\alpha x'\right) e^{j\gamma\omega\frac{f_1}{f_2}\frac{A_2}{A_1}x'} * p_3(x')\right] e^{j\frac{k}{f_3}A_3 x' x}.\end{aligned} \tag{A.72}$$

Making the change of variables

$$x'' = \alpha \frac{f_1}{f_2}\frac{A_2}{A_1} x' \tag{A.73}$$

and taking the spatial Fourier transform in light of the relations A.12, A.10, the field just before the output waveguide in the telescope is

$$\mathbf{E_{11}}(x,\omega) = C_T E(\omega)\, S''\left[-\frac{\gamma}{\alpha}\left(\omega + \frac{f_2}{f_3}\frac{A_3}{A_2}\frac{k}{\gamma f_1} A_1 x\right)\right] P_3\left(\frac{k}{f_3} A_3 x\right) e^{-j\frac{k}{2d_6}\left(\frac{f_3 - d_5 A_3}{f_3}\right)x^2}. \tag{A.74}$$

A.4 Effects of Fiber Coupling the DST / Telescope Output

To find the time domain fields out of the DST / telescope, the effects of the output waveguide (slit) must be treated. In contrast to [8, 7, 13], the slit cannot be treated as a δ function, e.g. a slit with zero width. The actual time domain field is found by performing an overlap integral of the field just prior to the waveguide and the effective waveguide mode and then taking an inverse Fourier transform with respect

to time. The method used to treat the effect of waveguide coupling is similar to [24]. Here the waveguide mode is assumed to centered at $x = 0$ and to be of the general form

$$f\left(\frac{x}{w_0}\right) \tag{A.75}$$

with the property

$$\int_{-\infty}^{\infty} dx \left| f\left(\frac{x}{w_0}\right)\right|^2 = 1. \tag{A.76}$$

To illustrate the general expression, consider the DST shaper output, prior to sampling $\mathbf{E_5}(x,\omega)$. In this case, the field coupled to the fiber can be written as

$$E_{DST}(x,\omega) = f\left(\frac{x}{w_0}\right) \int_{-\infty}^{\infty} dx'\, f\left(\frac{x'}{w_0}\right) \mathbf{E_5}(x',\omega). \tag{A.77}$$

The time domain field is then determined by taking the inverse temporal Fourier transform of the field coupled to the fiber. Writing the time-domain output fields of the DST shaper and the telescope, in terms of this overlap integral (using the expressions for the fields given by A.71 and A.74) we have

$$\begin{aligned} E_{DST}(x,t) &= \frac{C_{DST}}{\alpha} f\left(\frac{x}{w_0}\right) \frac{1}{\sqrt{2\pi}} \int_{-\infty}^{\infty} d\omega\, E(\omega)\, e^{j\omega t} \\ &\quad \cdot \int_{-\infty}^{\infty} dx'\, f\left(\frac{x'}{w_0}\right) e^{-j\frac{k}{2d_2}\left(\frac{f_1-d_1A_1}{f_1}\right)x'^2} S'\left[-\frac{\gamma}{\alpha}\left(\omega - \frac{k}{f_1\gamma}A_1x'\right)\right] \end{aligned} \tag{A.78}$$

$$\begin{aligned} E_{TEL}(x,t) &= \frac{C_T}{\alpha} f\left(\frac{x}{w_0}\right) \frac{1}{\sqrt{2\pi}} \int_{-\infty}^{\infty} d\omega\, E(\omega)\, e^{j\omega t} \\ &\quad \cdot \int_{-\infty}^{\infty} dx'\, f\left(\frac{x}{w_0}\right) S''\left[-\frac{\gamma}{\alpha}\left(\omega + \frac{f_2}{f_3}\frac{A_3}{A_2}\frac{k}{\gamma f_1}A_1x\right)\right] P_3\left(\frac{k}{f_3}A_3x\right) e^{-j\frac{k}{2d_6}\left(\frac{f_3-d_5A_3}{f_3}\right)x^2}. \end{aligned} \tag{A.79}$$

Interchanging the order of integration, and taking a temporal inverse Fourier transform using the shift and scaling properties A.6, A.7,

$$\begin{aligned} E_{DST}(x,t) &= \frac{C_{DST}}{\gamma} f\left(\frac{x}{w_0}\right) \\ &\int_{-\infty}^{\infty} dx'\ f\left(\frac{x}{w_0}\right) e^{-j\frac{k}{2d_2}\left(\frac{f_1-d_1A_1}{f_1}\right)x'^2} e(t) * \left\{ s'\left(-\frac{\alpha}{\gamma}t\right) e^{j\frac{k}{\gamma f_1}A_1x't} \right\} \end{aligned} \tag{A.80}$$

$$\begin{aligned} E_{TEL}(x,t) &= \frac{C_T}{\gamma} f\left(\frac{x}{w_0}\right) \\ &\int_{-\infty}^{\infty} dx'\ f\left(\frac{x}{w_0}\right) P_3\left(\frac{k}{f_3}A_3x\right) e^{-j\frac{k}{2d_6}\left(\frac{f_3-d_5A_3}{f_3}\right)x^2} \\ &e(t) * \left\{ s''\left(-\frac{\alpha}{\gamma}t\right) e^{-j\frac{f_2}{f_3}\frac{A_3}{A_2}\frac{k}{\gamma f_1}A_1x't} \right\} \end{aligned} \tag{A.81}$$

Interchanging the order of integration again, and treating the dx' integral as a spatial Fourier transform, these can be written as

$$\begin{aligned} E_{DST}(x,t) &= \sqrt{2\pi}w_0\frac{C_{DST}}{\gamma} f\left(\frac{x}{w_0}\right) \\ &e(t) * \left\{ s'\left(-\frac{\alpha}{\gamma}t\right) \left[F\left(\frac{kw_0}{\gamma f_1}t\right) * e^{j\frac{k}{2\gamma^2 f_1^2}A_1^2\left(\frac{f_1d_2}{f_1-d_1A_1}\right)t^2} \right] \right\} \end{aligned} \tag{A.82}$$

$$\begin{aligned} E_{TEL}(x,t) &= \sqrt{2\pi}w_0\frac{C_T}{\gamma} f\left(\frac{x}{w_0}\right) \\ &e(t) * \left\{ s''\left(-\frac{\alpha}{\gamma}t\right) \left[F\left(-\frac{f_2}{f_3}\frac{kw_0}{\gamma f_1}t\right) * p_4(t) \right] \right\} \end{aligned} \tag{A.83}$$

In the above expression,

$$p_4(t) = e^{-j\frac{k}{2f_3}\frac{f_2^2}{f_1^2}\frac{A_3^2}{A_2^2}A_1^2\mathbf{B_2}\frac{t^2}{\gamma^2}}, \tag{A.84}$$

$$\mathbf{B_2} = \frac{B_1}{(f_3 - d_5A_3)B_1 - A_3^2f_2d_4d_5d_6\left[f_2d_3(f_1 - d_1A_1) + f_1d_2(f_2 - d_4A_2)\right]}, \tag{A.85}$$

and

$$\begin{aligned} B_1 = &\\ &d_6\left[f_2d_3(f_1 - d_1A_1) + f_1d_2(f_2 - d_4A_2)\right]\left[f_3d_5(f_2 - d_3A_2) + f_2d_4(f_3 - d_6A_3)\right] \\ &- f_1f_3d_2d_3d_4d_5d_6A_2^2. \end{aligned} \tag{A.86}$$

Finally, evaluating the full expressions for $s'\left(-\frac{\alpha}{\gamma}t\right)$ and $s''\left(-\frac{\alpha}{\gamma}t\right)$, the full expressions for the temporal output of the DST / telescope are

$$\mathbf{E_{DST}}(x,t) = C_{DT} f\left(\frac{x}{w_0}\right) e(t) * \left\{ m\left(-\frac{\alpha}{\gamma}t\right) e^{-\frac{\alpha^2}{\gamma^2 w^2}t^2} e^{-j\frac{k}{2\gamma^2}\left(\frac{\alpha^2}{R}+\frac{f_1-d_2A_1}{f_1 d_1}\right)t^2} \left[F\left(\frac{kw_0}{\gamma f_1}A_1 t\right) * e^{j\frac{k}{2\gamma^2 f_1^2}A_1^2\left(\frac{f_1 d_2}{f_1-d_1A_1}\right)t^2}\right]\right\} \tag{A.87}$$

$$\begin{aligned}\mathbf{E_{TEL}}(x,t) = {} & C_{TT} f\left(\frac{x}{w_0}\right) e(t) * \\ & m\left(-\frac{\alpha}{\gamma}t\right) e^{-\frac{\alpha^2}{\gamma^2 w^2}t^2} e^{-j\frac{k}{2\gamma^2}\left[\frac{\alpha^2}{R}+\frac{f_1-d_2A_1}{f_1 d_1}+\frac{f_2^2}{f_1^2}\frac{A_1^2}{A_2^2}\left(\frac{f_2-d_3A_2}{f_2 d_4}+\frac{f_3-d_6A_3}{f_3 d_5}\right)\right]t^2} \\ & \left[F\left(-\frac{f_2}{f_3}\frac{A_3}{A_2}\frac{kw_0}{\gamma f_1}A_1 t\right) * p_4(t)\right]\end{aligned} \tag{A.88}$$

These expressions give the output field of the DST shaper / telescope for a general output waveguide (slit). The specific case of a singlemode fiber output is treated in Section 2.2. Additionally, though the diagram of Figure 2.3 illustrates a telescope constructed from two positive lenses, no assumptions were made during this derivation. The results also apply to a telescope consisting of a negative lens followed by a positive lens.

VITA

Jason D. McKinney received his B.S. and M.S. degrees in Electrical Engineering from Purdue University in 1997 and 1999, respectively. He began his Doctoral work in 1999, with a focus on space-time optical processing and arbitrary electromagnetic waveform generation. His research interests include optical pulse shaping, microwave photonics, optical signal processing, ultrafast optics, and optical devices. He has been recognized both by the School of ECE and the University for his teaching ability. He was a finalist for the Optical Society of America / New Focus Student award in 2002 and received the Chorafas Prize for outstanding Doctoral research in 2003. He is a member of IEEE / LEOS and the Optical Society of America.